

1 An [Emerging](#) Aerosol Climatology via Remote Sensing over Metro Manila, Philippines

2
3 Genevieve Rose Lorenzo^{1,2}, Avelino F. Arellano¹, Maria Obiminda Cambaliza^{2,3}, Christopher
4 Castro¹, Melliza Templonuevo Cruz^{2,4}, Larry Di Girolamo⁵, Glenn Franco Gacal², Miguel
5 Ricardo A. Hilario¹, Nofel Lagrosas⁶, Hans Jarett Ong², James Bernard Simpas^{2,3}, Sherdon Niño
6 Uy², and Armin Sorooshian^{1,7}

7
8 ¹Department of Hydrology and Atmospheric Sciences, University of Arizona, Tucson, Arizona,
9 85721, USA

10 ²Air Quality Dynamics-Instrumentation & Technology Development Laboratory, Manila
11 Observatory, Quezon City, 1108, Philippines

12 ³Department of Physics, School of Science and Engineering, Ateneo de Manila University,
13 Quezon City, 1108, Philippines

14 ⁴Institute of Environmental Science and Meteorology, University of the Philippines, Diliman,
15 Quezon City, 1101, Philippines

16 ⁵Department of Atmospheric Science, University of Illinois, Urbana-Champlain, Illinois, 61801,
17 USA

18 ⁶Center for Environmental Remote Sensing, Chiba University, Chiba, 263-8522, Japan

19 ⁷Department of Chemical and Environmental Engineering, University of Arizona, Tucson,
20 Arizona, 85721, USA

21
22 *Correspondence to:* armin@arizona.edu

23 **Abstract**

24 Aerosol particles in Southeast Asia ~~have a complex life cycle and consequently~~ are challenging
25 to characterize. ~~The~~ due to their complex life cycle within the diverse topography and weather in
26 the region ~~complicate the situation.~~ An emerging aerosol climatology was established based on
27 AERONET data (December 2009 to October 2018) for clear sky days in Metro Manila,
28 Philippines. ~~Aerosol optical depth (AOD) values were highest~~ infrom August, ~~coinciding with~~
29 the summer southwest monsoon, due to October, partly ~~to~~from fine ~~particles from~~ urban aerosol
30 particles, including soot. ~~Also, August corresponds to,~~ coinciding with the burning season in
31 Insular Southeast Asia when smoke is often transported to Metro Manila during the southwest
32 monsoon. Clustering of AERONET volume size distributions (VSD) resulted in five aerosol
33 particle sources based on the position and magnitude of their peaks in the VSD and the
34 contributions of specific particle species to AOD per cluster based on MERRA-2. The clustering
35 showed that the majority of aerosol particles above Metro Manila were from a clean marine
36 source (58%), which could be related to AOD values there being relatively smaller than in other
37 cities in the region. The following are the other particle sources over Metro Manila: fine polluted
38 (20%), mixed polluted dust (12%), urban/industrial (5%), and cloud processing (5%).
39 Furthermore, MERRA-2 AOD data over Southeast Asia were analyzed using empirical
40 orthogonal functions. Along with AOD fractional compositional contributions and wind regimes,
41 four dominant aerosol particle air masses emerged: two sulfate air masses from East Asia, an
42 organic carbon source from Indonesia, and a sulfate source from the Philippines. Knowing the
43 local and regional aerosol particle air masses that impact Metro Manila is useful in identifying
44 the sources while gaining insight on how aerosol particles are affected by long-range transport
45 and their impact on regional weather.

46 1. Introduction

47 Although Southeast Asia is one of the most rapidly developing regions in the world, ~~there have~~
48 ~~been limited studies characterizing with a growing number of extensive research conducted~~
49 ~~(Reid et al., 2023), there remain knowledge gaps related to~~ aerosol particles in the area (Tsay et
50 al., 2013; Lee et al., 2018; Chen et al., 2020; [Amnuaylojaroen, 2023](#)). The region represents a
51 complex geographic, meteorological, and hydrological environment making it challenging to
52 understand aerosol particle characteristics, especially interactions between aerosol particles with
53 their environment (Reid et al., 2013). The island of Luzon in the Philippines in particular is very
54 populated and is characterized by high levels of anthropogenic emissions superimposed on
55 natural emissions from the surrounding waters (AzadiAghdam et al., 2019) and long-range
56 transport of emissions from areas such as Indonesia and East Asia (Braun et al., 2020; Hilario et
57 al., 2020a; Hilario et al., 2020b; Hilario et al., 2021a). [Aerosol particle lifecycle in the region is](#)
58 [impacted by Philippine weather that is marked by two distinct monsoons, typhoons, the](#)
59 [intertropical convergent zone, and impacts from El Niño-Southern Oscillation and Madden-](#)
60 [Julian Oscillation \(Cruz et al., 2013; Xian et al., 2013; Reid et al., 2012; Reid et al., 2015; Hilario](#)
61 [et al., 2021b\)](#). Studying this area is informative owing to the wide dynamic range in aerosol
62 [particle and weather conditions, which are interconnected.](#) ~~The presence of~~ [The overlapping of](#)
63 [large fraction of cirrus clouds with lower](#) clouds in the area (Hong and Di Girolamo, 2020)
64 makes space-borne remote sensing of aerosol particles very challenging (Reid et al., 2013; Lin et
65 al., 2014). These reasons motivated the NASA Cloud, Aerosol, and Monsoon Processes
66 Philippines Experiment (CAMP²Ex) airborne measurement campaign in 2019 to understand the
67 interaction between tropical meteorology and aerosol particles (Di Girolamo et al., 2015; Reid et
68 al., 2023). ~~Prior to the airborne measurements, intensive surface based measurements were~~
69 ~~conducted as part of the CAMP²Ex weathER and CompoSition Monitoring (CHECSM) study~~
70 ~~between July 2018 and October 2019~~ [However, those short terms measurements cannot provide](#)
71 [an adequate assessment of aerosol behavior across all seasons and over many years.](#)

72 ~~Aerosol climatology studies in different regions have proved beneficial to understand temporal~~
73 ~~characteristics of aerosol particle concentrations and properties, in addition to identifying~~
74 ~~potential source regions along with interactions with clouds and rainfall (Stevens and Feingold,~~
75 ~~2009; Li et al., 2011; Tao et al., 2012; Crosbie et al., 2014; Kumar et al., 2015; Alizadeh-~~
76 ~~Choobari and Gharaylou, 2017; Mora et al., 2017; Aldhaif et al., 2021).~~ The NASA AeRosol
77 RObotic NETwork (AERONET) (Holben et al., 1998) is pivotal in providing broad temporal
78 coverage [of aerosol characteristics in specific locations with a column-based perspective from](#)
79 [the ground up.](#) ~~Aerosol climatology studies in different regions have proved beneficial to~~
80 ~~understand temporal characteristics of aerosol particle concentrations and properties, in addition~~
81 ~~to identifying potential source regions along with interactions with clouds and rainfall (Stevens~~
82 ~~and Feingold, 2009; Li et al., 2011; Tao et al., 2012; Crosbie et al., 2014; Kumar et al., 2015;~~
83 ~~Alizadeh-Choobari and Gharaylou, 2017; Mora et al., 2017; Aldhaif et al., 2021).~~ [in specific](#)
84 [locations with a column based perspective from the ground up.](#) To our knowledge, there has not
85 been a remote sensing-based aerosol climatology study for the Metro Manila region of Luzon,
86 which has approximately 16 cities, a population of 12.88 million, and a high population density
87 of 20,800 km⁻² (PSA, 2016; Alas et al., 2018). ~~Studying this area is informative owing to the~~
88 ~~wide dynamic range in aerosol particle and weather conditions, which are interconnected.~~
89 [Aerosol particle lifecycle in the region is impacted by Philippine weather that is marked by two](#)
90 [distinct monsoons, typhoons, and impacts from El Niño Southern Oscillation and Madden-Julian](#)

91 [Oscillation \(Cruz et al., 2013; Xian et al., 2013; Reid et al., 2012; Reid et al., 2015; Hilario et al.,](#)
92 [2021b\).](#)

93 [Regional analysis of aerosol particles in Southeast Asia and Asia in general show the prevalence](#)
94 [of biomass burning in the region, as well as the larger influence of anthropogenic emissions in](#)
95 [East Asia \(Nakata et al., 2018\).](#) ~~These large prevalent sources may overshadow other relevant but~~
96 ~~weaker sources in the region, such as local sources. Due to the complex nature of aerosol~~
97 ~~particles, analysis techniques such as principal component analysis and clustering along with~~
98 ~~recent improvements in gridded datasets help detect spatial and temporal patterns that would~~
99 ~~otherwise be difficult to make with noise interference and even weak signals (Li et al., 2013;~~
100 ~~Sullivan et al., 2017; Plymale et al., 2021).~~ [Understanding the dominant air masses around](#)
101 [Southeast Asia will help in distinguishing local and transported particles that influence the](#)
102 [aerosol climatology in Metro Manila.](#) [Most of the past studies involving long-term remotely](#)
103 [sensed aerosol particle data in Southeast Asia \(Cohen, 2014; Nakata et al., 2018; Nguyen et al.,](#)
104 [2019b\) had no specific focus on the Philippines. The Philippines is considered as part of the](#)
105 [Maritime Continent \(MC\), the island nations sub-region of Southeast Asia. The other Southeast](#)
106 [Asia sub-region, Peninsular Southeast Asia \(PSEA\), comprises those nations within the](#)
107 [continental Asia land mass. These two regions have separate aerosol sources and climate, where](#)
108 [MC is dependent on the intertropical convergent zone \(ITCZ\) and PSEA is dependent on both](#)
109 [the ITCZ and monsoon systems \(Dong and Fu, 2015\). Only the southern part of the Philippines](#)
110 [is climatologically part of MC \(Ramage, 1971\), however, and northwest Philippines, where](#)
111 [Metro Manila is located, is affected by the monsoons and tropical cyclones aside from the ITCZ](#)
112 [\(Chang et al., 2005; Yumul Jr et al., 2010; Bagtasa, 2017\). These unique meteorological](#)
113 [influences and extensive local aerosol particle sources warrant a unique aerosol climatology over](#)
114 [Metro Manila, one of a polluted source in a tropical marine environment, and its effects on cloud](#)
115 [formation in the area. Aerosol effects on clouds in the marine environment are associated with](#)
116 [the largest uncertainties in climate change research \(Hendrickson et al., 2021; Wall et al., 2022\)](#)
117 [and the Philippines was ranked as the 5th country globally as most at risk to climate change and](#)
118 [extreme weather from 1997 to 2018 \(Eckstein et al., 2018\). There have been several surface](#)
119 [measurements of aerosol particles made in Metro Manila for the past 20 years \(Oanh et al., 2006;](#)
120 [Bautista VII et al., 2014; Cruz et al., 2019\) but columnar ground-based measurements there are](#)
121 [just beginning to be established \(Dorado et al., 2001; Ong et al., 2016; Cruz et al., 2023\). The](#)
122 [AERONET sun photometer is one of the first long-term column-based aerosol instruments in](#)
123 [Metro Manila and the Philippines \(Ong et al., 2016\).](#)

124 The goal of this study is to use multi-year AERONET data [in Manila Observatory](#) along with
125 other complementary datasets ([MERRA-2, PERSIANN, MISR, HYSPLIT, and NAAPS](#)) to
126 address the following questions: (1) what are the monthly characteristics of aerosol particles over
127 Metro Manila, Philippines?; (2) what are the possible sources and factors influencing the
128 observed characteristics?; (3) what relationships are evident between aerosol particles and cloud
129 characteristics?; and (4) what are the regional and local aerosol particle air masses that influence
130 Metro Manila?
131

132 **2. Methods**

133 This work relies on analysis of several datasets summarized in Table 1 and the following
 134 subsections. The common time range used for all datasets is between January 2009 and October
 135 2018.

136 **Table 1:** Summary of datasets over Metro Manila used in this work covering the period from
 137 January 2009 to October 2018.

Parameter	Data Source	Spatial Coverage	Data Repository	Time Coverage
			(AERONET)	
Aerosol Optical Depth (500 nm)	AERONET	14.635°N, 121.078°E	https://aeronet.gsfc.nasa.gov/	Jan 2009 - Oct 2018
Asymmetry Factor (440 nm - 1020 nm)	AERONET	14.635°N, 121.078°E		Jan 2009 - Oct 2018
Extinction Angstrom Exponent (440 nm - 870 nm)	AERONET	14.635°N, 121.078°E		Jan 2009 - Oct 2018
Fine Mode Fraction	AERONET	14.635°N, 121.078°E		Jan 2009 - Oct 2018
Precipitable Water	AERONET	14.635°N, 121.078°E		Jan 2009 - Oct 2018
Single Scattering Albedo (440 nm - 1020 nm)	AERONET	14.635°N, 121.078°E		Jan 2009 - Oct 2018
Refractive Index (Real and Imaginary; 440 nm - 1020 nm)	AERONET	14.635°N, 121.078°E		Jan 2009 - Oct 2018
Volume Size Distribution	AERONET	14.635°N, 121.078°E		Jan 2009 - Oct 2018
			(MERRA-2)	
Low Cloud Fraction (MODIS)	MERRA-2	14.253°N - 14.758°N, 120.937575°E - 121.562525°E	https://disc.gsfc.nasa.gov/	Jan 2009 - Dec 2018
Planetary Boundary Layer Height	MERRA-2	14.253°N - 14.758°N, 120.937575°E - 121.562525°E		Jan 2009 - Dec 2018
Relative Humidity (975 mb)	MERRA-2	14.253°N - 14.758°N, 120.937575°E - 121.562525°E		Jan 2009 - Dec 2018
Sea Level Pressure	MERRA-2	14.253°N - 14.758°N, 120.937575°E - 121.562525°E		Jan 2009 - Dec 2018
Temperature (975 mb)	MERRA-2	14.253°N - 14.758°N, 120.937575°E - 121.562525°E		Jan 2009 - Dec 2018
Wind (975 mb)	MERRA-2	14.253°N - 14.758°N, 120.937575°E - 121.562525°E		Jan 2009 - Dec 2018
Total Extinction Aerosol Optical Depth (550 nm)	MERRA-2	14.3°N - 14.8°N, 120.75°E - 121.25°E		Jan 2009 - Dec 2018
Sulfate, Black Carbon, Organic Carbon, Dust, and Sea Salt Extinction Aerosol Optical Depth (550 nm)	MERRA-2	14.3°N - 14.8°N, 120.75°E - 121.25°E		Jan 2009 - Dec 2018
			(PERSIANN)	
Precipitation	PERSIANN	14.53°N - 15.0148°N, 120.75°E - 121.25°E	https://chrsdata.eng.uci.edu/	Jan 2009 - Dec 2018

138

139 **2.1 Datasets**

140 2.1.1 AERONET

141 The central dataset used is that of sun photometer measurements and derived (inversion)
 142 parameters from the AERONET (Holben et al., 1998) site at the Manila Observatory in Quezon
 143 City, Philippines (14.64°N, 121.08°E, ~70 m. a. s. l.). Direct sunlight extinction measurements
 144 were made at nominal wavelengths of 340, 380, 440, 500, 675, 870, 940, and 1020 nm, from

145 which aerosol optical depth (AOD) was calculated (except for 940 nm, which is for water vapor)
146 (Eck et al., 2013). AOD is a commonly used proxy for aerosol particle loading in the air column
147 from the ground up (Holben et al., 2001); higher AOD translates to more aerosol particle
148 extinction in the column above a location. The extinction angstrom exponent (EAE) and the fine
149 mode fraction (FMF) are also AERONET direct sun products that are retrieved after the
150 application of a spectral de-convolution algorithm (O'Neill et al., 2003). For the inversion
151 products, it is through radiative retrievals that the volume size distribution (VSD) and complex
152 refractive index (RI) are gathered ([Schuster et al., 2005](#)) ~~and from which single scattering albedo~~
153 ~~(SSA) and asymmetry factor (AF) are calculated, and from which single scattering albedo (SSA)~~
154 ~~and asymmetry factor (AF) are calculated. The AERONET observations were made during clear~~
155 ~~sky conditions, which has been shown (Hong and Di Girolamo, 2022) to be able to represent all~~
156 ~~sky conditions.~~

157 For the inversions, four wavelengths (440, 670, 870, and 1020 nm) of the radiometer spectral
158 channels were chosen for diffuse radiance measurements and to avoid gas absorption (Dubovik
159 et al., 1998). Version 3 Direct Sun and Inversion algorithms (AERONET, 2019; Giles et al.,
160 2019) were used with the AlmuCantar Sky Scan Scenario to derive the following parameters with
161 level 2.0 (automatically cloud-cleared and quality controlled datasets with pre- and post-field
162 calibrations) data quality: column AOD (500 nm), fine mode fraction (500 nm), extinction
163 angstrom exponent (440 – 870 nm), precipitable water (940 nm), [SSA single scattering albedo](#)
164 (440, 670, 870, and 1020 nm), asymmetry factor (440, 670, 870, and 1020 nm), refractive index
165 (440, 670, 870, and 1020 nm), and VSD. The version 3 products are able to keep fine mode
166 aerosol particle data (haze and smoke) as well as remove optically thin cirrus clouds in order to
167 retain more aerosol particle measurements in the database (Giles et al., 2019). Cloud screening in
168 the version 3 product improves remote sensing measurements in Southeast Asia in general,
169 where cirrus clouds are pervasive (Reid et al., 2013). At most, a total of 29,037 direct sun and
170 1419 inversion AERONET daytime data points were available between January 2009 and
171 October 2018.

172 2.1.2 MERRA-2

173 Modern Era-Retrospective Analysis for Research and Applications, Version 2 (MERRA-2: 0.5°
174 $\times 0.625^\circ$ approximate resolution) meteorological and aerosol particle composition [reanalysis](#) data
175 (Bosilovich, 2016; Gelaro et al., 2017; Randles et al., 2017) were acquired for the area around
176 Manila Observatory ($14.25^\circ\text{N} - 14.75^\circ\text{N}$, $120.9375^\circ\text{E} - 121.5625^\circ\text{E}$). [The aerosol reanalysis](#)
177 [data includes data assimilation of AOD from the Moderate Resolution Imaging](#)
178 [Spectroradiometer \(MODIS: Terra, 2000 to present and Aqua, 2002 to present\), Advanced Very](#)
179 [High Resolution Radiometer \(AVHRR, 1979-2002\), and Multiangle Imaging SpectroRadiometer](#)
180 [\(MISR, 2000-2014\) \(Buchard et al., 2017; Rizza et al., 2019\).](#) The following products were used:
181 M2I3NPASM Assimilated Meteorological Fields (3-hourly) for 975 mb level winds,
182 temperature, relative humidity, and sea level pressure; M2T1NXFLX Surface Flux Diagnostics
183 (1-hourly from 00:30 UTC time-averaged) 2D for planetary boundary layer height; ~~and~~
184 M2T1NXCSP COSP Satellite Simulator (1-hourly from 00:30 UTC time-averaged) for MODIS
185 mean low cloud fraction (cloud top pressure > 680 hPa); [and M2T1NXAER Aerosol Diagnostics](#)
186 [\(1-hourly from 00:30 UTC time-averaged\) for Total AOD and speciated AOD \(Sulfate, Black](#)
187 [Carbon \(BC\), Organic Carbon \(OC\), Dust, and Sea Salt\).](#)

188 MERRA-2 meteorological and aerosol particle composition monthly [mean reanalysis](#) data
189 (Bosilovich, 2016; Gelaro et al., 2017; Randles et al., 2017) were also acquired for a larger
190 region, [\(30° × 30°\)](#), the Southeast Asia region (0°–N– 30°N, 105°E – 135°E) for the period from
191 2009 to 2018. This is within the spatial domain of the CAMP²Ex airborne measurement
192 campaign which, as mentioned earlier, targets the interaction between tropical meteorology and
193 aerosol particles. The following datasets (0.5° latitude and 0.625° longitude resolution) were
194 used: MERRA-2 tavgM_2d_aer_Nx: Aerosol Assimilation (M2TMNXAER) for Total [500 nm](#)
195 AOD and speciated [500 nm](#) AOD (Sulfate, ~~Black Carbon (BC)~~, ~~Organic Carbon (OC)₂~~, Dust,
196 and Sea Salt) and MERRA-2 instM_3d_ana_Np: Analyzed Meteorological Fields
197 (M2IMNPANA) for 1000 hPa and 725 hPa level U and V winds. [The total MERRA-2 AOD for](#)
198 [the region \(mean over 30° x 30° region\) was used along with MISR AOD data \(mean over 30° x](#)
199 [30° region\) to assess the influence of long-range sources to the aerosol column over Manila](#)
200 [Observatory](#). The monthly meteorological and aerosol particle composition data for the region
201 will be used for empirical orthogonal functions, which will be described later.

202 2.1.3 MISR

203 [Monthly AOD data \(Level 3 Global Aerosol: 0.5° × 0.5° spatial resolution\) from 2009 to 2018](#)
204 [are used from the Multi-angle Imaging SpectroRadiometer \(MISR\), \(Diner et al., 2007; Garay et](#)
205 [al., 2018\). Level 3 products are global maps of parameters available in Level 2 \(measurements](#)
206 [derived from the instrument data\) products. MISR has relatively more accurate AOD and agrees](#)
207 [better with AERONET data compared to other satellite products due to its multi-angle](#)
208 [measurements \(Choi et al., 2019; Kuttippurath and Raj, 2021\). Monthly median AOD \(bin 0\)](#)
209 [were extracted for Southeast Asia \(0.25°– 30.25°N, 104.75°E – 134.75°E\) within the CAMP²Ex](#)
210 [region. They are used for comparison to the AERONET \(over Metro Manila\) and MERRA-2](#)
211 [\(Southeast Asia\) monthly AOD values.](#)

212 2.1.4 PERSIANN

213 Hourly precipitation data were obtained from the Precipitation Estimation from the Remotely
214 Sensed Information using Artificial Neural Networks (PERSIANN) (Nguyen et al., 2019a)
215 database of the Center for Hydrometeorology and Remote Sensing (CHRS) at the University of
216 California, Irvine (UCI). Hourly data were accumulated for running three-day totals, which were
217 compared to AERONET data. The data were averaged between the four grids that included the
218 area of interest as well as ensuring a similar spatial domain (14.5°N – 15.0°N, 120.75°E –
219 121.25°E) to the MERRA-2 dataset.

220 2.1.4 MISR

221 [Monthly 500 nm AOD data \(Level 3 Global Aerosol: 0.5° × 0.5° spatial resolution in the region](#)
222 [0.25°N – 30.25°N and 104.75°E – 134.75°E\) from 2009 to 2018 are used from the Multi-angle](#)
223 [Imaging SpectroRadiometer \(MISR\), \(Diner et al., 2007; Garay et al., 2018\) as regional](#)
224 [\(Southeast Asia\) baseline remote sensing data to support the Manila Observatory AERONET](#)
225 [data. The regional \(30° × 30°\) MISR data was used to confirm regional sources of aerosols that](#)
226 [may be influencing the AOD over Metro Manila. Level 3 MISR products are global maps of](#)
227 [parameters available in Level 2 \(measurements derived from the instrument data\) products.](#)
228 [MISR is ideal for remote sensing in the CAMP²Ex region because it has an overpass at 10:30](#)
229 [AM ECT \(descending mode\) \(when cirrus is minimal\) and its retrievals have been shown to be](#)
230 [unimpacted by small cumulus \(Zhao et al., 2009\), which are typical in the region. MISR has](#)
231 [relatively more accurate AOD and agrees better with AERONET data compared to other satellite](#)

232 [products due to its multi-angle measurements \(Choi et al., 2019; Kuttippurath and Raj, 2021\).](#)
233 [The MISR sampling noise is relatively small due to the large domain and seasonal averages that](#)
234 [are considered in this study. MISR is also the only passive sensor that speciates aerosol particle](#)
235 [size and shape. All these factors led to the choice of using regional MISR data to associate long-](#)
236 [range sources influencing AERONET data in Manila Observatory. Monthly mean AOD \(bin 0\)](#)
237 [were extracted for Southeast Asia \(0.25°N – 30.25°N, 104.75°E – 134.75°E\) within the](#)
238 [CAMP²Ex region. Monthly mean AOD values were then calculated for each 0.5° grid point and](#)
239 [then for the 30° × 30° region, where the standard error in the monthly mean for the region is less](#)
240 [than 0.002. MISR monthly mean time series of size, shape, and absorption speciated 550 nm](#)
241 [AOD and angstrom exponent in the CAMP²Ex domain \(6.5°N – 22.5°N, 116.5°E – 128.5°E;](#)
242 [March 2000 to December 2020\) are also used to support the findings from the AERONET data.](#)

243 2.1.5 NAAPS

244 Archived [maps of](#) total and speciated optical depths ~~along with~~ and surface concentrations of
245 sulfate, dust, and smoke [for Southeast Asia](#) are used from the Navy Aerosol Analysis and
246 Prediction System (NAAPS: 1/3° × 1/3° spatial resolution) (Lynch et al., 2016), ~~and~~ which ~~is~~ are
247 publicly available at <https://www.nrlmry.navy.mil/aerosol/>. This reanalysis product relies on the
248 Navy Global Environmental Model (NAVGEM) for meteorological fields (Hogan et al., 2014).
249 Hourly maps were downloaded for ~~Southeast Asia~~ for aerosol particle events of interest based on
250 AERONET data. These maps help ~~in the identification of~~ [associate possible](#) regional emission
251 sources. ~~— to extreme aerosol loading events in Manila Observatory. Previous studies have used~~
252 [NAAPS data for an overview of aerosol sources in specific regions of interest](#) (Ross et al., 2018;
253 Foth et al., 2019; Markowicz et al., 2021; Harenda et al., 2022; Mims III, 2022). [More recent](#)
254 [studies show the need to improve aerosol representation in NAAPS](#) (Edwards et al., 2022), ~~so we~~
255 [will use NAAPS qualitatively, together with MERRA-2 compositional AOD data and back-](#)
256 [trajectories, for an overview of aerosol sources that may contribute to extreme events with high](#)
257 [AOD from AERONET.](#)

258 2.1.6 ~~NASA Worldview~~ HYSPLIT

259 ~~Archived maps of cloud fraction (Aqua MODIS and Terra MODIS) were downloaded from~~
260 ~~NASA Worldview (https://worldview.earthdata.nasa.gov) for events of interest based on~~
261 ~~AERONET data.~~

263 ~~2.2.1 Clustering~~

264 ~~Available AERONET VSD data (0.050 μm to 15.000 μm particle radius in 22 logarithmically~~
265 ~~equidistant bins, 1419 data points) were clustered via k-means clustering (Lloyd, 1982). The~~
266 ~~algorithm used was k-means++ (Arthur and Vassilvitskii, 2006). The ideal number of clusters~~
267 ~~was chosen based on relatively highest (>0.5) average silhouette value and the presence of a~~
268 ~~cluster with a second peak in the larger accumulation mode of the VSD. The clusters were~~
269 ~~analyzed based on their associated meteorological conditions and aerosol particle characteristics~~
270 ~~and were classified into air mass types (Table 2) based on previous studies (Pace et al., 2006;~~
271 ~~Kaskaoutis et al., 2007; Sorooshian et al., 2013; Kumar et al., 2014; Sharma et al., 2014; Che et~~
272 ~~al., 2015; Kumar et al., 2015).~~

273 [Table 2: Summary of threshold values of aerosol optical depth \(AOD\), angstrom exponent \(AE\),](#)
274 [and fine mode fraction \(FMF\) used to identify air mass types.](#)

Air Mass Type	AOD	AE	FMF	Source
Clean Fine	<0.1	≥1	≥0.7	Sorooshian et al., 2013
Polluted Fine	≥0.1	≥1	≥0.7	Sorooshian et al., 2013
Clean Coarse	<0.1	<1	<0.3	Sorooshian et al., 2013
Polluted Coarse	≥0.1	<1	<0.3	Sorooshian et al., 2013
Desert Dust	≥0.3	-	<0.6	Kaskaoutis et al., 2007
Clean Marine	<0.2	-	<0.7	Kaskaoutis et al., 2007
Urban/Industrial	≥0.2	-	≥0.8	Kaskaoutis et al., 2007

~~2.3.2.1 Extreme Event Analysis~~

~~Selected types of aerosol particle events were identified to characterize different types of sources and processes impacting aerosol particle columnar properties above Metro Manila. The three events are described below.~~

~~2.3.12.1.1 Smoke Long Range Transport~~

~~Events related to transported biomass burning/smoke were chosen based on the highest black carbon contribution to total AOD from the MERRA-2 dataset, high smoke contributions to AOD from NAAPS, and a dominant submicrometer peak in the AERONET VSD (Eck et al., 1999) over Metro Manila. Maps of surface smoke contributions from NAAPS as well as back-trajectories from the National Oceanic and Atmospheric Administration's (NOAA) Hybrid Single-Particle Lagrangian Integrated Trajectory (HYSPLIT) model (Stein et al., 2015; Rolph et al., 2017) were used to identify the likely source and transport pathway for the smoke cases. Three provide support for the AERONET monthly aerosol characteristics and the chosen case studies. Three and seven-day back-trajectories with six-hour resolution were generated based on the NCEP/NCAR reanalysis meteorological dataset and with a resolution of 1° and a vertical wind setting of "model vertical velocity". The three-day data were used to map the density of trajectories reaching Manila Observatory in each month from 2008 to 2019. The seven-day data were used in the analysis of the case studies. Trajectories were computed for an end point with an altitude of 500 m above ground level at the Manila Observatory. This altitude represents the mixed layer based on related surface air quality studies (Crosbie et al., 2014; Mora et al., 2017; Schlosser et al., 2017; Aldhaif et al., 2020), including a previous study for the same area (Stahl et al., 2020).~~

2.1.7 NASA Worldview

Archived maps of cloud fraction (Aqua MODIS and Terra MODIS) over Metro Manila and Southeast Asia were downloaded from NASA Worldview (<https://worldview.earthdata.nasa.gov>) for events of interest based on AERONET data.

2.2 Clustering

Available AERONET VSD data (0.050 μm to 15.000 μm particle radius in 22 logarithmically equidistant discrete points, 1419 data points) were clustered via k-means clustering (Lloyd, 1982). The algorithm used was k-means++ (Arthur and Vassilvitskii, 2006). The ideal number of clusters was chosen based on relatively highest (>0.5) average silhouette value and the presence of a cluster with a second peak in the larger accumulation mode of the VSD. The clusters were analyzed based on their associated meteorological conditions and aerosol particle

310 characteristics and were classified into air mass types (Table 2) based on estimates from previous
 311 studies (Dubovik et al., 2002; Pace et al., 2006; Kaskaoutis et al., 2007; Kaskaoutis et al., 2009;
 312 Sorooshian et al., 2013; Kumar et al., 2014; Sharma et al., 2014; Che et al., 2015; Kumar et al.,
 313 2015; Deep et al., 2021). The first four mentioned air mass types in Table 2 are the most general,
 314 and four more classifications based on aerosol particle sources are included. The urban/industrial
 315 air mass type here refers to local combustion along with long-range transported biomass burning
 316 (Kaskaoutis et al., 2009). While these classifications are not rigid definitions of air masses, they
 317 help in understanding the sources that contribute to aerosols in Metro Manila and in identifying
 318 cases where certain sources are more influential than others.

319 **Table 2:** Summary of threshold values of aerosol optical depth (AOD), angstrom exponent (AE),
 320 fine mode fraction (FMF), and single scattering albedo (SSA) used to identify air mass types.

<u>Air Mass Type</u>	<u>AOD</u>	<u>AE</u>	<u>FMF</u>	<u>SSA</u>	<u>Source</u>
<u>Clean Fine</u>	$< 0.1^a$	$\geq 1^a$	$> 0.7^a$	-	<u>Sorooshian et al., 2013</u>
<u>Polluted Fine</u>	$\geq 0.1^a$	$\geq 1^a$	$> 0.7^a$	-	<u>Sorooshian et al., 2013</u>
<u>Clean Coarse</u>	$< 0.1^a$	$< 1^a$	$< 0.3^a$	-	<u>Sorooshian et al., 2013</u>
<u>Polluted Coarse</u>	$> 0.1^a$	$< 1^a$	$< 0.3^a$	-	<u>Sorooshian et al., 2013</u>
<u>Clean Marine</u>	$< 0.2^b$	$< 0.9^d$	-	0.98^e	<u>Kaskaoutis et al., 2009</u> <u>Dubovik et al., 2002</u>
<u>Urban/Industrial</u>	$\geq 0.2^b$	$\geq 1^d$	-	$0.9-$ 0.98^e	<u>Kaskaoutis et al., 2009</u> <u>Dubovik et al., 2002</u>
<u>Biomass Burning</u>	-	$> 1.4^a$	-	$0.89-$ 0.95^e	<u>Deep et al., 2021</u> <u>Dubovik et al., 2002</u> <u>Kaskaoutis et al., 2009</u>
<u>Desert Dust</u>	$\geq 0.3^c$	$< 1^d$	-	$0.92-$ 0.93^e	<u>Deep et al., 2021</u> <u>Dubovik et al., 2002</u>
<u>^a from MODIS</u>	-	<u>^c AOD at 400 nm</u>	-	<u>^e SSA at 440 nm</u>	
<u>^b AOD at 500 nm</u>	-	<u>^d AE at 380 nm to 870 nm</u>	-		

321

322 2.3 Extreme Event Analysis

323 Aerosol particle events based on the three clusters with the highest VSD concentrations were
 324 identified to characterize different types of sources and processes impacting aerosol particle
 325 columnar properties above Metro Manila. The three events are described below.

326 2.3.1 Smoke Long Range Transport

327 Events related to transported biomass burning/smoke were chosen from the AERONET VSD
 328 data that were clustered as urban/industrial (with a dominant submicrometer peak) (Eck et al.,
 329 1999) over Metro Manila. Cases with the highest black carbon contribution to total AOD from
 330 the MERRA-2 dataset were considered. Maps from NAAPS of high smoke contributions to
 331 AOD and surface smoke contributions in the direction of back-trajectories HYSPLIT were used
 332 to provide support for the likely source and transport pathway for the smoke cases.

333 2.3.2 Dust Long Range Transport

334 A dust transport case [over Metro Manila](#) was identified ~~based on the highest dust contribution to~~
335 ~~AOD from the MERRA-2 dataset, high dust contributions to AOD from NAAPS, and AERONET~~
336 ~~VSD dust cluster (with~~ an enhanced coarse peak in the AERONET VSD (compared to the
337 submicrometer fraction) (Eck et al., 1999) ~~over Metro Manila, the highest dust contribution to~~
338 ~~AOD from the MERRA-2 dataset, and high dust contributions to AOD from NAAPS.~~ Surface
339 dust concentrations from NAAPS along ~~with the~~ HYSPLIT back-trajectories ~~confirmed improved~~
340 the plausibility of dust for this case.

341 2.3.3 Cloud Processing

342 Cloud processing events were identified based on bimodal submicrometer VSDs (Eck et al.,
343 2012) and a relatively large sulfate contribution to AOD over Metro Manila from the MERRA-2
344 dataset, since this species is predominantly produced via cloud processing (Barth et al., 2000;
345 Faloon, 2009). The presence of clouds was verified [qualitatively](#) with [MODIS \(Aqua and Terra\)](#)
346 imagery from NASA Worldview in the path of air parcels reaching Metro Manila based on
347 HYSPLIT back-trajectories.

348 349 2.4 Empirical Orthogonal Functions

350 [Regional analysis of aerosol particles in Southeast Asia and Asia in general show the prevalence](#)
351 [of biomass burning in the region, as well as the larger influence of anthropogenic emissions in](#)
352 [East Asia \(Nakata et al., 2018\).](#) These large prevalent sources may overshadow other relevant but
353 [weaker sources in the region, such as local sources. Due to the complex nature of aerosol](#)
354 [particles, analysis techniques such as principal component analysis and clustering along with](#)
355 [recent improvements in gridded datasets help detect spatial and temporal patterns that would](#)
356 [otherwise be difficult to make with noise interference and even weak signals \(Li et al., 2013;](#)
357 [Sullivan et al., 2017; Plymale et al., 2021\).](#) Understanding the dominant air masses around
358 [Southeast Asia will help in distinguishing local and transported particles that influence the](#)
359 [aerosol climatology in Metro Manila.](#) ~~Empirical orthogonal function (EOF) analysis was~~
360 ~~performed to be able to associate the air mass clusters identified earlier with regional scale~~
361 ~~aerosol particle sources.~~

362 [To contextualize the analysis of aerosol particle masses in Metro Manila, major regional sources](#)
363 [of aerosol particles in Southeast Asia were identified based on the dominant principal](#)
364 [components from empirical orthogonal \(EOF\) analysis of AOD.](#) EOF analysis was done on the
365 monthly AOD data (January 2009 to December 2018) from MERRA-2 for the Southeast Asia
366 region for the months similar in scope to the AERONET data. EOF analysis needs a complete
367 dataset with no data gaps, which is not available with pure satellite retrievals; [like MISR; the](#)
368 MERRA-2 reanalysis ~~data alleviated dataset alleviates~~ this issue.

369 The monthly MERRA-2 AOD maps (0° - 30°N, 105°E – 135°E with 0.5° latitude and 0.625°
370 longitude resolution) (Lat: 61 rows x Lon: 49 columns) for the Southeast Asia region (presented
371 subsequently) were first deseasonalized. Then, the AOD anomaly per grid per year (of the 120
372 months) was calculated by subtracting the monthly mean AOD from each value of a given month
373 (Li et al., 2013). The anomalies per grid were weighted depending on their latitude by
374 multiplying the anomalies by the square root of the cosine of their latitudes.

375 EOF, specifically singular value decomposition (SVD), analysis (Björnsson and Venegas, 1997)
376 was then performed. To prepare the data for the analysis, they were transformed such that the
377 final matrix was a 2D matrix (120 x 2989) with each row representing a year, and each column
378 representing a grid in the map. The matrix was analyzed for eigenvalues using SVD in Matlab,
379 which ~~outputted outputs~~ the eigenvalue (S) and eigenvector (U: principal components and V:
380 empirical orthogonal functions) matrices. The eigenvalues were, by default, arranged in
381 descending order. Each PC time series was standardized by dividing each PC value by the
382 standard deviation per PC time series (120 months).

383 An eigenvalue spectrum was also plotted based on the variance explained by each eigenvalue
384 and error bars that were calculated using the North test (North et al., 1982). Then, the
385 unweighted AOD anomalies were regressed onto the first three standardized PCs. Each grid
386 therefore had a regression between 120 pairs (unweighted AOD anomalies vs standardized PCs).
387 From the linear regression equation, the regression coefficient per grid was calculated ~~and~~
388 plotted. Each grid on the Southeast Asia map was colored based on the calculated regression
389 coefficient value.

390

391 **2.5 Correlations**

392 The first three standardized PCs of AOD anomalies were correlated to deseasonalized
393 compositional AOD fractions (Sulfate, BC, OC, Dust, and Sea Salt). For each correlation, the t-
394 test value was calculated, and the resulting t-score was compared to a t-critical value for ~n= 100
395 pairs (n is the number of pairs of data, in this case 120 months) for 0.90 confidence level, which
396 is 1.660. Correlations that have t-values exceeding +1.660 or less than -1.660 (two-tailed test) are
397 significant (90% confidence).

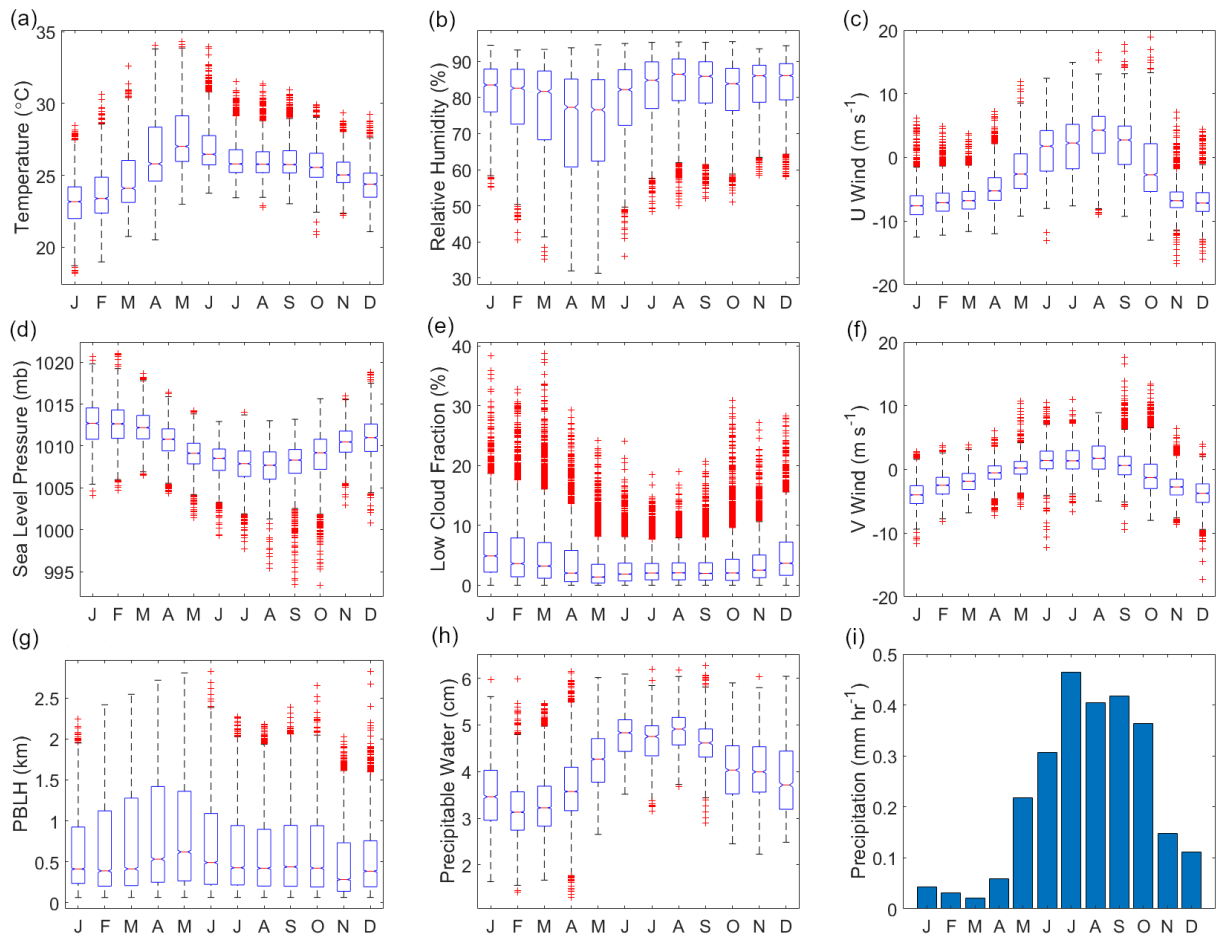
398

399 **3 Results and Discussion**

400 **3.1 Meteorology and Atmospheric Circulation**

401 Knowledge of monthly behavior of weather in the study region helps interpretation of aerosol
402 particle data. Philippine climate is influenced both by the winter northeast monsoon
403 (~November to April, Amihan) and the summer southwest monsoon (~May to October, Habagat)
404 (Coronas, 1920; Flores, 1969; Matsumoto et al., 2020). Median 3-hourly temperatures at 975 mb
405 per month (MERRA-2, 975 mb) (Fig. 1a) ranged from 23.2 °C in January during the winter
406 northeast monsoon, to 27.0 °C in May during the transition from the summer season, as defined
407 in (Bañares et al., 2021), to the southwest monsoon. May was also the month with the lowest
408 median 3-hourly relative humidity (76.6%) (MERRA-2, 975 mb) (Fig. 1b). The highest median
409 level of relative humidity at 975 mb for a month was in August (86.5 %) during the summer
410 southwest monsoon, which is also the time of the year (June to August) when rainfall peaks in
411 the region where the sampling station (Manila Observatory) is located (Coronas, 1920; Cruz et
412 al., 2013). The highest mean hourly precipitation (Fig. 1i) per month was from July (0.46 mm hr⁻¹)
413 to September (0.42 mm hr⁻¹), while March exhibited the lowest mean hourly rainfall (0.02 mm
414 hr⁻¹). Like relative humidity and precipitation, median precipitable water (from available
415 AERONET data) ~~(Fig. of 513 points in August, 4015 points in February, and 5049 points in~~
416 March) (Fig. 1h) was highest in August (4.9 cm) and lowest in February and March (3.1 cm and
417 3.2 cm, respectively).

418



419

420

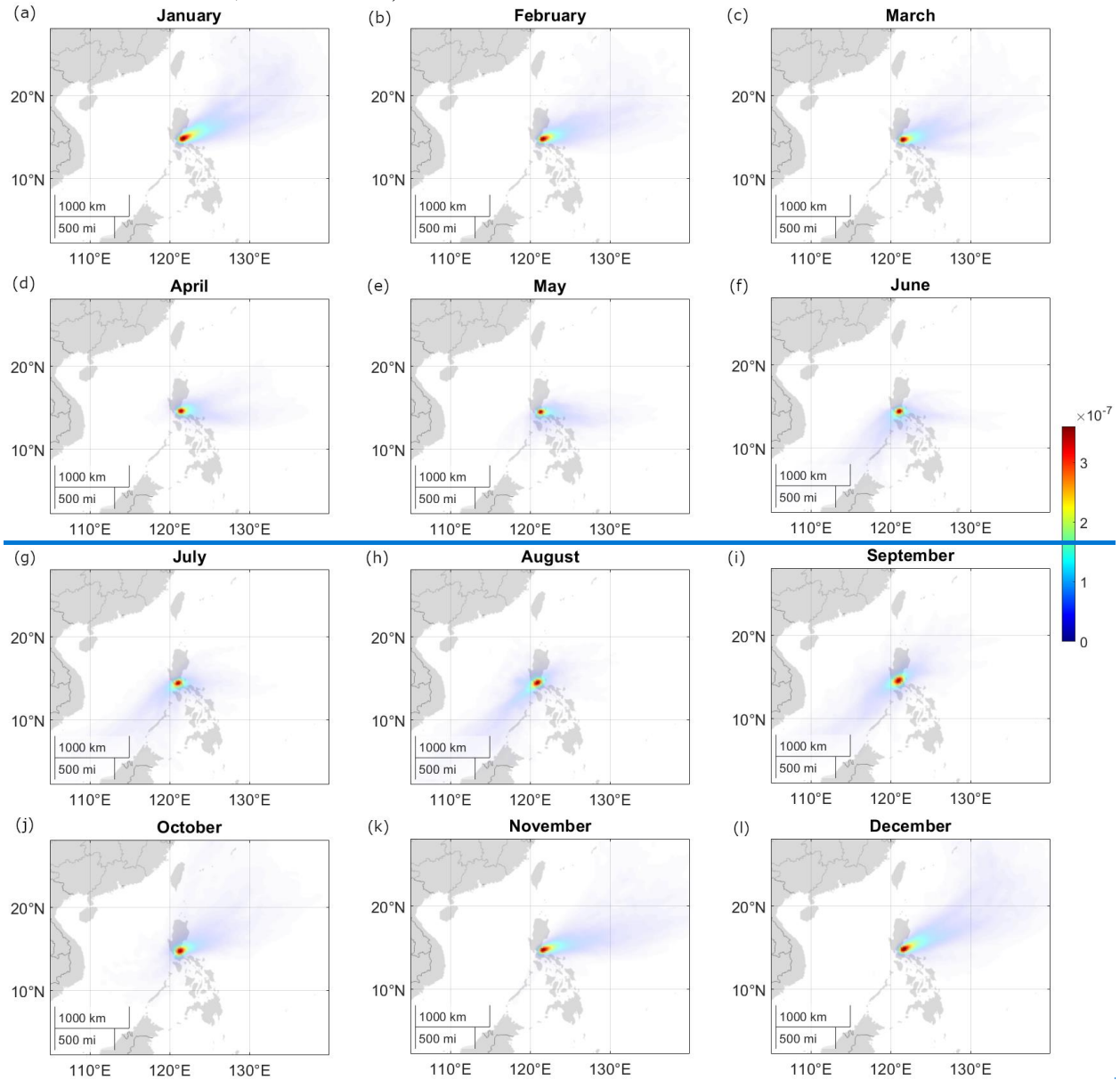
421 **Figure 1:** Monthly characteristics of meteorological parameters for Metro Manila, Philippines
 422 based on data between January 2009 and October 2018. MERRA-2 parameters: (a) temperature
 423 [at 975 mb](#), (b) relative humidity [at 975 mb](#), (c/f) u and v wind at 975 mb, (d) sea level pressure,
 424 (g) planetary boundary layer height (PBLH), (e) low cloud fraction; ([cloud top pressure > 680](#)
 425 [hPa](#)); AERONET: (h) precipitable water; ([data counts per month Jan: 2131, Feb: 4015, Mar:](#)
 426 [5049, Apr: 5844, May: 3448, Jun: 1696, Jul: 652, Aug: 513, Sep: 753, Oct: 1700, Nov: 2084,](#)
 427 [Dec: 1449](#)); PERSIANN: (i) mean hourly precipitation per month.

428

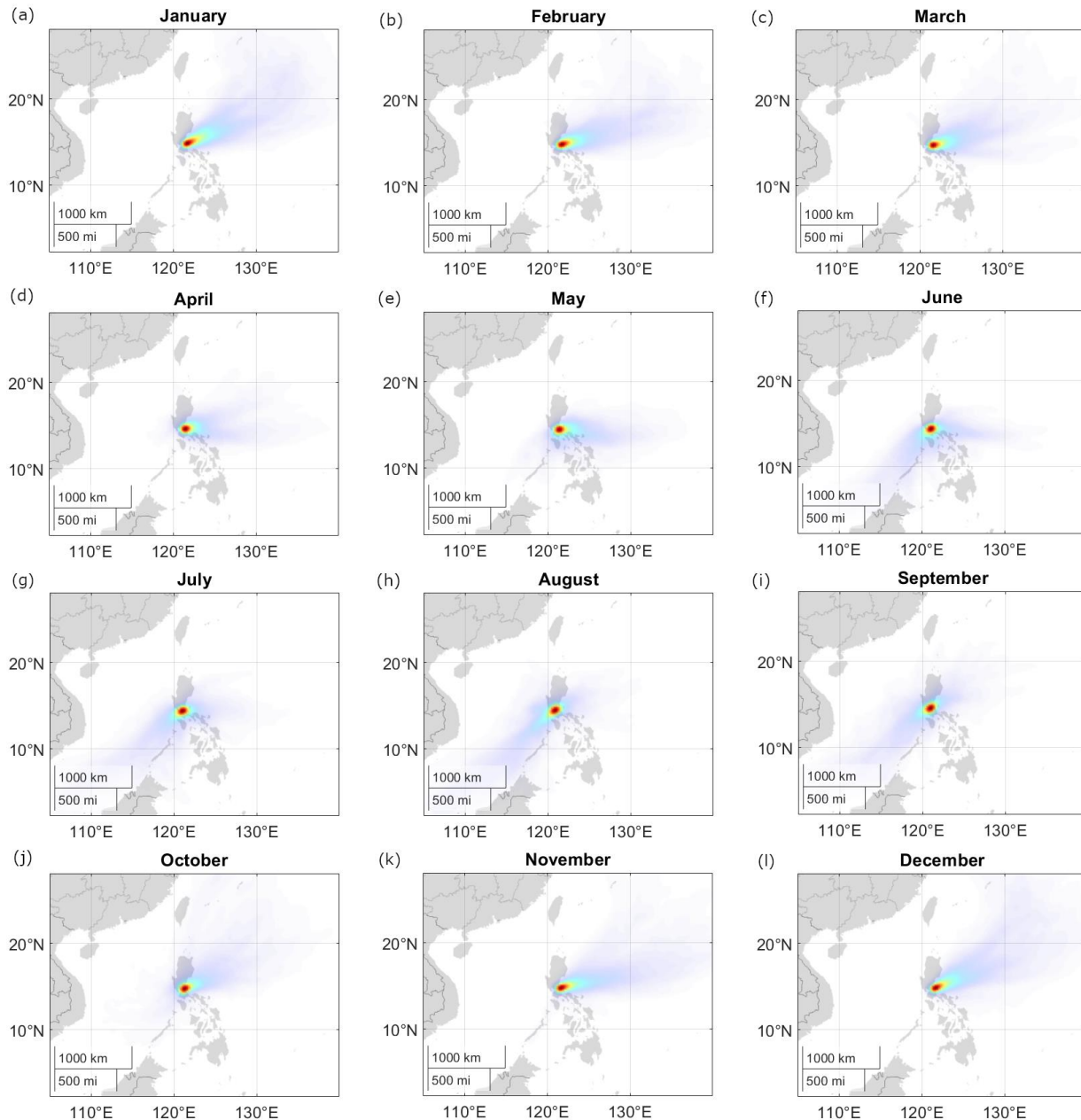
429 The lowest 3-hourly median pressures (MERRA-2) were observed (Fig. 1d) between July and
 430 September during the southwest monsoon season (~985.2 – 985.8 mb). This is also the time
 431 when the most number of tropical cyclones pass the island of Luzon (Wu and Choy, 2016). The
 432 highest 3-hourly median pressures (988.1 – 990.0 mb) were during the winter northeast
 433 monsoon.

434 Median winds (MERRA-2) were from the south/southwest direction from June to September
 435 (Fig. 1c and 1f), associated with the summer southwesterly monsoon. HYSPLIT back-
 436 trajectories show the same wind pattern (Fig. 2f to 2i). The highest median 3-hourly wind speeds
 437 (MERRA-2) (Fig. 1c and 1f) during the southwest monsoon were recorded for August (u: 4.2 m
 438 s⁻¹ and v: 1.7 m s⁻¹). Median winds begin to transition in October and November (to the northeast

439 monsoon: Amihan) (Fig. 2j and 2k) coming from the east/northeast and maintained until
 440 February (Fig. 2b), which is towards the end of the winter northeast monsoon. There were
 441 generally higher wind speeds and the highest median 3-hourly wind speeds of the year
 442 (MERRA-2) (Fig. 1c and 1d) in January (u : -7.6 m s^{-1} and v : -4.0 m s^{-1}). Median winds shifted
 443 toward a more easterly source from March to May (transition time before the Habagat monsoon)
 444 (Fig. 2c to 2e) accompanied by decreasing median 3-hourly wind speeds ($u = -6.8 \text{ m s}^{-1}$, $v = -1.9$
 445 m s^{-1} to u : -2.6 m s^{-1} , $v = 0.2 \text{ m s}^{-1}$).



446



447
 448 **Figure 2:** Density plots of [HYSPLIT](#) trajectories reaching Manila Observatory per month from
 449 2009 to 2018. [Red](#) denotes areas with the greatest number of back trajectories within a 100 km
 450 radius. The colors represent density value contributions to Matlab-calculated cumulative
 451 probability distribution surfaces (100 km radius) from coordinates of three-day back trajectories
 452 of the specific months.

453 The transition times between the monsoons (when the wind directions shift and wind speeds
 454 change) are also the times of the highest (May, Fig. 1g, 621.2 m) and lowest (November, Fig. 1g,
 455 279.6 m) median planetary boundary layer heights (MERRA-2). The median planetary boundary
 456 layer height was highest during the period (May) of highest temperatures, lowest relative
 457 humidity, reduced air pressure, and lowest monthly median low cloud fraction (MERRA-2) (Fig.
 458 1e) (1.4 %). The lowest monthly median planetary boundary layer height was observed during

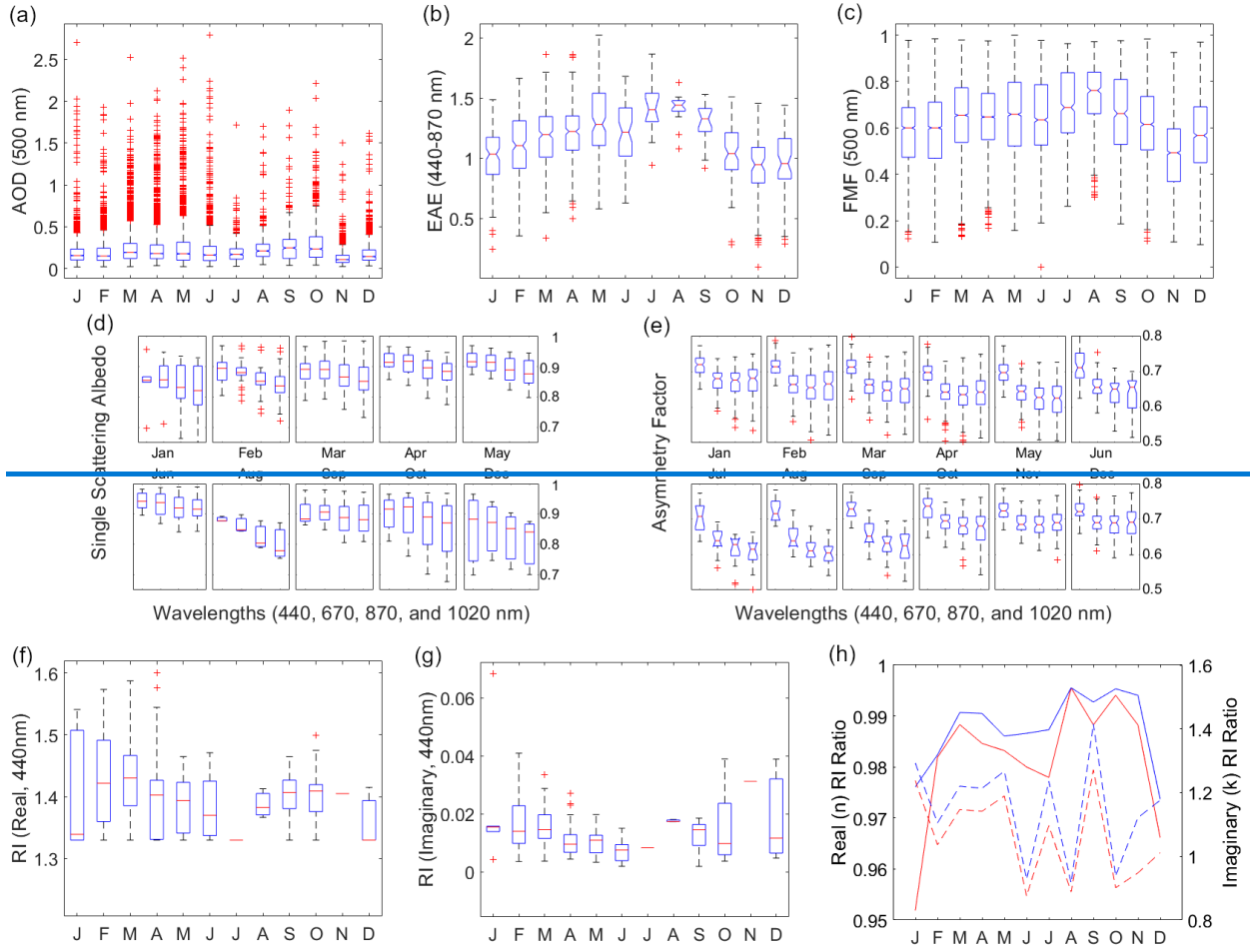
459 the period (November) when temperatures were beginning to cool and air pressure was rising.
460 The monthly maximum low cloud fraction was lowest in July (18.5 %) during the summer
461 southwest monsoon while the monthly median and monthly maximum low cloud fractions
462 (MERRA-2) (Fig. 1e) were highest (38.3 % max, 4.9 % median) in January during the winter
463 northeast monsoon.
464

465 **3.2 Aerosol Particle Characteristics**

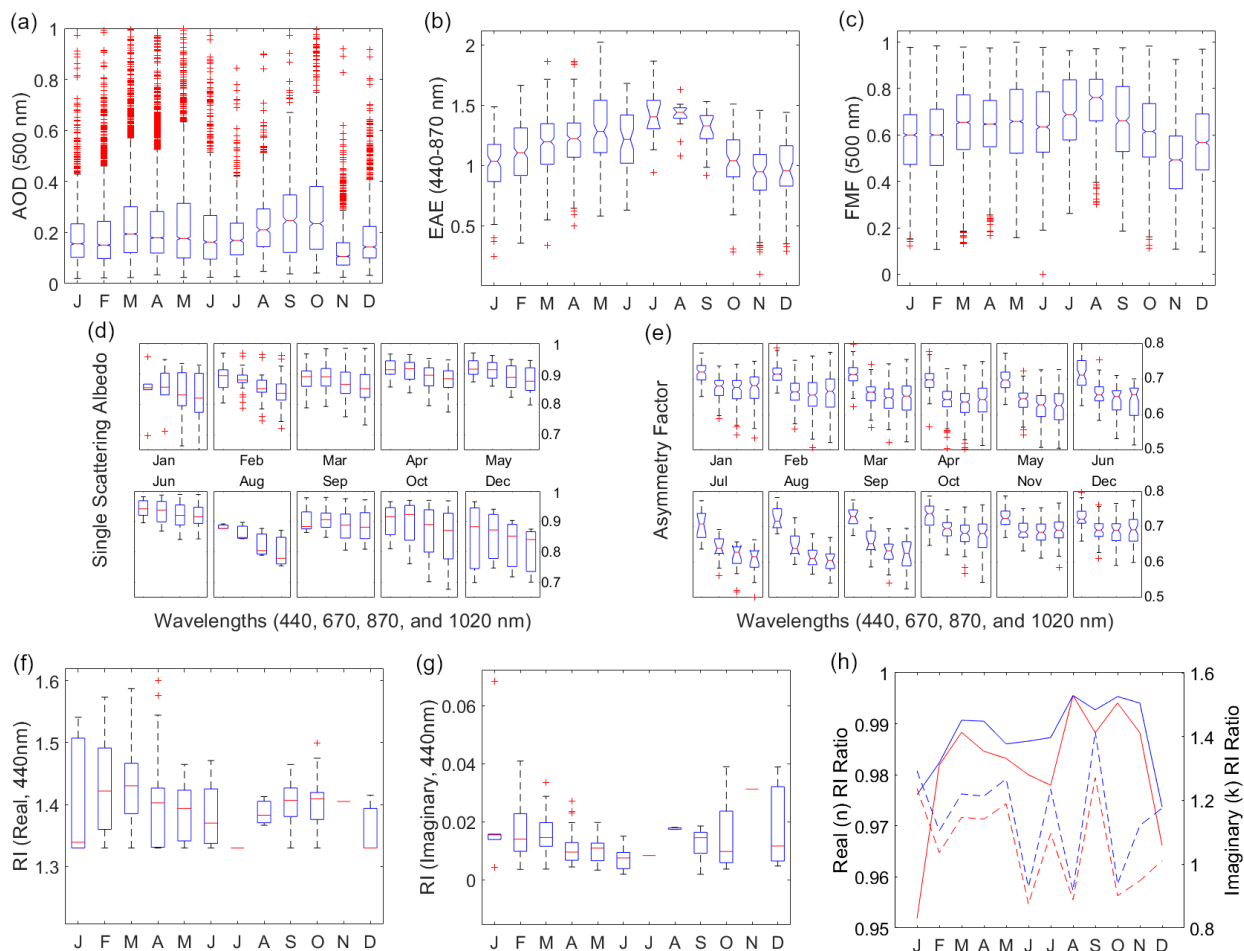
466 3.2.1 Aerosol Optical Depth

467 Monthly median AOD (AERONET, [500 nm](#)) (Fig. 3a) over the Manila Observatory was highest
468 from August (0.21) to October (0.23) around the time of the summer monsoon when winds were
469 coming from the southwest (Figs. 2h to 2i) (Holben et al., 2001). This is the same time of year
470 when biomass burning activities occur in the [Indonesian](#) region southwest of Metro Manila-
471 [\(Glover and Jessup, 1998; Kiely et al., 2019; Cahyono et al., 2022\)](#). [Studies have shown that](#)
472 [AOD in the Philippines increases during the biomass burning season in Indonesia \(Nguyen et al.,](#)
473 [2019b; Caido et al., 2022\)](#). [Regional AOD \(550 nm\)](#) over the larger Southeast Asia
474 [region/domain](#) from MISR and MERRA-2 (Fig. 4) had a similarly large peak ~~from~~ [around the](#)
475 [same time beginning in](#) September ~~to~~ [until](#) October which, however, was second only in
476 magnitude to a March peak, which is influenced by biomass burning in Peninsular Southeast
477 Asia (PSEA) (Gautam et al., 2013; Hyer et al., 2013; [Dong and Fu, 2015; Wang et al., 2015;](#)
478 [Yang et al., 2022\)](#). [This is consistent with the peak in speciated AOD due to fine \(radii <0.7](#)
479 [µm\), spherical, and absorbing aerosols that were observed by MISR from March to April \(Fig.](#)
480 [S1\)](#). This larger peak in March, attributed to PSEA [\(which is ~2000 km west of the](#)
481 [Philippines\)](#), was not as prevalent in the AERONET AOD data [over Manila Observatory in](#)
482 [Metro Manila](#) due to the dominant easterly winds in the Philippines in March (Fig. 2c) and more
483 localized sources.

484



485

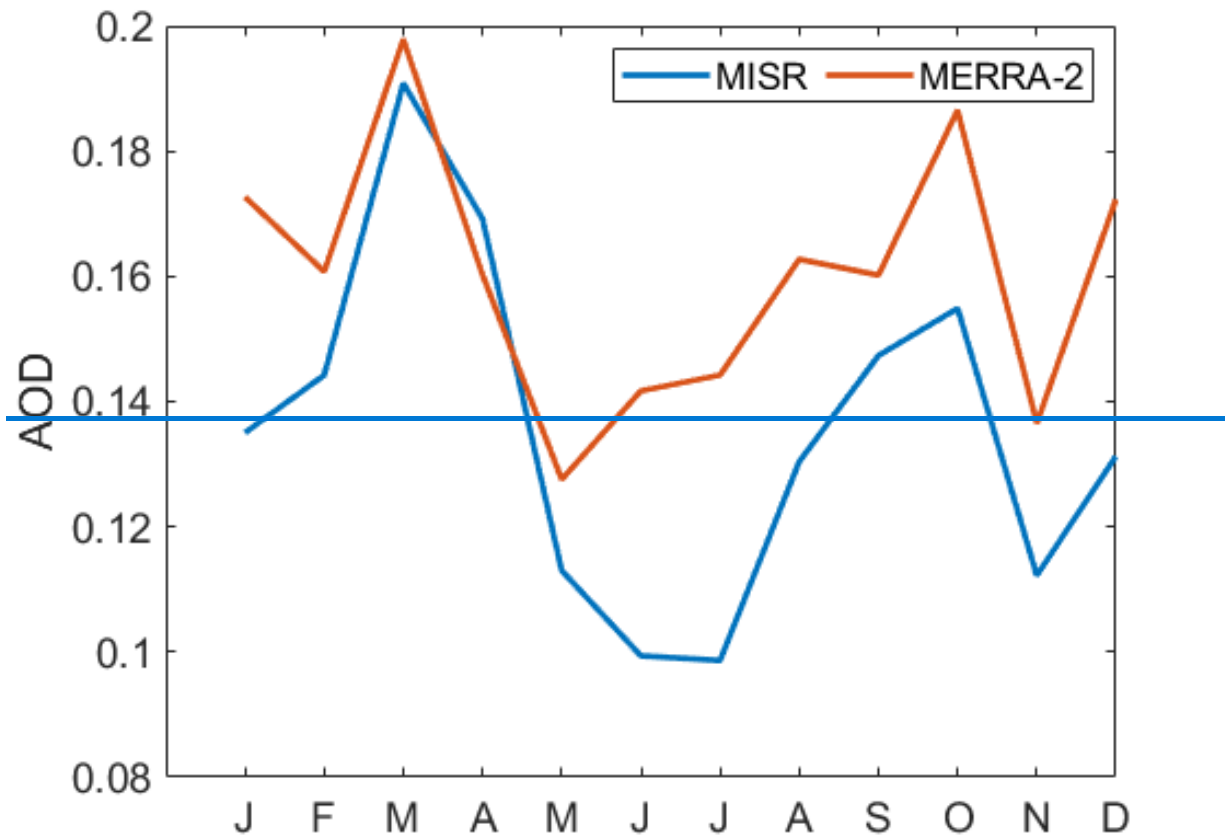


486
 487 **Figure 3:** Monthly characteristics of AERONET aerosol particle parameters: (a) aerosol optical
 488 depth (AOD at 500 nm with y-axis until 1.0 only for larger boxplot resolution) with counts (Jan:
 489 2107, Feb: 3931, Mar: 4923, Apr: 5755, May: 3389, Jun: 1653, Jul: 637, Aug: 483, Sep: 718,
 490 Oct: 1555, Nov: 2001, Dec: 1386), (b) extinction angstrom exponent (EAE at 440-870 nm) with
 491 counts (Jan: 102, Feb: 248, Mar: 312, Apr: 309, May: 137, Jun: 53, Jul: 14, Aug: 18, Sep: 18,
 492 Oct: 79, Nov: 77, Dec: 52), (c) spectral de-convolution algorithm (SDA) retrievals of fine mode
 493 fraction (FMF), at 500 nm) with the same counts as AOD, (d) single scattering albedo (SSA)
 494 from 440 nm (leftmost boxplot) to 1020 nm (rightmost boxplot) with counts (Jan: 6, Feb: 31,
 495 Mar: 62, Apr: 50, May: 29, Jun: 8, Aug: 3, Sep: 5, Oct: 17, Dec: 3), (e) asymmetry factor (AF),
 496 from 440 nm (leftmost boxplot) to 1020 nm (rightmost boxplot) with the same counts as EAE,
 497 (f) real and (g) imaginary refractive index (RI) values (440 nm), with the same counts as SSA,
 498 and (h) refractive index ratios (where the blue line is the ratio of RI at 440 nm and 670-670 nm,
 499 the red line is the ratio of RI at 440 nm and the average RI for the 670-1020 nm wavelengths,
 500 and the broken lines are the imaginary refractive index ratios) for Metro Manila, Philippines
 501 based on data between January 2009 and October 2018.

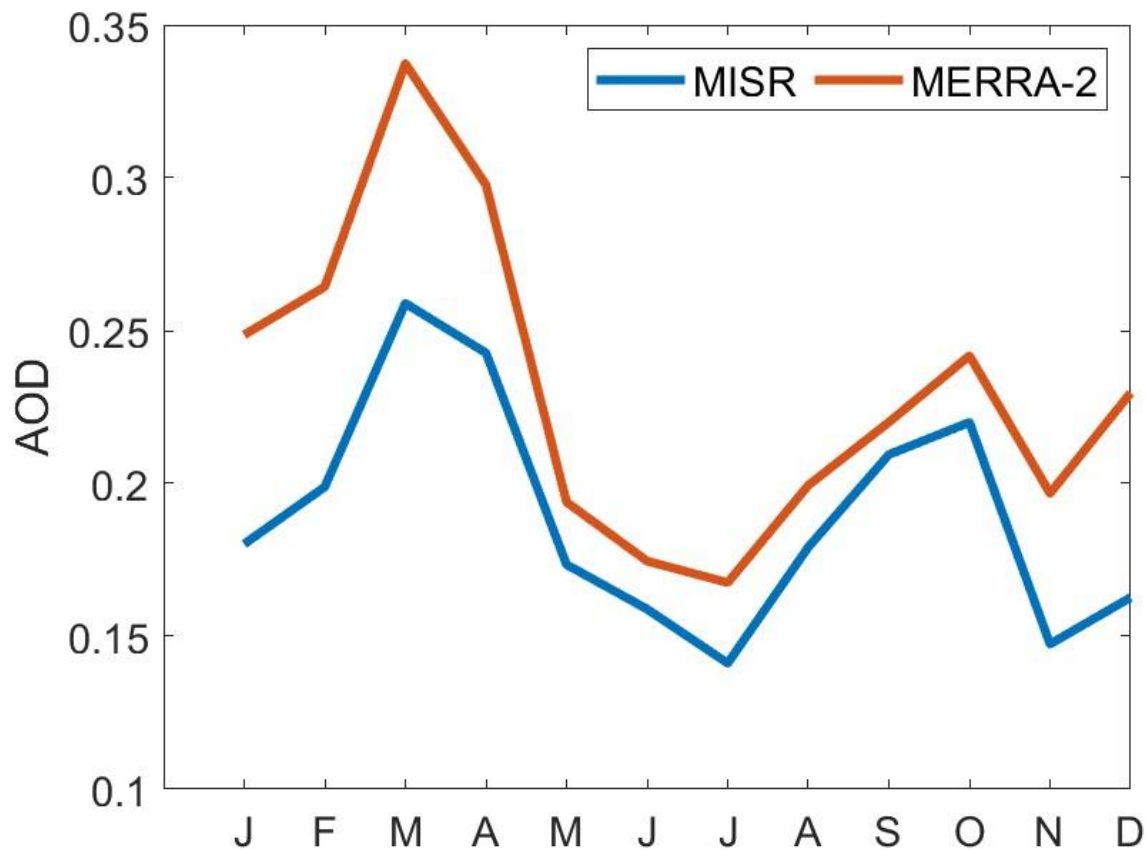
502 There is a notable dip in the monthly median AERONET AOD over Manila Observatory from
 503 the peak in October to the lowest monthly median AOD (0.11) in November, (Fig. 3a), just
 504 slightly above defined background levels (<0.1) (Holben et al., 2001), when the windspeeds
 505 were picking up and were coming from the east to northeast directions (Fig. 2k) in the direction
 506 of the Philippine Sea and the West Pacific Ocean. This dip was also observed in the regional

507 [AOD data \(MISR and MERRA-2, Fig. 4\).](#) This dip was also observed in the regional ($30^{\circ} \times 30^{\circ}$)
508 [AOD data \(MISR and MERRA-2, Fig. 4\).](#) This is most probably due to the decrease in the AOD
509 [contribution from fine \(radii \$<0.7 \mu\text{m}\$ \) and spherical particles based on size speciated MISR](#)
510 [AOD \(Fig. S1\).](#) Larger and non-spherical particle contributions to AOD increase in November in
511 [the Southeast Asia region.](#) The MERRA-2 AOD is relatively higher than the MISR AOD
512 [probably due to assimilation of MODIS data into MERRA-2.](#) Studies in Asia (Xiao et al., 2009;
513 [Qi et al., 2013; Choi et al., 2019\)](#) have observed relatively higher MODIS AOD compared to
514 [MISR AOD.](#)

515



516



517
 518 **Figure 4:** Monthly median mean AOD (550 nm) in Southeast Asia (30° x 30°) from 2009 to
 519 2018 from MISR (blue line) and MERRA-2 (red line).

520 There were 338 instances (~1.2 % of the time based on the total number of 28,538 valid
 521 AERONET AOD data points) of AOD values exceeding 1, indicative of heavy aerosol particle
 522 loading (Huang et al., 2021). Because AOD is extrinsic (it depends on mass), AOD describes
 523 total aerosol particle loading and we examine other aerosol particle parameters from AERONET
 524 to make more informed inferences about size and composition.

525 3.2.2 Extinction Angstrom Exponent and Fine Mode Fraction

526 The extinction angstrom exponent (EAE) relates the extinction of light at specific wavelengths
 527 and is indicative of aerosol particle size (Ångström, 1929). ~~The EAE is usually greater for~~
 528 ~~smaller particles (~4 for very small particles that undergo Rayleigh scattering and 0 for particles~~
 529 ~~as large as cloud drops) (Bergstrom et al., 2007), except for when the coarse mode has a large~~
 530 ~~impact on the angstrom exponent (Schuster et al., 2006).~~ The EAE is usually greater for smaller
 531 particles (~4 for very small particles that undergo Rayleigh scattering, > 2 for small particles, <
 532 1 for large particles like sea salt and dust, and 0 for particles as large as cloud drops) (Schuster et
 533 al., 2006; Bergstrom et al., 2007). The highest monthly median EAE (Fig. 3b) from 2009 to 2018
 534 over the Manila Observatory was observed from July (~1.4) to September (~1.3), during the
 535 southwest monsoon. This period is associated with the biomass burning southwest of the

536 Philippines (Oanh et al., 2018; Stahl et al., 2021; Crosbie et al., 2022). The median (per month)
537 EAE ranged from ~0.9 in November to ~1.4 in August, a range which is within the values from
538 previous studies collected from mixed sites and urban/industrial areas with both fine and coarse
539 particles (Eck et al., 2005; Giles et al., 2012). The high EAE over Manila Observatory from July
540 to September is probably regional in nature based on the MISR data showing increased EAE
541 with increased AOD from fine, spherical, and absorptive particles (Fig. S1) in Southeast Asia
542 during the same months. The high EAE over Manila Observatory from July to September is
543 consistent with the regional (30° latitude x 30° longitude) MISR data that shows increased AOD
544 from fine, spherical, and absorptive particles (Fig. S1) in Southeast Asia during the same months.
545 This suggests that the high EAE observed at the Manila Observatory during these months is not
546 necessarily from local sources.

547 EAE increases with AOD (Fig. S1S2), which means that the greater particle loading is
548 contributed by smaller particles (Smirnov et al., 2002). Of the high loading cases (AOD >1),
549 over Manila Observatory, the EAE values ranged from were mostly greater than 0.6 to 1.6, 8
550 indicating fine mode particles (Che et al., 2015). The EAE values in August were the highest
551 compared to other months including having the highest minimum value of any month (0.71)
552 (Fig. S1S2), due to smaller particles (~EAE >1 for fine particles, Table 2). The lowest EAE
553 values (0.08) and thus the largest particles were observed in December, which again may be
554 regional in nature with MISR EAE also lowest during this time with increased AOD from larger
555 and non-spherical particles (Fig. S1).

556 The fine mode fraction (FMF) describes the prevalence of fine mode particles in the column of
557 air above the surface. The fine mode fraction (Fig. 3c) from 2009 to 2018 was highest in August
558 (monthly median of 0.75) and lowest in November (monthly median of 0.45). This is consistent
559 with the EAE values discussed earlier with the prevalence of smaller particles in August and
560 larger particles in November. In August (Fig. 2h) the southwest monsoon is known to coincide
561 with ~~transported~~ the transporting of fine smoke particles to Luzon. In November (Fig. 2k), the
562 prevalent winds may have already shifted to easterly (Matsumoto et al., 2020) implying more
563 marine-related sources associated with coarser particles.

564 3.2.3 Single Scattering Albedo

565 The single scattering albedo (SSA) is the most important aerosol particle parameter determining
566 whether aerosol particles will have a warming or cooling effect (Reid et al., 1998). SSA is the
567 ratio of the scattering coefficient to the total extinction (scattering and absorption) coefficient
568 (Bohren and Clothiaux, 2006) of aerosol particles. Higher SSAs are related to more reflective
569 aerosol particles while more absorbing aerosol particles will have lower SSA values; values
570 range from 1 (reflective) to 0 (absorbing). Monthly median SSA values were largest in June
571 (0.94, at 440 nm), suggesting the presence of more reflective aerosol particles, and smallest in
572 August (0.78, 88 at 440 nm and 0.78 at 1020 nm) suggesting more absorptive particles that are
573 similar in range to the SSA of biomass burning particles (Table 2). August is when biomass
574 burning is prevalent to the southwest of the Philippines and associated with soot particles that are
575 absorptive.

576 The sensitivity of SSA to different wavelengths depends on the type of aerosol particles present.
577 More specifically, aerosol particle size and refractive index (which is related to aerosol particle
578 composition) both affect the SSA (Dubovik and King, 2000; Bergstrom et al., 2007; Moosmüller

579 and Sorensen, 2018). For dust-type particles, SSA increases with wavelength because of lower
580 dust absorption in the higher visible to infrared wavelengths (Dubovik et al., 2002), while for
581 urban particles (including black carbon), which absorb light at longer wavelengths, SSA
582 decreases with wavelength (Reid et al., 1998; Bergstrom et al., 2002). The presence of organic
583 carbon may affect this spectral dependence; however, because organic particles absorb in the
584 UV, this lowers SSA at wavelengths shorter than 440 nm (Kirchstetter et al., 2004). Monthly
585 median SSA generally decreased with increasing wavelength for all months with available data
586 (Fig. 3d) presumably due to the influence of more urban particles in contrast to dust.
587 Noteworthy though are the monsoon transition months of April, September, and October (Fig.
588 3d), which had increased SSA from 440 nm to 670 nm, possibly from organics along with black
589 carbon due to transported smoke. The back-trajectories for these months (Figs. 2d, 2i, and 2j)
590 suggest sources from the northeast that are closer to Luzon during these months compared to
591 other months. This indicates the possibility of more local sources. Increasing the certainty of
592 sources associated with aerosol particles necessitates looking at other available aerosol particle
593 parameters, discussed subsequently.

594 3.2.4 Asymmetry Factor

595 The asymmetry factor quantifies the direction of scattering of light due to aerosol particles, with
596 values ranging from -1 (back scatter) to 0 (uniform scattering) to 1 (forward scatter). It is
597 important in modeling climate forcing because it affects the vertical distribution of the radiation
598 in the atmosphere (Kudo et al., 2016; Zhao et al., 2018). The asymmetry factor is dependent on
599 particle size, shape, and composition and the value of 0.7 is used in radiative models (Pandolfi et
600 al., 2018).

601 Lower asymmetry factors are related to smaller particles (at constant AOD) (Bi et al., 2014).
602 Measured values due to biomass burning, for example, are 0.54 (550 nm) in Brazil (Ross et al.,
603 1998) and 0.45 – 0.53 (550 nm and including dust) over central India (Jose et al., 2016). There
604 have been relatively higher values observed in western, central, and eastern Europe (0.57 – 0.61
605 at 520 – 550 nm) (Pandolfi et al., 2018) and the U.S. East Coast (0.7 at 550 nm) (Hartley and
606 Hobbs, 2001). In Norway, the asymmetry factor for background summer conditions was 0.62
607 and was higher in the springtime at 0.81 (862 nm) during Arctic haze events (Herber et al.,
608 2002). Highest values are associated with dust such as those measured in the Sahara being 0.72 –
609 0.73 (500 nm) (Formenti et al., 2000). Over Metro Manila, the asymmetry factors from the
610 AERONET data at the 675, 870, and 1020 nm were similar across months (Fig. 3e). The monthly
611 median asymmetry factors at 440 nm ranged from 0.70 (April and May) to 0.74 (October), while
612 for 670, 870, and 1020 nm the monthly median asymmetry factors were smaller and ranged from
613 0.62 – 0.69. These values were closely related to those observed over the U.S. East Coast as
614 mentioned earlier, perhaps due to the proximity of the location to the coast (10 km east of Manila
615 Bay and 100 km west of the Philippine Sea) as well as its location in Manila, which is a large
616 local source due mostly to vehicles (Cruz et al., 2019).

617 The monthly median asymmetry factor in Metro Manila was greatest towards the end of the year
618 (October to December) for all the wavelengths, suggesting larger particles when winds (Figs. 2j
619 to 2l) come from the Philippine Sea in the northeast. It was in March and April that the monthly
620 median asymmetry factor was minimal for 440 nm and in August for 670, 870, and 1020 nm.
621 These were the times when ~~the~~ aerosol particles were smallest. March to April represents the
622 driest time of the year in Manila (Fig. 1b and 1h) perhaps preventing particle growth and where

623 the local sources may be dominating, even as back-trajectories (Fig. 2c and 2d) extend all the
624 way from the Philippine Sea to the east. This is corroborated by results from other studies
625 showing that the asymmetry factor seems to be enhanced by relative humidity (Zhao et al.,
626 2018). The unexpected low asymmetry factor values in August, however, are probably because
627 of the source of the particles. August had the highest relative humidity and precipitable water
628 (Fig. 1b and 1h) but is also when the back-trajectories (Fig. 2h) were from the southwest,
629 possibly affected by the Indonesia fires, which could have transported more non-hygroscopic
630 fine particles.

631 Fine particles have been observed to exhibit decreasing asymmetry factors with increasing
632 wavelength (Bergstrom et al., 2003). This trend is observed in all the months for the monthly
633 median asymmetry factors (Fig. 3e) suggesting the predominance of smaller aerosol particles.
634 The greatest decrease in the asymmetry factor (all wavelengths) was in August, consistent with
635 the lowest observed values of the year (670, 870, and 1020 nm). Transported biomass burning
636 particles are the probable dominant particles during this time. They are usually composed of
637 hygroscopic inorganics, non-hygroscopic soot, and relative non-hygroscopic organic fractions
638 (Petters et al., 2009). Knowing the composition of biomass burning particles over the study
639 region will help in the understanding of hygroscopicity and its impacts on radiation.

640 3.2.5 Refractive Index

641 Refractive index is an intrinsic parameter as it does not depend on the mass or the size of
642 particles, and thus can be used to infer aerosol particle composition (Schuster et al., 2016). [For](#)
643 [the case of the AERONET data, which include refractive index values that are insensitive to](#)
644 [coarse particles \(Sinyuk et al., 2020\), the focus of the discussion will be for fine mode particles](#)
645 [and may be limited when coarse particles are involved.](#) Refractive index measurements are
646 complex since they include real and imaginary parts related to light scattering and absorption,
647 respectively. All aerosol particles scatter light but only certain types absorb light significantly.
648 The most prominent particle absorbers in the atmosphere are soot carbon, brown carbon (organic
649 carbon that absorbs light), and free iron from dust (hematite and goethite in the ultraviolet to
650 mid-visible) (Schuster et al., 2016). [For this study, we examine refractive index values at 440 nm](#)
651 [wavelength because this is the wavelength used to calculate SSA \(Andrews et al., 2017\).](#)[For this](#)
652 [study, we examine refractive index values at 440 nm wavelength.](#) Pure sources of soot carbon
653 have the highest real refractive index values (~1.85) as well as the highest imaginary refractive
654 index (~0.71), both independent of wavelength (Koven and Fung, 2006; Van Beelen et al.,
655 2014). Brown carbon and dust have relatively lower real refractive index values at 440 nm
656 (~1.57 and ~1.54) and imaginary refractive index values (~0.063 and ~0.008) that decrease with
657 increasing wavelength (Xie et al., 2017).

658 In this study the range of the monthly median real refractive index values (440 nm) was from
659 1.33 (December and January) to 1.43 (March) (Fig. 3f). Water uptake by aerosol particles
660 decreases the real refractive index values (Xie et al., 2017) and thus the lowered real refractive
661 indices over the Manila Observatory can be due to the presence of more water in the atmosphere
662 in general and/or the increased presence of more hygroscopic particles. December and January
663 are not necessarily the months that have the highest moisture content, but they are months when
664 back-trajectories reaching the column over the Manila Observatory are from the Philippine Sea
665 to the northeast presumably transporting hygroscopic particles. As reported in previous sections,
666 relatively larger particles are observed around this time of the year and thus sea salt can be an

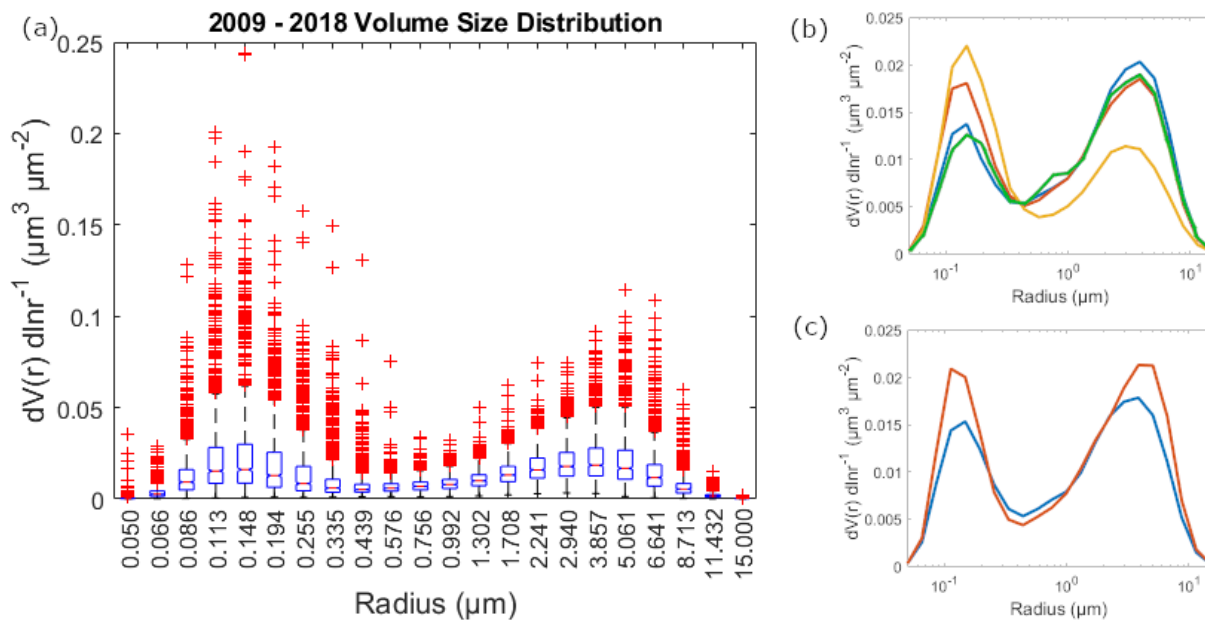
667 important contributor. The greatest change in the monthly median real refractive index with
668 increasing wavelength also was observed in December (Fig. 3h), possibly due the increased
669 fractional contribution of constituents other than soot carbon (because the real refractive index of
670 soot carbon is invariant with wavelength). Noteworthy as well is the month of August (Fig. 3f),
671 which has the smallest range of real refractive index values, possibly indicating a more
672 homogenous aerosol particle source compared to other months. August is the month with the
673 highest relative humidity (Fig. 1b) as well as highest precipitable water (Fig. 1h), while this is
674 also the month when long-range biomass burning emissions are observed to be highest, and
675 when the real refractive index values would otherwise be expected to be highest.

676 Water content seems to play a significant role in the real refractive index values in Manila.
677 March, when the monthly median real refractive index values are highest (Fig. 3f), is when
678 precipitable water vapor (Fig. 1h) is among the lowest in the year. The months around March are
679 also when maximum real refractive indices (1.57 in February, 1.59 in March, and 1.60 in April)
680 were observed (Fig. 3f). March was when there was a relatively small change in real refractive
681 index value with wavelength perhaps related to greater soot carbon fractions during this time,
682 due possibly to the contribution of biomass burning from Peninsular Southeast Asia (Shen et al.,
683 2014). Looking more closely at the imaginary refractive index values will help elucidate this
684 issue.

685 Monthly median imaginary refractive index values (440 nm) ranged from 0.007 in June to 0.015
686 in September and December (Fig. 3g). These are low compared to those of the pure soot carbon
687 mentioned earlier because of the mixed nature of the sampling site with contributions from
688 brown carbon and dust. The highest imaginary refractive index values in September and
689 December suggest the greatest fractional contribution of soot because the highest imaginary
690 refractive index values are associated with soot. These are also similar in magnitude to biomass
691 burning particles in the Amazon (0.013) (Guyon et al., 2003). The key distinction between soot
692 carbon and other major absorbers (brown carbon and dust) is that its imaginary refractive index
693 is invariant with wavelength. Both brown carbon and dust exhibit a decrease in the imaginary
694 refractive index with increasing wavelength (Xie et al., 2017). The ratios of imaginary refractive
695 index values (440 nm to average of 670–1020 nm) (Fig. 3h) show a relative invariance with
696 wavelength (ranging from 0.88 to 1.4), which indicates the dominance of soot as the major
697 absorber in the region (Eck et al., 2003). While observed wavelength invariance points to high
698 soot contributions, the size of the particles can help distinguish between brown carbon, which
699 reside mainly in the fine mode, and dust sources, which yield more coarse particles (Schuster et
700 al., 2016). September is during the southwest monsoon, which is when, as noted in the earlier
701 sections, fine particles were most prevalent. This is also the time when the imaginary refractive
702 index varied most with wavelength (1.4 ratio of the imaginary refractive index at 440 nm and the
703 imaginary refractive index average for 670 nm to 1020 nm in Fig. 3h) possibly with greater
704 absolute contributions from brown carbon, even with the highest soot carbon fractional
705 contributions. Brown carbon has been observed both from primary and aged aerosol particle
706 emissions from biomass burning (Saleh et al., 2013). As noted earlier, December also had the
707 highest imaginary refractive index values as well as relatively coarser particles, possibly due to
708 larger dust absolute contributions even with the highest soot carbon fraction contributions. The
709 lowest monthly median imaginary refractive index values in June, on the other hand, when fine
710 mode particles prevail suggest highest fractional contributions of brown carbon relative to other
711 months (Fig. 3h).

712 3.2.6 Volume Size Distributions

713 The volume size distribution (VSD) is another way to be able to more deeply characterize
 714 aerosol particles, specifically related to their effect on climate, weather, and clouds (Haywood
 715 and Boucher, 2000; Feingold, 2003). In the Manila Observatory dataset, there was a bi-modal
 716 VSD for the entire dataset (Fig. 5a). The fine mode median values peaked in the accumulation
 717 mode at 0.148 μm particle radius while the coarse mode median values peaked at 3.857 μm -
 718 (Fig. 5a and Table S1). The median coarse mode amplitudes and volume concentrations were
 719 higher than the fine mode amplitudes and volume concentrations for most of the year (DJF,
 720 MAM, and SON, Fig. 5b and Table S1), except during the southwest monsoon (JJA) when the
 721 fine mode amplitude and volume concentration was higher. This is consistent with observations
 722 earlier of fine mode prevalence during the southwest monsoon. Median VSD amplitudes (Fig.
 723 5c) were greater in the afternoon, with higher peaks and volume concentrations for both the fine
 724 and coarse modes, compared to the morning. There was a slightly larger coarse median
 725 amplitude and volume concentration, compared to the accumulation mode median amplitude and
 726 volume concentration, for both the morning and afternoon size distributions. While the VSDs
 727 confirm several observations based on the analysis of the aerosol particle parameters presented
 728 earlier, not much further information is gained especially regarding chemical composition. Size
 729 distributions are a result of contributions from multiple sources, and thus being able to
 730 discriminate the sources based on their characteristic size distributions will help identify relevant
 731 sources.
 732



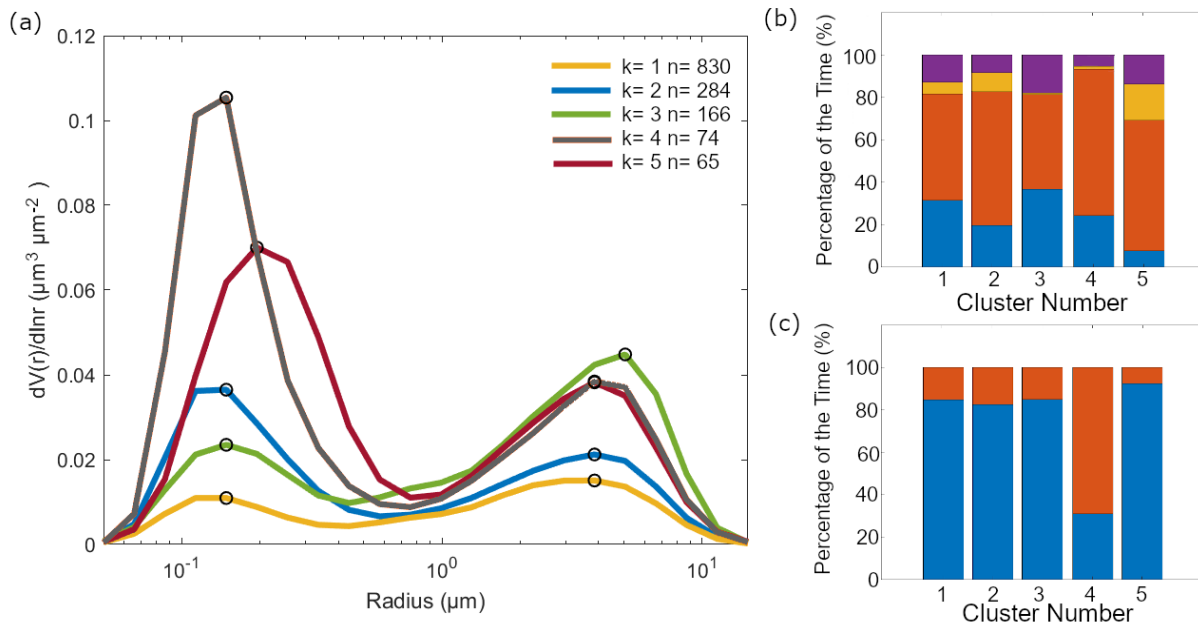
733 **Figure 5:** (a) VSD results derived from AERONET measurements at Metro Manila between
 734 January 2009 and October 2018. Median VSDs over the study period based on (b) season (blue:
 735 DJF, red: MAM, orange: JJA, green: SON) and (c) time of day (blue: AM, red: PM).
 736

737 **3.3 Clusters**

738 3.3.1 VSD Cluster Profiles

740 Five clusters were identified to best represent the VSD (Fig. 6a). The average of the VSDs in
 741 each cluster varied depending on the height of the peaks in the accumulation mode and the
 742 coarse mode. In Metro Manila, the accumulation mode is associated with aged aerosol particles
 743 and combustion (Cruz et al., 2019). The majority of the data (830 count out of 1419 total VSD
 744 profiles) were clustered together in a profile (cluster 1) that had relatively low average
 745 magnitudes of volume concentration for both the accumulation ($0.01 \mu\text{m}^3 \mu\text{m}^{-2}$) and coarse (0.02
 746 $\mu\text{m}^3 \mu\text{m}^{-2}$) modes, with the volume concentration magnitude of the coarse mode peak slightly
 747 higher than the volume concentration magnitude of the accumulation mode peak. The next
 748 prevalent cluster profile (284 counts, cluster 2) had an average fine mode peak for the volume
 749 concentration ($0.04 \mu\text{m}^3 \mu\text{m}^{-2}$) which was more than twice as much than the previous profile but
 750 with a similar coarse mode peak for the volume concentration ($0.02 \mu\text{m}^3 \mu\text{m}^{-2}$). The average
 751 coarse mode peak for the volume concentration ($0.04 \mu\text{m}^3 \mu\text{m}^{-2}$) was the highest (compared to
 752 the four other cluster profiles) for the third prevalent cluster profile (166 counts, cluster 3);
 753 cluster 3 ~~was also~~ had a slightly shifted volume concentration peak in the coarse mode to a
 754 higher radius ($5.06 \mu\text{m}$) compared to other clusters. The coarse mode dominated this VSD
 755 compared to other profiles (lower magnitude for the accumulation mode peak for the volume
 756 concentration, $0.02 \mu\text{m}^3 \mu\text{m}^{-2}$). The two remaining cluster profiles exhibited high average
 757 magnitudes of volume concentration in both the accumulation and coarse modes. The fourth
 758 prevalent cluster profile (74 counts, cluster 4) had the highest average absolute magnitude for the
 759 volume concentration in the accumulation mode ($0.11 \mu\text{m}^3 \mu\text{m}^{-2}$), while the fifth prevalent
 760 cluster profile (65 counts, cluster 5) had a slightly smaller accumulation mode peak for the
 761 volume concentration ($0.07 \mu\text{m}^3 \mu\text{m}^{-2}$) that was shifted to a slightly higher radius ($0.19 \mu\text{m}$
 762 compared to $0.15 \mu\text{m}$). Both clusters 4 and 5 had similar average coarse mode peak volume
 763 concentration magnitudes ($0.04 \mu\text{m}^3 \mu\text{m}^{-2}$).

764



765

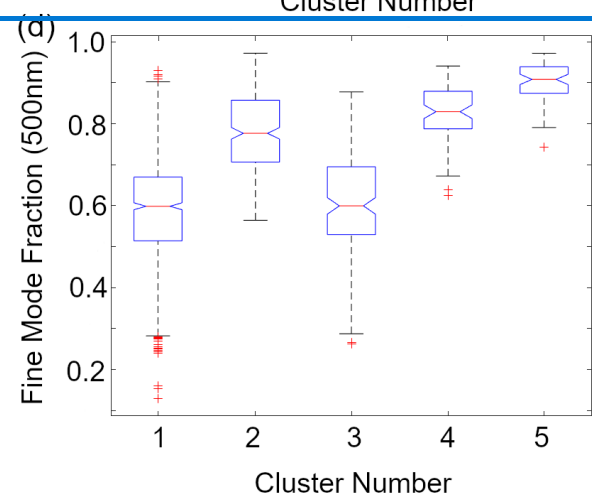
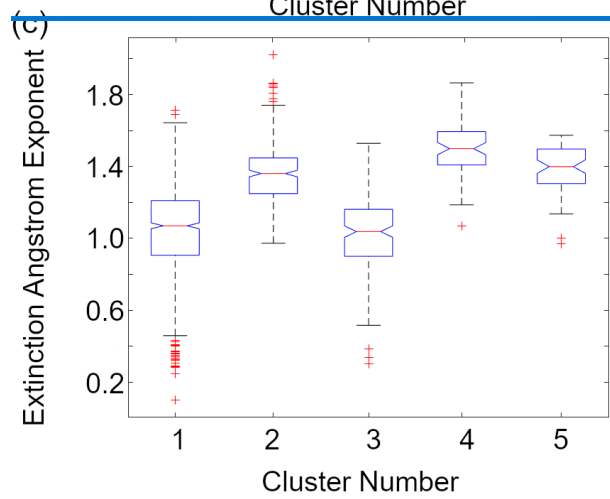
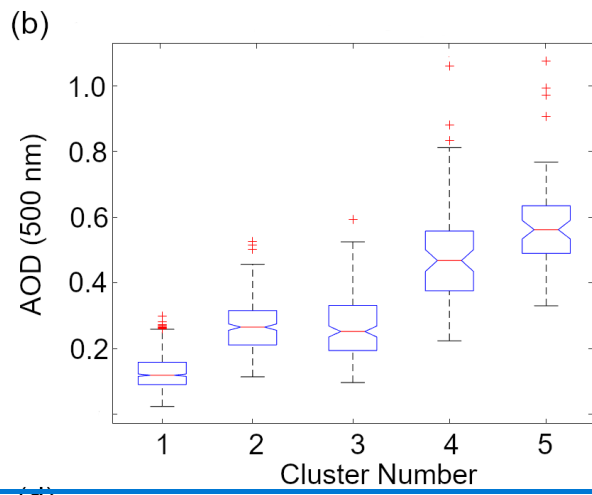
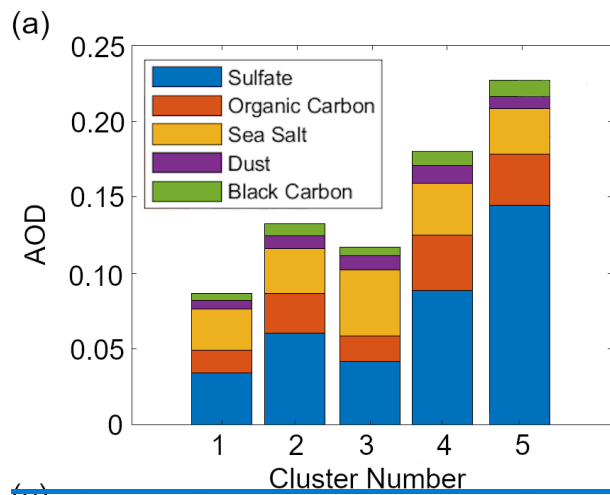
766 **Figure 6:** (a) Cluster analysis of VSD data yielding five characteristic and averaged VSDs with
 767 the number of points per cluster shown in the legend. The black circles on the curves show the

768 peak locations in the submicrometer ($<1 \mu\text{m}$) and coarse ($\geq 1 \mu\text{m}$) modes. The relative abundance
769 of each cluster is shown for different (b) seasons (blue: DJF, red: MAM, orange: JJA, violet:
770 SON) and (c) times of day (blue: AM, red: PM).

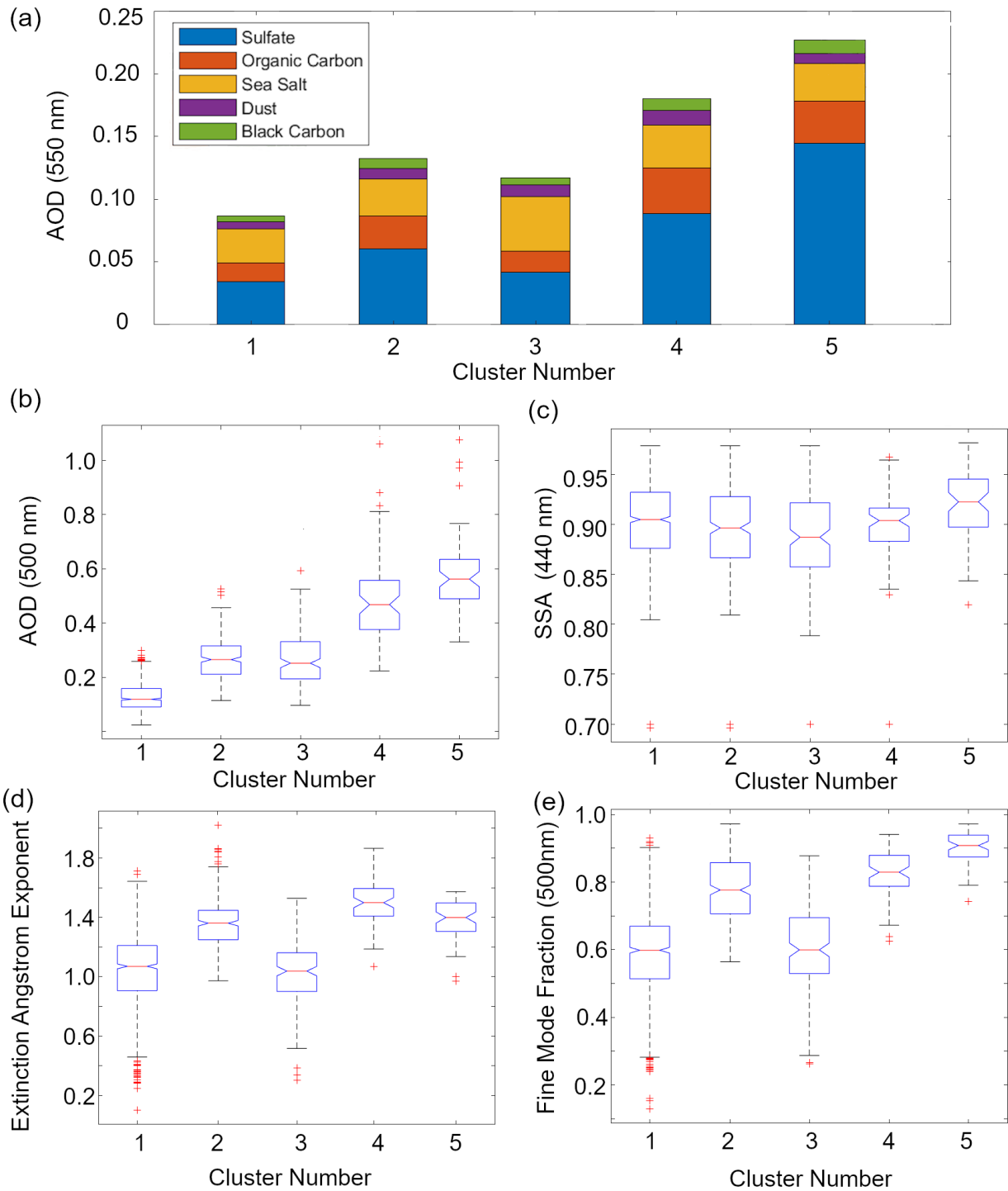
771 The clusters were distributed across seasons (Fig. 6b), with clusters 1 and 2 being the most
772 evenly distributed among the clusters. Cluster 3, which had the highest coarse mode peak, had
773 the greatest contribution from September to November compared to other clusters. Cluster 4,
774 which had the highest accumulated mode peak compared to other clusters, had the greatest
775 contribution from March to May as well as to afternoon VSDs compared to other clusters (Fig.
776 6b and 6c). Relative contributions of VSDs from June to August were highest for cluster 5,
777 which had the shifted accumulated mode peak.

778 Median total (AERONET) AOD values (Fig. 7b) were lowest (0.12) for cluster 1, though it had
779 the second highest sea salt fractional contributions (31%) (Fig. 7a) to total AOD (MERRA-2)
780 (31%) among all the clusters. Cluster 2 had relatively mid-range median total AOD values (0.27)
781 that, along with clusters 4 and 5, were dominated by sulfate and organic carbon (46% and 20%).
782 Cluster 3 had similar, but slightly lower median total AOD (0.25) compared to cluster 2. Cluster
783 3 was distinct because it had the largest total (0.04) and fractional contribution (37%) from sea
784 salt among all clusters. Clusters 4 and 5 had the highest median total AOD values (0.47 and
785 0.56), with cluster 5 having the highest absolute and fractional sulfate contributions (0.14 and
786 64%) among the clusters. Integrating the above results with their corresponding aerosol particle
787 properties can help associate the clusters to air masses.

788



789



790

791 **Figure 7:** (a) Average compositional contributions to aerosol optical depth (AOD at 550 nm)

792 from MERRA-2 per identified cluster: (counts per cluster from 1 to 5: 830, 284, 166, 74, 65).

793 Boxplots of AERONET (b) total AOD (500 nm), (c) [single scattering albedo \(SSA at 440 nm\)](#),

794 [\(d\) extinction angstrom exponent \(EAE, at 440 nm – 870 nm total\)](#), and [\(e\) fine mode fraction](#)

795 [\(FMF, at 500 nm\)](#) per cluster.

796

797 3.3.2 Air Mass Types

798 Air masses have been classified in previous studies based on their AOD, EAE, [FMF](#), and
799 [FMFSSA](#) values (e.g., [Lee et al., 2010](#) and [Aldhaif et al., 2021](#)). The criteria from different
800 studies (Table 2) were applied per cluster. Median total AOD of cluster 1 (0.12) was less than 0.2
801 (Fig. 7b), which is the threshold for sea salt sources ([Kaskaoutis et al., 2007](#); [Kaskaoutis et al.,](#)
802 [2009](#)). Half of the data points in cluster 1 also fall below the threshold for clean environments
803 (AOD < 0.1) ([Sorooshian et al., 2013](#)). Based on its median ~~FMF (0.60)~~ and EAE (1.07, where
804 EAE < 1 is coarse and EAE >1 is fine) and [FMF \(0.60\)](#) values (Fig. ~~7e7d~~ and ~~7e7e~~), cluster 1 is
805 a mixture of fine and coarse particles. [The fine](#) Cluster 1 is the only cluster with a median that
806 meets that threshold value for clean marine sources (AOD < 0.2), and we know from Sect. 3.3.1
807 that its average VSD magnitude was greater for the coarse fraction and that its sea salt
808 contribution to total AOD was second greatest among the clusters. Thus, ~~we can say that~~ most
809 probably, cluster 1 is a background clean marine source, since it also is predominant throughout
810 the seasons (Fig. 6b). This makes sense given the proximity of the ocean to Metro Manila from
811 both the east and the west. [The median SSA \(0.90 at 440 nm\) for cluster 1 \(Fig. 7c\), however,](#)
812 [suggests the presence of absorbing particles most probably due to high black carbon in the local](#)
813 [source \(\[Cruz et al., 2019\]\(#\)\) that is mixed in with this generally clean marine source.](#)

814 Most of the data from the other clusters all fall in the polluted category (Table 2), based on their
815 median total AODs (>0.1) (Fig. 7b). Cluster 2 has a median FMF value of 0.78 (Fig. ~~7e7e~~),
816 which suggests that most of the particles in this air mass are in the fine fraction. They are,
817 however, not sufficiently dominant in the aerosol for them to be typical of urban/industrial
818 sources. The average VSDs (Fig. 6a) of cluster 2 similarly suggest that their relative
819 accumulation mode magnitude is higher than the coarse magnitude, but not much higher. Like
820 cluster 1, cluster 2 is also more evenly distributed across the seasons (Fig. 6b). [The median SSA](#)
821 [for cluster 2 \(0.90 at 440 nm\) is also similar to the SSA of cluster 1 \(Fig. 7c\) where the local and](#)
822 [background particles are mixed. Cluster 2](#) could be a fine polluted background source
823 [superimposed on the dominant marine source.](#) Metro Manila is a megacity with continuous and
824 large amounts of sources that could be, due to its proximity to the ocean, interacting with the
825 background.

826 Based on its median EAE value (1.04) (Fig. 7d), cluster 3 is mixed but mostly in the coarse
827 fraction, consistent with its VSD profile (Fig. 6a) which has the highest coarse magnitude (FMF
828 = 0.60) compared to the other clusters. The contribution of data from September to February is
829 greatest in cluster 3, consistent with expected coarser particles during this period when the winds
830 are initially shifting from the southwest before becoming more northeasterly, as previously
831 noted. ~~This air mass can be a mixed polluted air mass, which is possibly transported due to the~~
832 ~~large sea salt contribution to total AOD (Sect. 3.3.1).~~ [Median SSA \(0.89 at 440 nm\) was lowest](#)
833 [for cluster 3 \(Fig. 7c\), this and the relatively high coarse particle contribution suggests cluster 3](#)
834 [as a possible dust source based on past studies \(\[Lee et al., 2010\]\(#\)\). This air mass can be a mixture](#)
835 [of local sources and transported dust air masses, the large sea salt contribution \(~37%\) to total](#)
836 [AOD \(Sect. 3.3.1\) can be related to long-range transport.](#)

837 Both clusters 4 and 5 have median total FMF (0.83 and 0.91) (Fig. ~~7e7e~~) values exceeding the
838 mark (> 0.8, Table 2) for urban/industrial air masses. Combining this and results from the
839 previous sections confirms that cluster 4 can be an urban/industrial source given that it had the
840 highest median accumulated mode peak and organic carbon contribution ([~20%](#)) to total AOD
841 among the clusters. [The median SSA for cluster 4 \(0.90 at 440 nm\) was similar to the median](#)

842 [SSA of clusters 1 and 2 \(Fig. 7c\), but the maximum SSA value for this cluster was lowest in](#)
843 [general among all the clusters suggesting cluster 4 has the net most absorptive effect. The cluster](#)
844 [4 air mass is probably from local sources and transported biomass burning emissions. The high](#)
845 [median EAE \(1.40, Fig. 7d\) may be associated with aerosol particles due to biomass burning](#)
846 [\(Deep et al., 2021\).](#)

847 Cluster 5 had the highest median total AOD ([0.56](#)) and FMF ([0.91](#)) values (Fig. [7e7b and 7e](#)). It
848 also had the highest (~~Fig. 7a~~) sulfate contribution ([~64%](#)) to total AOD ~~as well as (Fig. 7a), the~~
849 [highest median SSA \(0.92 at 440 nm, thus most reflective particles among the clusters\) \(Fig. 7c\),](#)
850 [and](#) a shifted accumulation mode peak (Fig. 6a). These characteristics suggest that cluster 5 is a
851 possible cloud processing air mass (Eck et al., 2012). The larger peak in the accumulation mode
852 is possibly the cloud signature. Previous studies have attributed this larger mode to cloud
853 processing due to the conversion of SO₂ to sulfate (Hoppel et al., 1994). Cloud processing is a
854 major source of sulfate (Barth et al., 2000).

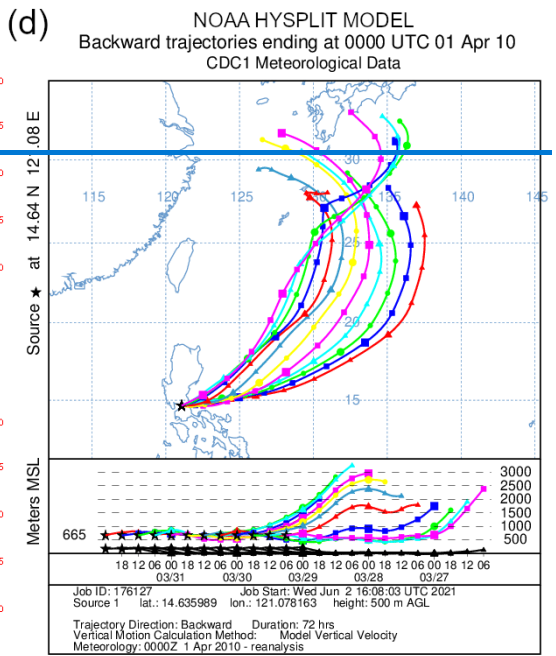
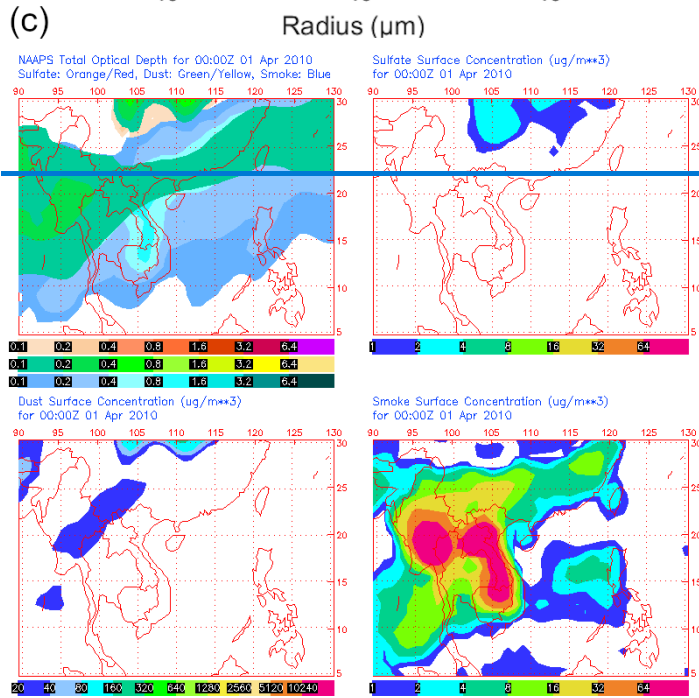
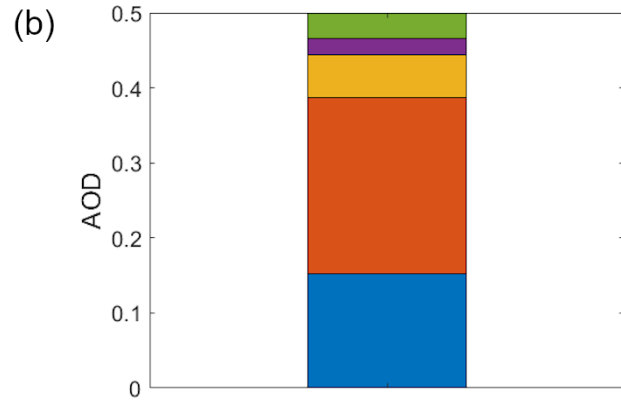
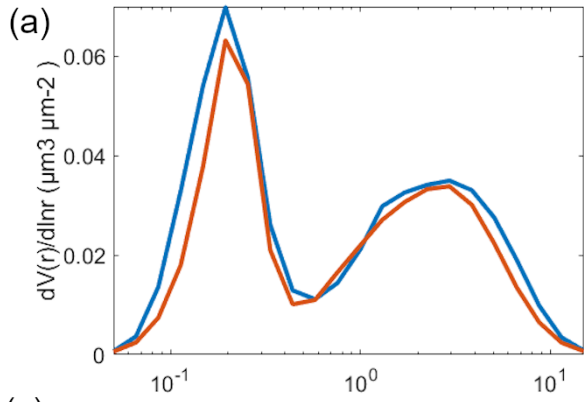
855 The distribution of the air masses based on the abundance of the VSD profiles per cluster suggest
856 prevalent clean marine (58% of the total VSD counts) and background fine polluted (20%) air
857 masses over Metro Manila. The mixed ~~polluted dust~~ (12%), urban/industrial (5%), and cloud
858 processing (5%) air masses contribute 22% ~~all together altogether~~. We can investigate more
859 deeply and look at specific case studies that can better describe the air masses identified here.
860

861 **3.4 Case Studies**

862 Selected case studies are used to highlight periods with the highest AOD values and strongest
863 clear sky (no rain and heavy clouds) daytime aerosol particle sources within the sampling period.
864 As such, the clusters that are associated with the selected case studies are the clusters (3-5) with
865 higher VSD [concentration](#) magnitudes.
866

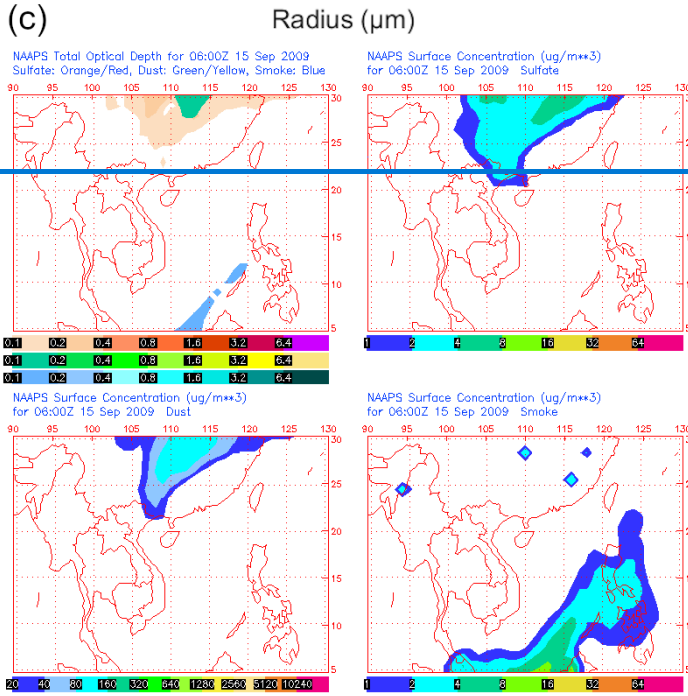
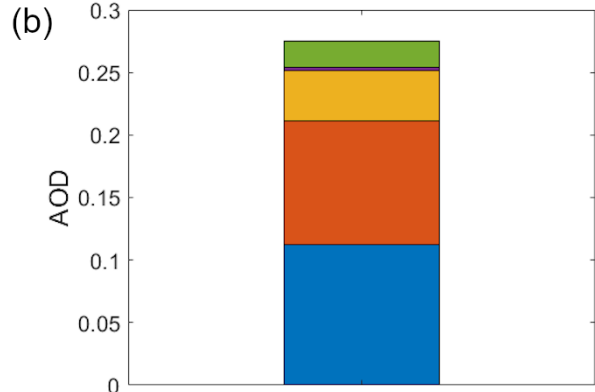
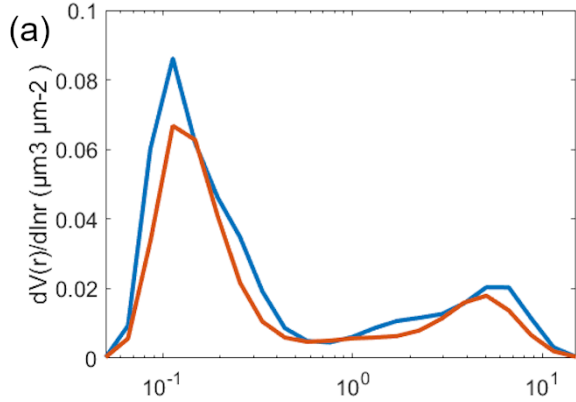
867 **3.4.1 Long Range Transport of Smoke**

868 Both cases of long-range transport of smoke discussed below have similar VSDs (Fig. 8a and 9a)
869 to the urban/industrial cluster VSD (cluster 4, Fig. 6a). Organic carbon was the dominant
870 contributor to AOD (Fig. 8b and 9b) for both long-range transport cases. The first of two events
871 occurred around 1 April 2020 with smoke presumed to come from East Asia. The VSD of this
872 specific case (Fig. 8a) is most like the urban/industrial cluster (cluster 4 in 3.3.2, Fig. 6a) because
873 of the high magnitude of its accumulated mode peak, its timing (April), and the enhanced
874 organic carbon contribution to AOD in the area (Fig. 8b). Though the absolute black carbon
875 contribution to AOD was highest here compared to the other case studies, and in general for the
876 AERONET data, it was organic carbon that was more prevalent in terms of contribution to total
877 AOD. Smoke is comprised of both soot carbon and organic carbon, amongst other constituents
878 (Reid et al., 2005).

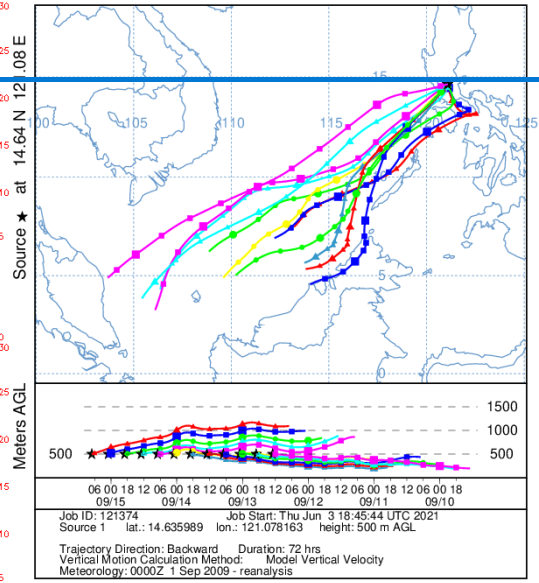


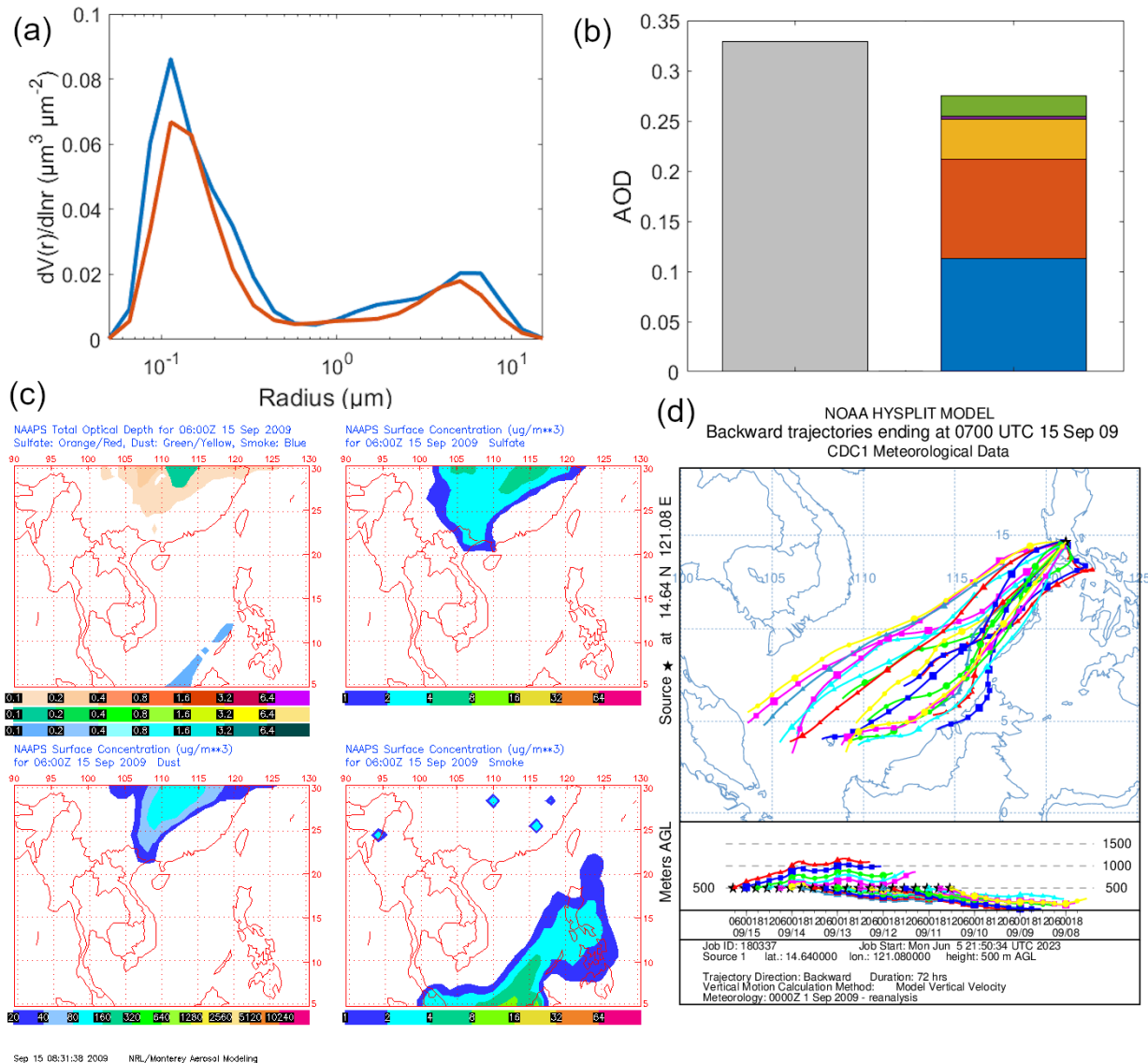
894 burning emissions in the Peninsular Southeast Asia (southern China, Burma, and Thailand) at
895 this time (Shen et al., 2014). The direction of the air mass coming into Metro Manila was from
896 the northeast, which curved from the west in the direction of East Asia based on HYSPLIT back-
897 trajectories (Fig. 8d).

898 The second smoke case was on 15 September 2009 with the source being Southeast Asia. The
899 back-trajectories of this case study (Fig. 9d) are from the southwest of the Philippines, and in the
900 direction of the Malaysia and Indonesia. NAAPS maps likewise show elevated AOD,
901 specifically smoke contribution to AOD (Fig. 9c), as well as enhanced smoke surface
902 contributions in the area around Metro Manila for this second smoke case study. The observed
903 AOD and smoke surface concentration increased specifically from the southwest of the
904 Philippines in the same direction of the back-trajectories. There were fires in the lowland (peat)
905 forests of Borneo around this time (NASA, 2009). MERRA-2 AOD contributions for this case
906 were greatest due to organic carbon as well as sulfate (Fig. 9b), and the absolute black carbon
907 contributions were greatest compared to other cases. The VSD of this smoke case from Southeast
908 Asia (Fig. 9a) resembled that from long-range transported smoke from East Asia (Fig. 8a) and
909 the urban/industrial air mass (cluster 4, Fig. 6a). This case occurred in the afternoon, which was
910 the prevalent time that the urban/industrial air mass was observed (Fig. 6c).



(d) NOAA HYSPLIT MODEL
Backward trajectories ending at 0700 UTC 15 Sep 09
CDC1 Meteorological Data



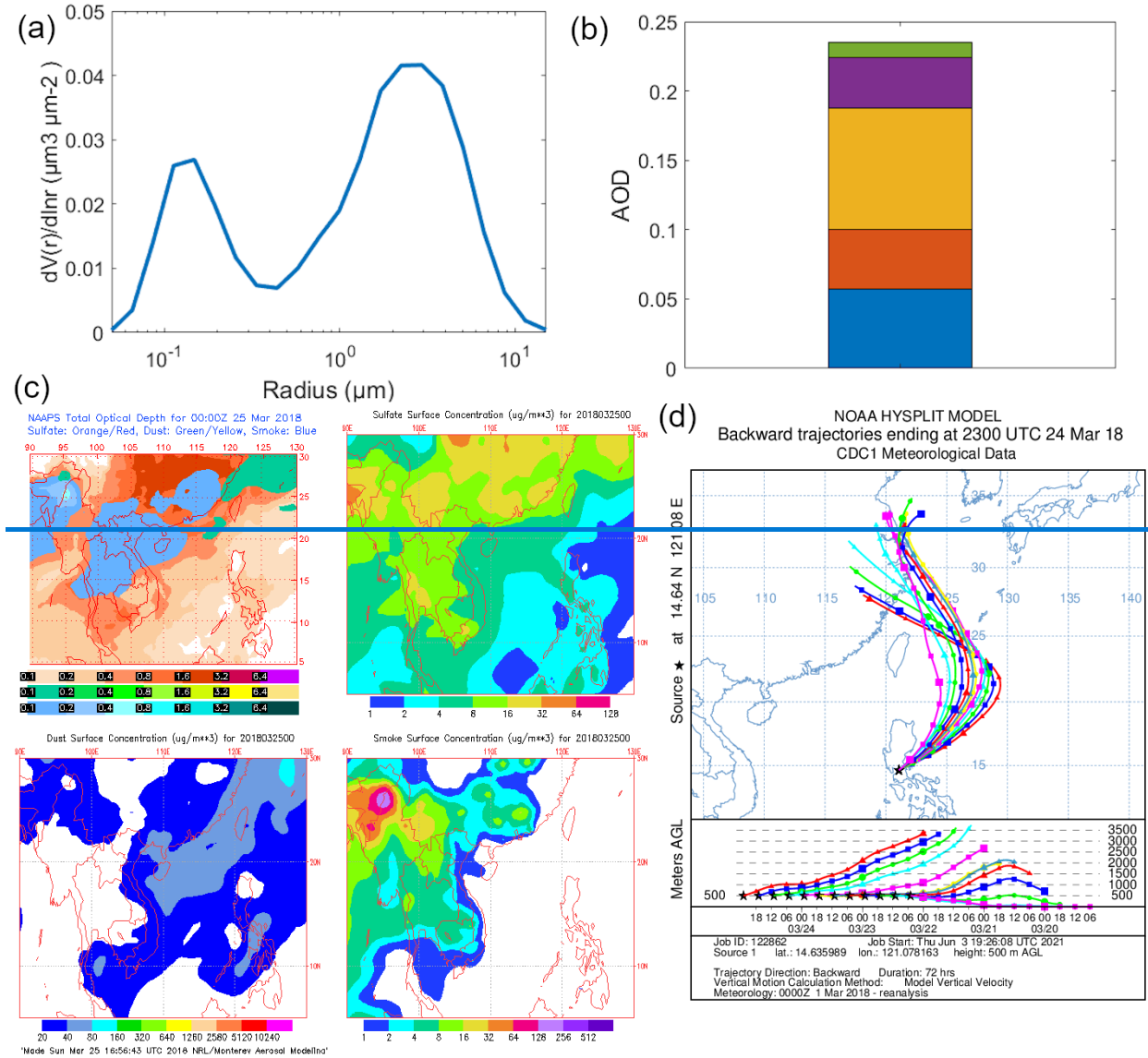


912
 913 **Figure 9:** Case study of long-range transport (smoke – Southeast Asia) around 15 September
 914 2009. (a) AERONET VSDs at (blue) 07:27 and (red) 07:52 UTC, (b) AOD from AERONET
 915 (gray: median AOD at 500 nm) and MERRA-2 hourly (green: black carbon, violet: dust, yellow:
 916 sea salt, orange: organic carbon, blue: sulfate) compositional contributions to AOD (550 nm)
 917 closest in time to 07:27 UTC, (c) NAAPS maps of total and compositional hourly AOD
 918 (orange/red: sulfate, green/yellow: dust, blue: smoke) and sulfate, dust, and smoke surface
 919 concentrations at 06:00 UTC, and (d) HYSPLIT three-seven-day back-trajectories arriving at
 920 Manila Observatory at 07:00 UTC.

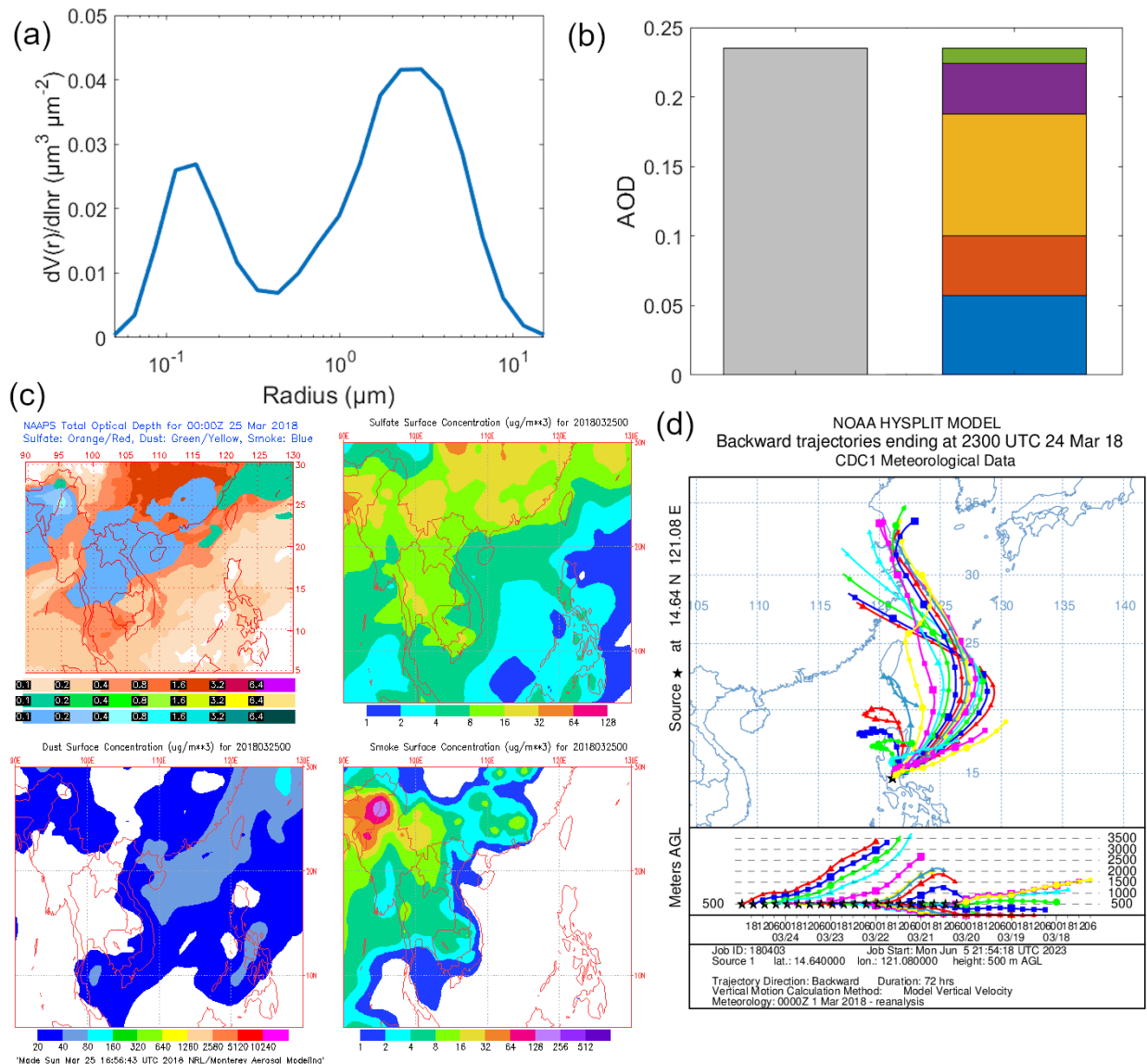
922 3.4.2 Long Range Transport of Dust

923 The VSD of this specific case on 24 March 2018 (Fig. 10a) was most similar to the mixed
 924 polluted dust cluster (cluster 3), which had a mixed size distribution but a more dominant coarse
 925 contribution. This is consistent with the most dominant contribution to AOD in the area, which
 926 was sea salt and dust (Fig. 10b). The back-trajectories were from East Asia around the same
 927 latitude as Taiwan (Fig. 10d). That area, at that time, had increased AOD in general from sulfate

928 and dust (Fig. 10c). The AOD from both AERONET and MERRA-2 (Fig. 10b) are lower than
 929 0.3 (the AOD threshold for dust in other studies, Table 2) because of the long distance from the
 930 source (thousands of kilometers). The dust and sulfate seemed to have been transported to Metro
 931 Manila from East Asia based on the NAAPS sulfate and dust surface concentrations (Fig. 10c).
 932



933

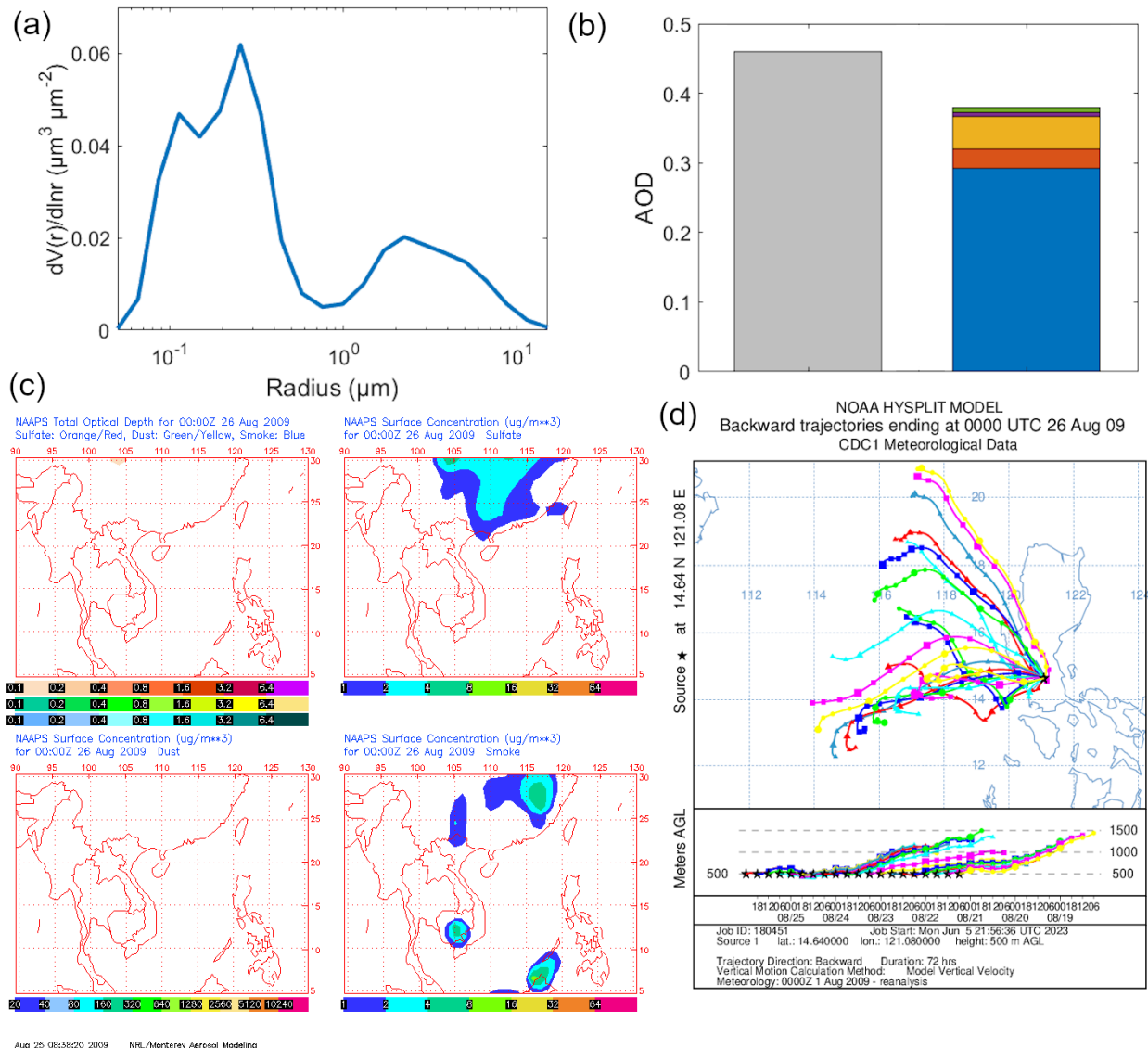


934
 935 **Figure 10:** Case study of long-range transport (dust) around 24-25 March 20092018. (a)
 936 AERONET VSD at (blue) 23:23 UTC, (b) AOD from AERONET (gray: AOD at 550 nm) and
 937 MERRA-2 hourly (green: black carbon, violet: dust, yellow: sea salt, orange: organic carbon,
 938 blue: sulfate) compositional contributions to AOD (550 nm) closest in time to 23:23 UTC, (c)
 939 NAAPS maps of total and compositional hourly AOD (orange/red: sulfate, green/yellow: dust,
 940 blue: smoke) and sulfate, dust, and smoke surface concentrations at 00:00 UTC on March 25,
 941 and (d) HYSPLIT ~~three~~seven-day back-trajectories arriving at Manila Observatory at 23:00
 942 UTC.

943
 944 3.53.4.3 Cloud Processing

945 Sulfate dominated the AOD (Fig. 11b) for this case on 26 August 2009 in the area around Metro
 946 Manila. This along with its VSD exhibiting a second peak (Fig. 11a) in the accumulation mode
 947 make it very similar to the cloud processing cluster (cluster 5). Sulfate has been known to be
 948 enhanced through chemical productions in clouds and is used as a signature for cloud processing
 949 (Barth et al., 2000; Ervens et al., 2018). Aqueous production of sulfate is significant in areas with

950 sources and clouds (Barth et al., 2000), and this case study has both. Aside from the high sulfate
951 contribution to AOD, the cloud fraction ([Aqua/MODIS, Terra/MODIS, Fig. S3](#)) is very high
952 (~100%) in the area of the back-trajectories (~~[Aqua/MODIS, Terra/MODIS, Fig. S211d](#)~~).
953 Interestingly, there is no regional AOD elevation observed in the NAAPS maps (Fig. 11c) for
954 this time. There are increased surface smoke and sulfate levels in East Asia as well as southwest
955 of the Philippines, and though the back-trajectories (~~[Fig. 11d](#)~~) do show a northeastward direction,
956 they do not reach far enough into mainland East Asia. It is possible that even while there are
957 known regional sources of sulfate in Southeast Asia (Smith et al., 2011; Li et al., 2017), this case
958 could be local to the Philippines. There is in fact a large power plant northwest of Metro Manila
959 (Jamora et al., 2020).
960

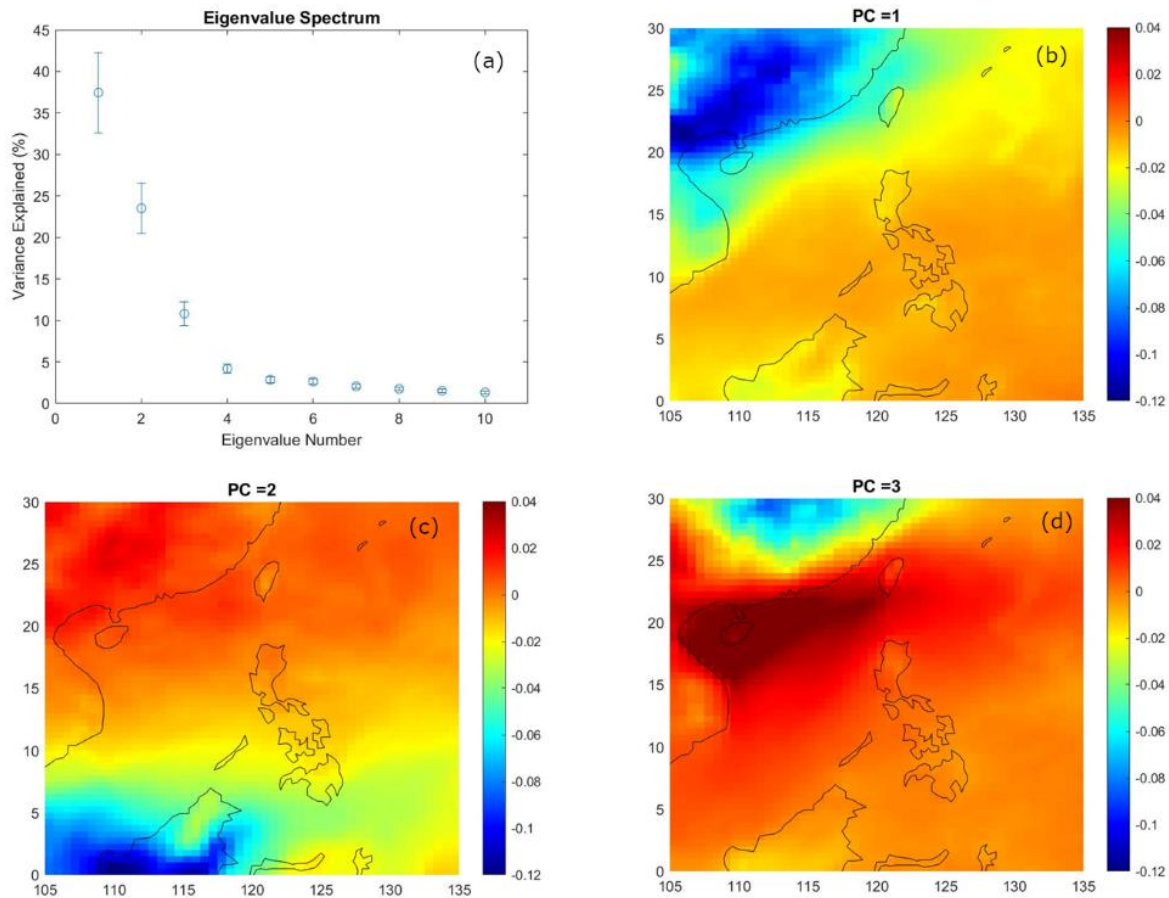


962
 963 **Figure 11:** Case study of cloud processing on 26 August 2009. (a) AERONET VSDs at 00:18
 964 UTC, (b) [AOD from AERONET](#) (gray: median AOD at 500 nm) and [MERRA-2 hourly](#) (green:
 965 black carbon, violet: dust, yellow: sea salt, orange: organic carbon, blue: sulfate) compositional
 966 contributions to AOD (550 nm) closest in time to 00:18 UTC, (c) NAAPS maps of total and
 967 compositional hourly AOD and contributions and smoke surface concentrations at 00:00 UTC,
 968 and (d) HYSPLIT [three-seven](#)-day back-trajectories arriving at Manila Observatory at 00:00
 969 UTC.

970
 971 **3.63.5 EOF Analysis of AOD in Southeast Asia**
 972 [To contextualize the analysis of aerosol particle](#)

973 [The air](#) masses in Metro Manila, [major are influenced by](#) regional sources [of aerosol particles in](#)
 974 [Southeast Asia](#) which were identified [based on the dominant principal components from](#) through
 975 EOF analysis of AOD. Three principal components (PC, Fig. 12) explained most of the data
 976 variance (73.77%) (Fig. 12a) and were all well-separated from each other and are therefore most

977 probably the major distinct aerosol particle sources in the region. They will be the focus of the
978 subsequent discussion.

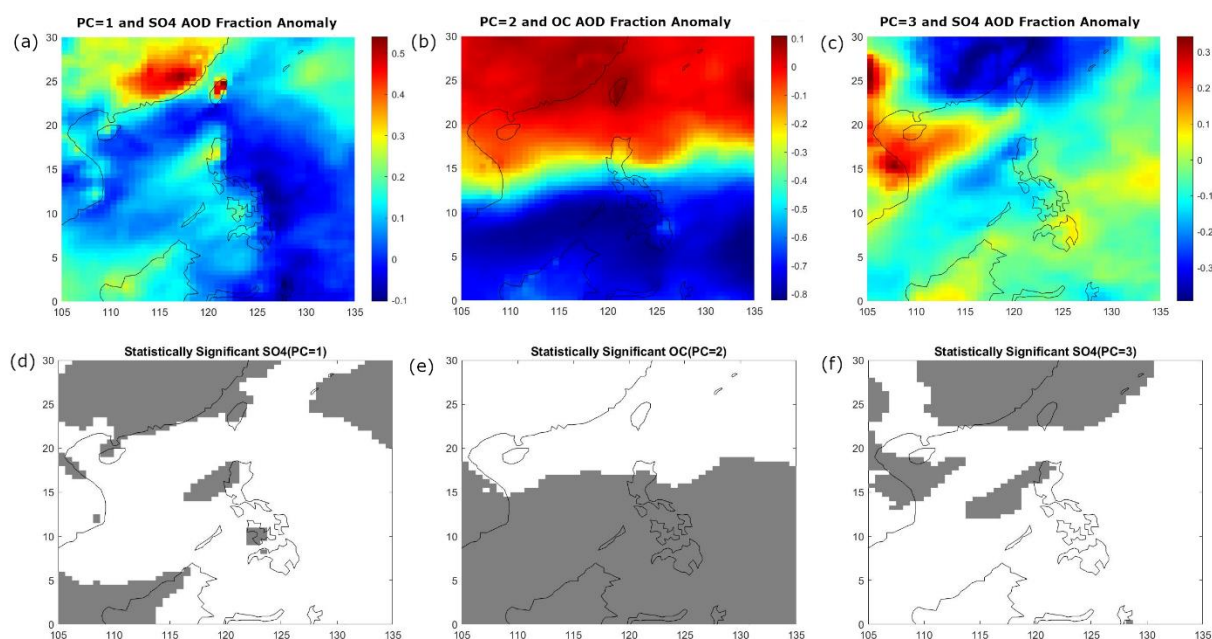


979 **Figure 12:** Results of the singular value decomposition. (a) Eigenvalue spectrum of the first ten
980 eigenvalues, (b-d) maps of the coefficients of regression AOD anomalies onto the first three
981 principal components.
982

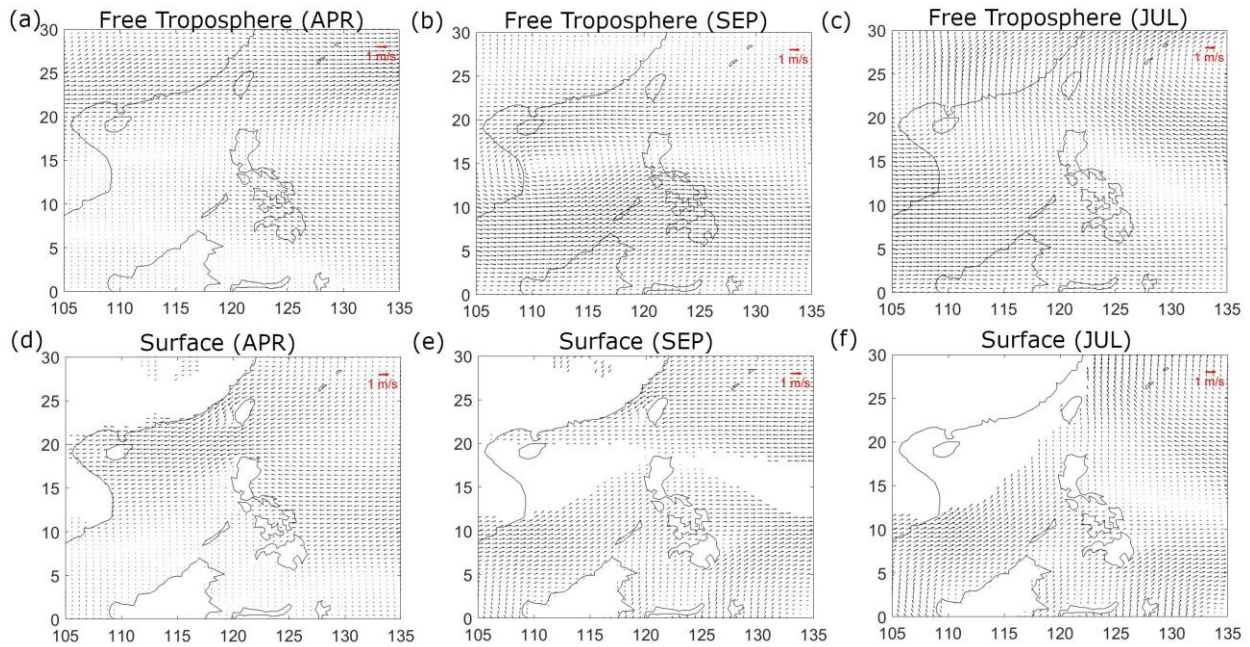
983 The first PC explains 37.46% of the data variance (Fig. 12a) and, based on the map of the
984 regression coefficients (Fig. 12b), separates mainland East Asia from the Philippines and
985 Indonesia. East Asia is a globally recognized source for high AOD (Li et al., 2013), and its
986 contribution to particles in Southeast Asia possibly corresponds to the first PC. The second PC
987 explains 25.51% of the data variance (Fig. 12a) and separates ~~the~~ southern Southeast Asia from
988 northern Southeast Asia at around 15°N (Fig. 12c). Southern Southeast Asia is a known regional
989 source of aerosol particles due to biomass burning (Cohen et al., 2017) and could be associated
990 with the second PC. The third PC explains 10.80% of the data variance (Fig. 12a) and separates
991 northern East Asia from southern East Asia mainland and the rest of Southeast Asia (Fig. 12d).

992 To gain confidence in the association of the PCs with their sources, we present correlation maps
993 between the first three PCs to the fractional contributions of sulfate and organic carbon to AOD
994 for the entire dataset.

995 The correlation maps of the first PC and the sulfate contribution to AOD (Fig. 13a and 13d)
 996 show high and statistically significant correlations (gray areas) in mainland East Asia and
 997 Taiwan, parts of western Philippines and Borneo, which are the probable sulfate sources. Clues
 998 from the mean monthly wind vector maps in April (Fig. 14a and 14d) and mean monthly AOD in
 999 either March or April (Fig. S3c or S3e) most resembling the features of regression map of the
 1000 first PC (Fig. 12b) and the PC time series peaking in March (Fig. S4) together suggest that the
 1001 first PC may be associated with air masses that are present around March or April. Emissions
 1002 sources and meteorology that are dominant during the peak dates in the PC time series offer
 1003 clues to the attribution of each PC. The Southeast Asia region and the Philippines is influenced
 1004 by the monsoon systems (Coronas, 1920; Matsumoto et al., 2020) and February to March is the
 1005 time when the winds are transitioning from the northeasterly to easterly. The first PC could be
 1006 affected by the easterly winds, which are dominant around March when its PC values peaked.
 1007 The higher-level winds (free troposphere) (Fig. 14a) in April are from the west in mainland East
 1008 Asia and are from the east in the Philippines and it is possible that the different wind regimes are
 1009 distinguishing the sulfate sources in East Asia and the Philippines and beyond. Sulfate is a
 1010 known product of industry in East Asia (Smith et al., 2011; Li et al., 2017) while the West Luzon
 1011 and West Visayas islands have large power plants (Jamora et al., 2020).



1012 **Figure 13:** Correlation coefficients of principal components with (a/c) sulfate AOD fraction and
 1013 (b) organic carbon AOD fraction. Statistically significant (90%, d-f) areas are shaded gray.
 1014



1015 **Figure 14:** Monthly averaged winds for (a & d) April, (b & e) September, and (c & f) July from
 1016 MERRA-2 at (725 hPa, a-c) the free troposphere approximate and at (1000 hPa, d-f) the surface.
 1017

1018 The correlation maps of the second PC and the OC contribution to AOD (Fig. 13b and 13e) show
 1019 high and statistically significant correlations from 0°N to 15°N. The large magnitude of the
 1020 correlation coefficient (gray areas in Fig. 13b) stands out in the southern Southeast Asia and is
 1021 the potential OC source. In this case, it is known that Indonesia is a major source of biomass
 1022 burning during its fire season (Glover and Jessup, 1998), and thus the local significance
 1023 established in the southern Southeast Asia is most likely due to the Indonesia biomass burning
 1024 source. The burning season in Indonesia is from August to October, and that is the same time
 1025 when the AOD values peak in the area (Fig. S3h, S3i, and S3j), as well as the peak of the second
 1026 PC in the time series (Fig. S4). Winds are usually from the southwest and west due to the
 1027 southwest monsoon from September to October, when the second PC peaked, and thus the
 1028 second PC may be related to the southwest monsoon. During the same time the surface and free
 1029 troposphere mean monthly winds (Fig. 14b and 14e) are from the southwest (in the general
 1030 direction of Indonesia) towards the south portion of Southeast Asia and thus corroborate the
 1031 observation that the second PC may be highlighting the regional effect of the Indonesia forest
 1032 fires. Of interest is the line of separation of the northern and southern Southeast Asia in the
 1033 principal component that is within the area of the monsoon trough (Wang et al., 2007). This line
 1034 is also evident in the surface and the free troposphere maps where the southwest winds from the
 1035 area of Indonesia meet the easterlies in north Southeast Asia (Fig. 14b and 14e) and which thus
 1036 appears to be limiting the dispersion of the biomass burning emissions to southern Southeast
 1037 Asia.

1038 The third PC was also well correlated to the sulfate AOD fraction though, compared to the first
 1039 PC correlation maps, there were distinctions between the northern and southern East Asia
 1040 regions (Fig. 13c and 13f). The local Philippine source still came out in the correlation maps as a
 1041 significant source. It was not clear from the PC time series (Fig. S4), which showed peaks in the
 1042 third PC in February, how the dates were related to the PC profile. The free troposphere winds in

1043 July (Fig. 14c), as well as the AOD monthly mean map in July (Fig. 14c), however, showed
1044 more similarities to the third PC regression map. Both showed a delineation between the
1045 northern East Asia and southern East Asia (including Hong Kong) features. Mean winds (Fig.
1046 14c) in the free troposphere are from the west, due to the southwest monsoon, in the area around
1047 the Philippines, and they were from the northeast in north Southeast Asia. The interface of the
1048 winds is within the approximate location of the monsoon trough in July (Wang et al., 2007), and
1049 it is thus possible that the monsoon trough is causing the separation of the sulfate sources. This
1050 could be investigated further. The monsoon trough has been noted to scavenge aerosol particles
1051 from southern Southeast Asia (Reid et al., 2013). It is evident from the analysis that meteorology
1052 affects the transport and processing of aerosol particles in region which along with local sources
1053 contribute to the aerosol composition in Southeast Asia (Cruz et al., 2019; AzadiAghdam et al.,
1054 2019; Braun et al., 2020; Hilario et al., 2020b; Hilario et al., 2022).

1056 4. Conclusion

1057 Metro Manila has both urban and industrial local sources known to contribute to the dominance
1058 of fine mode particles in its air (Cruz et al., 2019). Ten years of AERONET data in Manila
1059 Observatory suggest that aerosol particles in Metro Manila were mixed in size but with a
1060 prevalent fine mode fraction (>50% FMF) throughout the year. Background clean marine aerosol
1061 particles (58% of the time) and fine polluted aerosol particles (20% of the time) were the most
1062 dominant clear sky day sources impacting the atmospheric column over Metro Manila based on
1063 cluster analysis of volume size distributions. The proximity of Metro Manila to the sea, both in
1064 the east and west, along with local sources, transportation being the most prominent, [together](#)
1065 contribute to the prevalence of the marine and fine particles. The prevalence of marine particles
1066 could explain the relatively small AOD values in Metro Manila compared to other Southeast
1067 Asian megacities (Reid et al., 2013).

1068 Regional sources and meteorology also impact monthly aerosol optical depth trends in Metro
1069 Manila from EOF analysis. Biomass burning from Borneo and Sumatra emerged in the study as
1070 the second most prevalent regional anthropogenic aerosol particle source in Southeast Asia.
1071 Though the monsoon trough limits the dispersion of aerosol particles throughout the entire
1072 Southeast Asia, biomass burning emissions impact southern Southeast Asia including Metro
1073 Manila during the southwest monsoon (July to September). The monsoon winds facilitate the
1074 transport of fine particles during the peak burning season in Borneo and Sumatra (August-
1075 September). This is experienced in Metro Manila as higher than usual aerosol particle loadings
1076 [during around](#) the same period: [\(August to October\)](#). Climatologically, August ~~is was~~ also when
1077 [aerosol optical depth peaked over Metro Manila, concurrent there were particles](#) with [the](#) greatest
1078 fine mode fractions that were relatively absorbing and non-hygroscopic possibly due to increased
1079 organic and elemental carbon fractional contributions. Though not as strong a source as the
1080 Borneo and Sumatra case, the peninsular Southeast Asia burning season (March-April) also
1081 contributed to extreme aerosol particle concentrations over Metro Manila.

1082 High aerosol particle loadings due to transported dust, probably from East Asia, were observed
1083 in Metro Manila during the transition period between the southwest and northeast monsoons and
1084 during the northeast monsoon (December to February). These extreme events are transient
1085 because the lowest median aerosol particle loadings of the year were observed during the
1086 northeast monsoon when annual wind speeds were highest. Particles then were observed to be

1087 largest in diameter, with the greatest coarse fraction contribution, [relatively high absorptivity](#),
1088 and most hygroscopicity, compared to other months of the year. This is probably due to
1089 constituents other than soot, especially aged dust (Kim and Park, 2012; Geng et al., 2014) and
1090 sea salt which the northeast winds appear to be bringing in from the general direction of the
1091 Luzon Island and the Philippine Sea (West Pacific Ocean).

1092 Cloud processing is one of the cases that were linked to very high aerosol particle loading in
1093 Metro Manila. This is associated with sulfate sources, which appear more localized in nature
1094 because of a power plant nearby. This sulfate source seems to be distinct from the industrial
1095 sulfate air mass from East Asia, which is the most dominant regional aerosol particle source in
1096 Southeast Asia (Li et al., 2013). Winds appear to limit the mixing of this notable East Asia air
1097 mass with local industrial sources in the region including the Philippines and Indonesia.

1098 The formation of cloud systems in Southeast Asia is complex due to intersecting large- and
1099 small-scale mechanisms. Additionally, the interaction of particles and clouds in Southeast Asia is
1100 not yet well understood. In Metro Manila, both topography and meteorology affect aerosol
1101 particle distribution (Cruz et al., 2023). This baseline study on the aerosol particle characteristics
1102 in Metro Manila and in regional Southeast Asia shows how meteorology impacts varied aerosol
1103 particle sources (e.g., sulfate, elemental carbon, and organic carbon) and their distribution in the
1104 region. This can help in mitigating aerosol particle sources in the region and in the deepening of
1105 the understanding of the relationship of aerosol particles, meteorology, and clouds.

1106

1107 **Data availability**

1108 Aerosol Robotic Network (AERONET) (2020), Version 3 Direct Sun Algorithm, Site: Manila
1109 Observatory, Philippines, Accessed: [**28 September 2020**], [https://aeronet.gsfc.nasa.gov/cgi-](https://aeronet.gsfc.nasa.gov/cgi-bin/webtool_aod_v3?stage=3®ion=Asia&state=Philippines&site=Manila_Observatory&place_code=10&if_polarized=0)
1110 [bin/webtool_aod_v3?stage=3®ion=Asia&state=Philippines&site=Manila_Observatory&plac](https://aeronet.gsfc.nasa.gov/cgi-bin/webtool_aod_v3?stage=3®ion=Asia&state=Philippines&site=Manila_Observatory&place_code=10&if_polarized=0)
1111 [e_code=10&if_polarized=0](https://aeronet.gsfc.nasa.gov/cgi-bin/webtool_aod_v3?stage=3®ion=Asia&state=Philippines&site=Manila_Observatory&place_code=10&if_polarized=0)

1112 Aerosol Robotic Network (AERONET) (2020), Version 3 Direct Sun and Inversion Algorithm,
1113 Site: Manila Observatory, Philippines, Accessed: [**28 September 2020**],
1114 [https://aeronet.gsfc.nasa.gov/cgi-](https://aeronet.gsfc.nasa.gov/cgi-bin/webtool_inv_v3?stage=3®ion=Asia&state=Philippines&site=Manila_Observatory&place_code=10&if_polarized=0)
1115 [bin/webtool_inv_v3?stage=3®ion=Asia&state=Philippines&site=Manila_Observatory&place](https://aeronet.gsfc.nasa.gov/cgi-bin/webtool_inv_v3?stage=3®ion=Asia&state=Philippines&site=Manila_Observatory&place_code=10&if_polarized=0)
1116 [_code=10&if_polarized=0](https://aeronet.gsfc.nasa.gov/cgi-bin/webtool_inv_v3?stage=3®ion=Asia&state=Philippines&site=Manila_Observatory&place_code=10&if_polarized=0)

1117 Multi-angle Imaging SpectroRadiometer (MISR) Jet Propulsion Laboratory (2018), Level 3
1118 Component Global Aerosol product in netCDF format covering a month V004, Accessed: [**22**
1119 **November 2021**], <https://search.earthdata.nasa.gov/>

1120 Global Modeling and Assimilation Office (GMAO) (2015), MERRA-2 inst3_3d_asm_Np: 3d,3-
1121 Hourly,Instantaneous,Pressure-Level,Assimilation,Assimilated Meteorological Fields V5.12.4,
1122 Greenbelt, MD, USA, Goddard Earth Sciences Data and Information Services Center (GES
1123 DISC), Accessed: [**10 March 2021**], <https://doi.org/10.5067/QBZ6MG944HW0>

1124 Global Modeling and Assimilation Office (GMAO) (2015), MERRA-2 tavg1_2d_flux_Nx: 2d,1-
1125 Hourly,Time-Averaged,Single-Level,Assimilation,Surface Flux Diagnostics V5.12.4, Greenbelt,

1126 MD, USA, Goddard Earth Sciences Data and Information Services Center (GES DISC),
1127 Accessed: [10 March 2021], <https://doi.org/10.5067/7MCPBJ41Y0K6>

1128 Global Modeling and Assimilation Office (GMAO) (2015), MERRA-2 tavg1_2d_csp_Nx: 2d,1-
1129 Hourly,Time-averaged,Single-Level,Assimilation,COSP Satellite Simulator V5.12.4, Greenbelt,
1130 MD, USA, Goddard Earth Sciences Data and Information Services Center (GES DISC),
1131 Accessed: [13 July 2021], <https://doi.org/10.5067/H0VVAD8F6MX5>

1132 Nguyen, P., E.J. Shearer, H. Tran, M. Ombadi, N. Hayatbini, T. Palacios, P. Huynh, G.
1133 Updegraff, K. Hsu, B. Kuligowski, W.S. Logan, and S. Sorooshian, The CHRS Data Portal, an
1134 easily accessible public repository for PERSIANN global satellite precipitation data, Nature
1135 Scientific Data, Vol. 6, Article 180296, 2019, Accessed: [11 March 2021],
1136 <https://doi.org/10.1038/sdata.2018.296>

1137
1138 **Author contributions**

1139 GRL and AS designed the experiment. NL, SNU, GRL, GFG, HJO, JBS, and MTC, carried out
1140 various aspects of the data collection. GRL, AS, JBS, MOC, MRH, [CC](#), and [ECLDG](#) conducted
1141 analysis and interpretation of the data. GRL prepared the manuscript draft with contributions
1142 from the coauthors. AFA, LDG, MRH, GRL, and AS reviewed and edited the manuscript. AS
1143 led the management and funding acquisition. All authors approved the final version of the
1144 manuscript.

1145
1146 **Competing interests**

1147 We declare that Armin Sorooshian is a member of the editorial board of Atmospheric Chemistry
1148 and Physics. The peer-review process was guided by an independent editor, and the authors have
1149 also no other competing interests to declare.

1150
1151 **Acknowledgements**

1152 The authors acknowledge support from NASA grant 80NSSC18K0148 in support of the NASA
1153 CAMP²Ex project, in addition to ONR grant N00014-21-1-2115. We acknowledge the US Naval
1154 Research Laboratory for providing the AERONET instrument. We acknowledge the use of
1155 imagery from the NASA Worldview application (<https://worldview.earthdata.nasa.gov>), part of
1156 the NASA Earth Observing System Data and Information System (EOSDIS).

1157
1158 **References:**

1159 AERONET Inversion Products (Version 3):
1160 https://aeronet.gsfc.nasa.gov/new_web/Documents/Inversion_products_for_V3.pdf, access: June
1161 25, 2021, 2019.

1162 Alas, H. D., Müller, T., Birmili, W., Kecorius, S., Cambaliza, M. O., Simpas, J. B. B., Cayetano,
1163 M., Weinhold, K., Vallar, E., and Galvez, M. C.: Spatial characterization of black carbon mass
1164 concentration in the atmosphere of a southeast asian megacity: an air quality case study for
1165 Metro Manila, Philippines, Aerosol Air Qual. Res., 18, 2301-2317,
1166 <https://doi.org/10.4209/aaqr.2017.08.0281>, 2018.

- 1167 Aldhaif, A. M., Lopez, D. H., Dadashazar, H., and Sorooshian, A.: Sources, frequency, and
 1168 chemical nature of dust events impacting the United States East Coast, *Atmos. Environ.*, 231,
 1169 117456, <https://doi.org/10.1016/j.atmosenv.2020.117456>, 2020.
- 1170 Aldhaif, A. M., Lopez, D. H., Dadashazar, H., Painemal, D., Peters, A. J., and Sorooshian, A.:
 1171 An Aerosol Climatology and Implications for Clouds at a Remote Marine Site: Case Study Over
 1172 Bermuda, *J. Geophys. Res.- Atmos.*, 126, e2020JD034038,
 1173 <https://doi.org/10.1029/2020JD034038>, 2021.
- 1174 Alizadeh-Choobari, O., and Gharaylou, M.: Aerosol impacts on radiative and microphysical
 1175 properties of clouds and precipitation formation, *Atmos. Res.*, 185, 53-64,
 1176 <https://doi.org/10.1016/j.atmosres.2016.10.021>, 2017.
- 1177 [Andrews, E., Ogren, J. A., Kinne, S., and Samset, B.: Comparison of AOD, AAOD and column
 1178 single scattering albedo from AERONET retrievals and in situ profiling measurements, *Atmos.
 1179 Chem. Phys.*, 17, 6041-6072, <https://doi.org/10.5194/acp-17-6041-2017>, 2017.](#)
 1180 [Amnuaylojaroen, T.: Air Pollution Modeling in Southeast Asia—An Overview, *Vegetation Fires
 1181 and Pollution in Asia*, 531-544, \[https://doi.org/10.1007/978-3-031-29916-2_31\]\(https://doi.org/10.1007/978-3-031-29916-2_31\), 2023.](#)
- 1182 Ångström, A.: On the atmospheric transmission of sun radiation and on dust in the air,
 1183 *Geografiska Annaler*, 11, 156-166, 1929.
- 1184 Arthur, D., and Vassilvitskii, S.: *k-means++: The advantages of careful seeding*, Stanford, 2006.
- 1185 AzadiAghdam, M., Braun, R. A., Edwards, E.-L., Bañaga, P. A., Cruz, M. T., Betito, G.,
 1186 Cambaliza, M. O., Dadashazar, H., Lorenzo, G. R., and Ma, L.: On the nature of sea salt aerosol
 1187 at a coastal megacity: Insights from Manila, Philippines in Southeast Asia, *Atmos. Environ.*, 216,
 1188 116922, <https://doi.org/10.1016/j.atmosenv.2019.116922>, 2019.
- 1189 [Bagtasa, G.: Contribution of tropical cyclones to rainfall in the Philippines, *Journal of Climate*,
 1190 30, 3621-3633, <https://doi.org/10.1175/JCLI-D-16-0150.1>, 2017.](#)
- 1191 Bañares, E. N., Narisma, G. T. T., Simpas, J. B. B., Cruz, F. A. T., Lorenzo, G. R. H.,
 1192 Cambaliza, M. O. L., and Coronel, R. C.: Seasonal and diurnal variations of observed convective
 1193 rain events in metro Manila, Philippines, *Atmos. Res.*, 105646,
 1194 <https://doi.org/10.1016/j.atmosres.2021.105646>, 2021.
- 1195 Barth, M., Rasch, P., Kiehl, J., Benkovitz, C., and Schwartz, S.: Sulfur chemistry in the National
 1196 Center for Atmospheric Research Community Climate Model: Description, evaluation, features,
 1197 and sensitivity to aqueous chemistry, *J. Geophys. Res.- Atmos.*, 105, 1387-1415,
 1198 <https://doi.org/10.1029/1999JD900773>, 2000.
- 1199 [Bautista VII, A. T., Pabroa, P. C. B., Santos, F. L., Racho, J. M. D., and Quirrit, L. L.:
 1200 Carbonaceous particulate matter characterization in an urban and a rural site in the Philippines,
 1201 *Atmospheric Pollution Research*, 5, 245-252, <https://doi.org/10.5094/APR.2014.030>, 2014.](#)
- 1202 Bergstrom, R. W., Russell, P. B., and Hignett, P.: Wavelength dependence of the absorption of
 1203 black carbon particles: Predictions and results from the TARFOX experiment and implications

- 1204 for the aerosol single scattering albedo, *J. Atmos. Sci.*, 59, 567-577,
 1205 [https://doi.org/10.1175/1520-0469\(2002\)059<0567:WDOTAO>2.0.CO;2](https://doi.org/10.1175/1520-0469(2002)059<0567:WDOTAO>2.0.CO;2), 2002.
- 1206 Bergstrom, R. W., Pilewskie, P., Schmid, B., and Russell, P. B.: Estimates of the spectral aerosol
 1207 single scattering albedo and aerosol radiative effects during SAFARI 2000, *J. Geophys. Res.-*
 1208 *Atmos.*, 108, <https://doi.org/10.1029/2002JD002435>, 2003.
- 1209 Bergstrom, R. W., Pilewskie, P., Russell, P. B., Redemann, J., Bond, T. C., Quinn, P. K., and
 1210 Sierau, B.: Spectral absorption properties of atmospheric aerosols, *Atmos. Chem. Phys.*, 7, 5937-
 1211 5943, <https://doi.org/10.5194/acp-7-5937-2007>, 2007.
- 1212 Bi, J., Huang, J., Hu, Z., Holben, B., and Guo, Z.: Investigating the aerosol optical and radiative
 1213 characteristics of heavy haze episodes in Beijing during January of 2013, *J. Geophys. Res.-*
 1214 *Atmos.*, 119, 9884-9900, <https://doi.org/10.1002/2014JD021757>, 2014.
- 1215 Björnsson, H., and Venegas, S.: A manual for EOF and SVD analyses of climatic data, CCGCR
 1216 Report, 97, 112-134, 1997.
- 1217 Bohren, C. F., and Clothiaux, E. E.: Fundamentals of atmospheric radiation: an introduction with
 1218 400 problems, John Wiley & Sons, 2006.
- 1219 Braun, R. A., Aghdam, M. A., Bañaga, P. A., Betito, G., Cambaliza, M. O., Cruz, M. T.,
 1220 Lorenzo, G. R., MacDonald, A. B., Simpas, J. B., and Stahl, C.: Long-range aerosol transport
 1221 and impacts on size-resolved aerosol composition in Metro Manila, Philippines, *Atmos. Chem.*
 1222 *Phys.*, 20, 2387-2405, <https://doi.org/10.5194/acp-20-2387-2020>, 2020.
- 1223 [Buchard, V., Randles, C., Da Silva, A., Darmenov, A., Colarco, P., Govindaraju, R., Ferrare, R.,](#)
 1224 [Hair, J., Beyersdorf, A., and Ziemba, L.: The MERRA-2 aerosol reanalysis, 1980 onward. Part](#)
 1225 [II: Evaluation and case studies, *Journal of Climate*, 30, 6851-6872, \[https://doi.org/10.1175/JCLI-\]\(https://doi.org/10.1175/JCLI-D-16-0613.1\)](#)
 1226 [D-16-0613.1, 2017.](#)
- 1227 [Cahyono, W. E., Setyawati, W., Hamdi, S., Cholianawati, N., Kombara, P. Y., and Sari, W. J.:](#)
 1228 [Observations of aerosol optical properties during tropical forest fires in Indonesia, *Materials*](#)
 1229 [Today: Proceedings](#), 63, S445-S450, <https://doi.org/10.1016/j.matpr.2022.04.113>, 2022.
- 1230 [Caido, N. G., Ong, P. M., Rempillo, O., Galvez, M. C., and Vallar, E.: Spatiotemporal analysis](#)
 1231 [of MODIS aerosol optical depth data in the Philippines from 2010 to 2020, *Atmosphere*, 13, 939,](#)
 1232 [https://doi.org/10.3390/atmos13060939, 2022.](#)
- 1233 [Chang, C.-P., Wang, Z., McBride, J., and Liu, C.-H.: Annual cycle of Southeast Asia—Maritime](#)
 1234 [Continent rainfall and the asymmetric monsoon transition, *Journal of climate*, 18, 287-301,](#)
 1235 [https://doi.org/10.1175/JCLI-3257.1, 2005.](#)
- 1236 Che, H., Xia, X., Zhu, J., Wang, H., Wang, Y., Sun, J., Zhang, X., and Shi, G.: Aerosol optical
 1237 properties under the condition of heavy haze over an urban site of Beijing, China, *Environ. Sci.*
 1238 *Pollut. R.*, 22, 1043-1053, <https://doi.org/10.1007/s11356-014-3415-5>, 2015.
- 1239 Chen, Q., McGowan, S., Gouramanis, C., Fong, L., Balasubramanian, R., and Taylor, D.:
 1240 Rapidly rising transboundary atmospheric pollution from industrial and urban sources in

- 1241 Southeast Asia and its implications for regional sustainable development, *Environ. Res. Lett.*, 15,
1242 1040a1045, <https://doi.org/10.1088/1748-9326/abb5ce>, 2020.
- 1243 Choi, M., Lim, H., Kim, J., Lee, S., Eck, T. F., Holben, B. N., Garay, M. J., Hyer, E. J., Saide, P.
1244 E., and Liu, H.: Validation, comparison, and integration of GOCI, AHI, MODIS, MISR, and
1245 VIIRS aerosol optical depth over East Asia during the 2016 KORUS-AQ campaign, *Atmos.*
1246 *Meas. Tech.*, 12, 4619-4641, <https://doi.org/10.5194/amt-12-4619-2019>, 2019.
- 1247 Cohen, J. B.: [Quantifying the occurrence and magnitude of the Southeast Asian fire climatology,](https://doi.org/10.1088/1748-9326/9/11/114018)
1248 [Environmental Research Letters](https://doi.org/10.1088/1748-9326/9/11/114018), 9, 114018, <https://dx.doi.org/10.1088/1748-9326/9/11/114018>,
1249 [2014](https://doi.org/10.1088/1748-9326/9/11/114018).
- 1250 [Cohen, J. B.](https://doi.org/10.5194/acp-17-721-2017), Lecoecur, E., and Hui Loong Ng, D.: Decadal-scale relationship between
1251 measurements of aerosols, land-use change, and fire over Southeast Asia, *Atmos. Chem. Phys.*,
1252 17, 721-743, <https://doi.org/10.5194/acp-17-721-2017>, 2017.
- 1253 Coronas, J.: *The Climate and Weather of the Philippines, 1903-1918*, by Rev. José Coronas. SJ,
1254 Chief, Meteorological Division, Weather Bureau, Manila Observatory, Manila,: Bureau of
1255 Printing, 1920.
- 1256 Crosbie, E., Sorooshian, A., Monfared, N. A., Shingler, T., and Esmaili, O.: A multi-year aerosol
1257 characterization for the greater Tehran area using satellite, surface, and modeling data,
1258 *Atmosphere*, 5, 178-197, <https://doi.org/10.3390/atmos5020178>, 2014.
- 1259 Crosbie, E., Ziemba, L. D., Shook, M. A., Robinson, C. E., Winstead, E. L., Thornhill, K. L.,
1260 Braun, R. A., MacDonald, A. B., Stahl, C., and Sorooshian, A.: Measurement report: Closure
1261 analysis of aerosol–cloud composition in tropical maritime warm convection, *Atmos. Chem.*
1262 *Phys.*, 22, 13269-13302, <https://doi.org/10.5194/acp-22-13269-2022>, 2022.
- 1263 Cruz, F., Narisma, G. T., Villafuerte II, M. Q., Chua, K. C., and Olaguera, L. M.: A
1264 climatological analysis of the southwest monsoon rainfall in the Philippines, *Atmos. Res.*, 122,
1265 609-616, <https://doi.org/10.1016/j.atmosres.2012.06.010>, 2013.
- 1266 Cruz, M. T., Bañaga, P. A., Betito, G., Braun, R. A., Stahl, C., Aghdam, M. A., Cambaliza, M.
1267 O., Dadashazar, H., Hilario, M. R., Lorenzo, G. R., Ma, L., MacDonald, A. B., Pabroa, C., Yee,
1268 J. R., Simpas, J. B., and Sorooshian, A.: Size-resolved composition and morphology of
1269 particulate matter during the southwest monsoon in Metro Manila, Philippines, *Atmos. Chem.*
1270 *Phys.*, 19, 10675–10696, <https://doi.org/10.5194/acp-19-10675-2019>, 2019.
- 1271 Cruz, M. T., Simpas, J. B., Sorooshian, A., Betito, G., Cambaliza, M. O. L., Collado, J. T.,
1272 Eloranta, E. W., Holz, R., Topacio, X. G. V., and Del Socorro, J.: Impacts of regional wind
1273 circulations on aerosol pollution and planetary boundary layer structure in Metro Manila,
1274 Philippines, *Atmos. Environ.*, 293, 119455, <https://doi.org/10.1016/j.atmosenv.2022.119455>,
1275 2023.
- 1276 [Deep, A., Pandey, C. P., Nandan, H., Singh, N., Yadav, G., Joshi, P., Purohit, K., and Bhatt, S.:](https://doi.org/10.1016/j.atmosenv.2022.119455)
1277 [Aerosols optical depth and Ångström exponent over different regions in Garhwal Himalaya,](https://doi.org/10.1016/j.atmosenv.2022.119455)

1278 [India, Environmental Monitoring and Assessment, 193, 324, https://doi.org/10.1007/s10661-021-](https://doi.org/10.1007/s10661-021-09048-4)
1279 [09048-4, 2021.](https://doi.org/10.1007/s10661-021-09048-4)

1280 Di Girolamo, L., Holz, R., Reid, J., Tanelli, S., van den Heever, S., Narsma, G., and Simpas, J.:
1281 Cloud and aerosol monsoonal processes-Philippines experiment (CAMP2Ex), NASA White
1282 Paper, 2015.

1283 Diner, D. J., Di Girolamo, L., and Nolin, A.: Preface to the MISR special issue, Remote Sens.
1284 Environ., 107, 1, <https://doi.org/10.1016/j.rse.2006.11.001>, 2007.

1285 [Dong, X., and Fu, J. S.: Understanding interannual variations of biomass burning from](https://doi.org/10.1016/j.atmosenv.2015.05.052)
1286 [Peninsular Southeast Asia, part II: Variability and different influences in lower and higher](https://doi.org/10.1016/j.atmosenv.2015.05.052)
1287 [atmosphere levels, Atmospheric Environment, 115, 9-18,](https://doi.org/10.1016/j.atmosenv.2015.05.052)
1288 [https://doi.org/10.1016/j.atmosenv.2015.05.052, 2015.](https://doi.org/10.1016/j.atmosenv.2015.05.052)

1289 [Dorado, S. V., Holdsworth, J. L., Lagrosas, N. C., Villarin, J. R., Narisma, G., Ellis, J., and](https://doi.org/10.1016/j.lsr.2001.05.001)
1290 [Perez, R.: Characterization of urban atmosphere of Manila with lidar, filter sampling, and](https://doi.org/10.1016/j.lsr.2001.05.001)
1291 [radiosonde, Lidar Remote Sensing for Industry and Environment Monitoring, 2001, 591-598,](https://doi.org/10.1016/j.lsr.2001.05.001)

1292 Dubovik, O., Holben, B., Kaufman, Y., Yamasoe, M., Smirnov, A., Tanré, D., and Slutsker, I.:
1293 Single-scattering albedo of smoke retrieved from the sky radiance and solar transmittance
1294 measured from ground, J. Geophys. Res.- Atmos., 103, 31903-31923,
1295 <https://doi.org/10.1029/98JD02276>, 1998.

1296 Dubovik, O., and King, M. D.: A flexible inversion algorithm for retrieval of aerosol optical
1297 properties from Sun and sky radiance measurements, J. Geophys. Res.- Atmos., 105, 20673-
1298 20696, <https://doi.org/10.1029/2000JD900282>, 2000.

1299 Dubovik, O., Holben, B., Eck, T. F., Smirnov, A., Kaufman, Y. J., King, M. D., Tanré, D., and
1300 Slutsker, I.: Variability of absorption and optical properties of key aerosol types observed in
1301 worldwide locations, J. Atmos. Sci., 59, 590-608, [https://doi.org/10.1175/1520-](https://doi.org/10.1175/1520-0469(2002)059<0590:VOAAOP>2.0.CO;2)
1302 [0469\(2002\)059<0590:VOAAOP>2.0.CO;2](https://doi.org/10.1175/1520-0469(2002)059<0590:VOAAOP>2.0.CO;2), 2002.

1303 Eck, T., Holben, B., Reid, J., O'Neill, N., Schafer, J., Dubovik, O., Smirnov, A., Yamasoe, M.,
1304 and Artaxo, P.: High aerosol optical depth biomass burning events: A comparison of optical
1305 properties for different source regions, Geophys. Res. Lett., 30,
1306 <https://doi.org/10.1029/2003GL017861>, 2003.

1307 Eck, T., Holben, B., Dubovik, O., Smirnov, A., Goloub, P., Chen, H., Chatenet, B., Gomes, L.,
1308 Zhang, X. Y., and Tsay, S. C.: Columnar aerosol optical properties at AERONET sites in central
1309 eastern Asia and aerosol transport to the tropical mid-Pacific, J. Geophys. Res.- Atmos., 110,
1310 <https://doi.org/10.1029/2004JD005274>, 2005.

1311 Eck, T., Holben, B., Reid, J., Mukelabai, M., Piketh, S., Torres, O., Jethva, H., Hyer, E., Ward,
1312 D., and Dubovik, O.: A seasonal trend of single scattering albedo in southern African biomass-
1313 burning particles: Implications for satellite products and estimates of emissions for the world's
1314 largest biomass-burning source, J. Geophys. Res.- Atmos., 118, 6414-6432,
1315 <https://doi.org/10.1002/jgrd.50500>, 2013.

1316 Eck, T. F., Holben, B., Reid, J., Dubovik, O., Smirnov, A., O'Neill, N., Slutsker, I., and Kinne, S.:
1317 Wavelength dependence of the optical depth of biomass burning, urban, and desert dust aerosols,
1318 *J. Geophys. Res.- Atmos.*, 104, 31333-31349, <https://doi.org/10.1029/1999JD900923>, 1999.

1319 Eck, T. F., Holben, B. N., Reid, J., Giles, D., Rivas, M., Singh, R. P., Tripathi, S., Bruegge, C.,
1320 Platnick, S., and Arnold, G.: Fog-and cloud-induced aerosol modification observed by the
1321 Aerosol Robotic Network (AERONET), *J. Geophys. Res.- Atmos.*, 117,
1322 <https://doi.org/10.1029/2011JD016839>, 2012.

1323 [Edwards, E.-L., Reid, J. S., Xian, P., Burton, S. P., Cook, A. L., Crosbie, E. C., Fenn, M. A.,](#)
1324 [Ferrare, R. A., Freeman, S. W., and Hair, J. W.: Assessment of NAAPS-RA performance in](#)
1325 [Maritime Southeast Asia during CAMP 2 Ex, *Atmospheric Chemistry and Physics*, 22, 12961-](#)
1326 [12983, <https://doi.org/10.5194/acp-22-12961-2022>, 2022.](#)

1327 Ervens, B., Sorooshian, A., Aldhaif, A. M., Shingler, T., Crosbie, E., Ziemba, L., Campuzano-
1328 Jost, P., Jimenez, J. L., and Wisthaler, A.: Is there an aerosol signature of chemical cloud
1329 processing?, *Atmos. Chem. Phys.*, 18, 16099-16119, <https://doi.org/10.5194/acp-18-16099-2018>,
1330 2018.

1331 Faloon, I.: Sulfur processing in the marine atmospheric boundary layer: A review and critical
1332 assessment of modeling uncertainties, *Atmos. Environ.*, 43, 2841-2854,
1333 <https://doi.org/10.1016/j.atmosenv.2009.02.043>, 2009.

1334 Feingold, G.: Modeling of the first indirect effect: Analysis of measurement requirements,
1335 *Geophys. Res. Lett.*, 30, <https://doi.org/10.1029/2003GL017967>, 2003.

1336 Flores, J.: Climate of the Philippines, *Climates of the Northern and Eastern Asia*, 159-213, 1969.

1337 Formenti, P., Andreae, M. O., and Lelieveld, J.: Measurements of aerosol optical depth above
1338 3570 m asl in the North Atlantic free troposphere: results from ACE-2, *Tellus B*, 52, 678-693,
1339 <https://doi.org/10.1034/j.1600-0889.2000.00006.x>, 2000.

1340 [Foth, A., Kanitz, T., Engelmann, R., Baars, H., Radenz, M., Seifert, P., Barja, B., Fromm, M.,](#)
1341 [Kalesse, H., and Ansmann, A.: Vertical aerosol distribution in the southern hemispheric](#)
1342 [midlatitudes as observed with lidar in Punta Arenas, Chile \(53.2° S and 70.9° W\), during](#)
1343 [ALPACA, *Atmospheric Chemistry and Physics*, 19, 6217-6233, \[https://doi.org/10.5194/acp-19-\]\(https://doi.org/10.5194/acp-19-6217-2019\)](#)
1344 [6217-2019, 2019.](#)

1345 Garay, M. J., Bull, M. A., Nastan, A. M., Witek, M. L., Seidel, F. C., Diner, D. J., Kahn, R. A.,
1346 Limbacher, J. A., and Kalashnikova, O. V.: Data Product Specification for the MISR Level 2
1347 Aerosol Product, Jet Propulsion Laboratory, California Institute of Technology. JPL D-100649.
1348 https://asdc.larc.nasa.gov/documents/misr/DPS_AEROSOL_V023.20180125.pdf, 2018.

1349 Gautam, R., Hsu, N. C., Eck, T. F., Holben, B. N., Janjai, S., Jantarach, T., Tsay, S.-C., and Lau,
1350 W. K.: Characterization of aerosols over the Indochina peninsula from satellite-surface
1351 observations during biomass burning pre-monsoon season, *Atmos. Environ.*, 78, 51-59,
1352 <https://doi.org/10.1016/j.atmosenv.2012.05.038>, 2013.

- 1353 Gelaro, R., McCarty, W., Suárez, M. J., Todling, R., Molod, A., Takacs, L., Randles, C. A.,
1354 Darmenov, A., Bosilovich, M. G., and Reichle, R.: The modern-era retrospective analysis for
1355 research and applications, version 2 (MERRA-2), *J. Climate*, 30, 5419-5454,
1356 <https://doi.org/10.1175/JCLI-D-16-0758.1>, 2017.
- 1357 Geng, H., Hwang, H., Liu, X., Dong, S., and Ro, C.-U.: Investigation of aged aerosols in size-
1358 resolved Asian dust storm particles transported from Beijing, China, to Incheon, Korea, using
1359 low-Z particle EPMA, *Atmos. Chem. Phys.*, 14, 3307-3323, [https://doi.org/10.5194/acp-14-](https://doi.org/10.5194/acp-14-3307-2014)
1360 3307-2014, 2014.
- 1361 Giles, D. M., Holben, B. N., Eck, T. F., Sinyuk, A., Smirnov, A., Slutsker, I., Dickerson, R.,
1362 Thompson, A., and Schafer, J.: An analysis of AERONET aerosol absorption properties and
1363 classifications representative of aerosol source regions, *J. Geophys. Res.- Atmos.*, 117,
1364 <https://doi.org/10.1029/2012JD018127>, 2012.
- 1365 Giles, D. M., Sinyuk, A., Sorokin, M. G., Schafer, J. S., Smirnov, A., Slutsker, I., Eck, T. F.,
1366 Holben, B. N., Lewis, J. R., and Campbell, J. R.: Advancements in the Aerosol Robotic Network
1367 (AERONET) Version 3 database—automated near-real-time quality control algorithm with
1368 improved cloud screening for Sun photometer aerosol optical depth (AOD) measurements,
1369 *Atmos. Meas. Tech.*, 12, 169-209, <https://doi.org/10.5194/amt-12-169-2019>, 2019.
- 1370 Glover, D., and Jessup, T.: The Indonesian fires and haze of 1997: the economic toll, *Economy*
1371 *and Environment Program for SE Asia (EEPSEA)* Singapore and the World Wildlife Fund
1372 (WWF) Indonesia, Jakarta, 1998.
- 1373 Guyon, P., Boucher, O., Graham, B., Beck, J., Mayol-Bracero, O. L., Roberts, G. C., Maenhaut,
1374 W., Artaxo, P., and Andreae, M. O.: Refractive index of aerosol particles over the Amazon
1375 tropical forest during LBA-EUSTACH 1999, *J. Aerosol Sci.*, 34, 883-907,
1376 [https://doi.org/10.1016/S0021-8502\(03\)00052-1](https://doi.org/10.1016/S0021-8502(03)00052-1), 2003.
- 1377 [Harenda, K. M., Markowicz, K. M., Poczta, P., Stachlewska, I. S., Bojanowski, J. S., Czernecki,](#)
1378 [B., McArthur, A., Schuetemeyer, D., and Chojnicki, B. H.: Estimation of the effects of aerosol](#)
1379 [optical properties on peatland production in Rzecin, Poland, *Agricultural and Forest*](#)
1380 [Meteorology, 316, 108861, <https://doi.org/10.1016/j.agrformet.2022.108861>, 2022.](#)
- 1381 Hartley, W. S., and Hobbs, P. V.: An aerosol model and aerosol-induced changes in the clear-sky
1382 albedo off the east coast of the United States, *J. Geophys. Res.- Atmos.*, 106, 9733-9748,
1383 <https://doi.org/10.1029/2001JD900025>, 2001.
- 1384 Haywood, J., and Boucher, O.: Estimates of the direct and indirect radiative forcing due to
1385 tropospheric aerosols: A review, *Rev. Geophys.*, 38, 513-543,
1386 <https://doi.org/10.1029/1999RG000078>, 2000.
- 1387 [Hendrickson, B. N., Brooks, S. D., Thornton, D. C., Moore, R. H., Crosbie, E., Ziemba, L. D.,](#)
1388 [Carlson, C. A., Baetge, N., Mirrieles, J. A., and Alsante, A. N.: Role of sea surface microlayer](#)
1389 [properties in cloud formation, *Frontiers in Marine Science*, 7, 596225,](#)
1390 <https://doi.org/10.3389/fmars.2020.596225>, 2021.

- 1391 Herber, A., Thomason, L. W., Gernandt, H., Leiterer, U., Nagel, D., Schulz, K. H., Kaptur, J.,
 1392 Albrecht, T., and Notholt, J.: Continuous day and night aerosol optical depth observations in the
 1393 Arctic between 1991 and 1999, *J. Geophys. Res.- Atmos.*, 107, AAC 6-1-AAC 6-13,
 1394 <https://doi.org/10.1029/2001JD000536>, 2002.
- 1395 Hilario, M. R. A., Cruz, M. T., Bañaga, P. A., Betito, G., Braun, R. A., Stahl, C., Cambaliza, M.
 1396 O., Lorenzo, G. R., MacDonald, A. B., AzadiAghdam, M., Pabroa, P. C., Yee, J. R., Simpas, J.
 1397 B., and Sorooshian, A.: Characterizing weekly cycles of particulate matter in a coastal megacity:
 1398 The importance of a seasonal, size-resolved, and chemically-speciated analysis, *J. Geophys.*
 1399 *Res.- Atmos.*, 125, e2020JD032614, <https://doi.org/10.1029/2020JD032614>, 2020a.
- 1400 Hilario, M. R. A., Cruz, M. T., Cambaliza, M. O. L., Reid, J. S., Xian, P., Simpas, J. B.,
 1401 Lagrosas, N. D., Uy, S. N. Y., Cliff, S., and Zhao, Y.: Investigating size-segregated sources of
 1402 elemental composition of particulate matter in the South China Sea during the 2011 Vasco
 1403 cruise, *Atmos. Chem. Phys.*, 20, 1255-1276, <https://doi.org/10.5194/acp-20-1255-2020>, 2020b.
- 1404 Hilario, M. R. A., Crosbie, E., Shook, M., Reid, J. S., Cambaliza, M. O. L., Simpas, J. B. B.,
 1405 Ziemba, L., DiGangi, J. P., Diskin, G. S., and Nguyen, P.: Measurement report: Long-range
 1406 transport patterns into the tropical northwest Pacific during the CAMP 2 Ex aircraft campaign:
 1407 chemical composition, size distributions, and the impact of convection, *Atmos. Chem. Phys.*, 21,
 1408 3777-3802, <https://doi.org/10.5194/acp-21-3777-2021>, 2021a.
- 1409 Hilario, M. R. A., Olaguera, L. M., Narisma, G. T., and Matsumoto, J.: Diurnal characteristics of
 1410 summer precipitation over Luzon Island, Philippines, *Asia-Pacific Journal of Atmospheric*
 1411 *Sciences*, 57, 573-585, <https://doi.org/10.1007/s13143-020-00214-1>, 2021b.
- 1412 Hilario, M. R. A., Bañaga, P. A., Betito, G., Braun, R. A., Cambaliza, M. O., Cruz, M. T.,
 1413 Lorenzo, G. R., MacDonald, A. B., Pabroa, P. C., and Simpas, J. B.: Stubborn aerosol: why
 1414 particulate mass concentrations do not drop during the wet season in Metro Manila, Philippines,
 1415 *Environmental Science: Atmospheres*, 2, 1428-1437, <https://doi.org/10.1039/D2EA00073C>,
 1416 2022.
- 1417 Hogan, T. F., Liu, M., Ridout, J. A., Peng, M. S., Whitcomb, T. R., Ruston, B. C., Reynolds, C.
 1418 A., Eckermann, S. D., Moskaitis, J. R., and Baker, N. L.: The navy global environmental model,
 1419 *Oceanography*, 27, 116-125, <https://doi.org/10.5670/oceanog.2014.73>, 2014.
- 1420 Holben, B. N., Eck, T. F., Slutsker, I. a., Tanre, D., Buis, J., Setzer, A., Vermote, E., Reagan, J.
 1421 A., Kaufman, Y., and Nakajima, T.: AERONET—A federated instrument network and data
 1422 archive for aerosol characterization, *Remote Sens. Environ.*, 66, 1-16,
 1423 [https://doi.org/10.1016/S0034-4257\(98\)00031-5](https://doi.org/10.1016/S0034-4257(98)00031-5), 1998.
- 1424 Holben, B. N., Tanre, D., Smirnov, A., Eck, T., Slutsker, I., Abuhassan, N., Newcomb, W.,
 1425 Schafer, J., Chatenet, B., and Lavenu, F.: An emerging ground-based aerosol climatology:
 1426 Aerosol optical depth from AERONET, *J. Geophys. Res.- Atmos.*, 106, 12067-12097,
 1427 <https://doi.org/10.1029/2001JD900014>, 2001.

- 1428 Hong, Y., and Di Girolamo, L.: Cloud phase characteristics over Southeast Asia from A-Train
1429 satellite observations, *Atmos. Chem. Phys.*, 20, 8267-8291, [https://doi.org/10.5194/acp-20-8267-](https://doi.org/10.5194/acp-20-8267-2020)
1430 2020, 2020.
- 1431 [Hong, Y., and Di Girolamo, L.: An overview of aerosol properties in clear and cloudy sky based](#)
1432 [on CALIPSO observations, *Earth and Space Science*, 9, e2022EA002287,](#)
1433 <https://doi.org/10.1029/2022EA002287>, 2022.
- 1434 Hoppel, W., Frick, G., Fitzgerald, J., and Larson, R.: Marine boundary layer measurements of
1435 new particle formation and the effects nonprecipitating clouds have on aerosol size distribution,
1436 *J. Geophys. Res.- Atmos.*, 99, 14443-14459, <https://doi.org/10.1029/94JD00797>, 1994.
- 1437 Huang, C., Li, J., Sun, W., Chen, Q., Mao, Q.-J., and Yuan, Y.: Long-Term Variation
1438 Assessment of Aerosol Load and Dominant Types over Asia for Air Quality Studies Using
1439 Multi-Sources Aerosol Datasets, *Remote Sensing*, 13, 3116, <https://doi.org/10.3390/rs13163116>,
1440 2021.
- 1441 Hyer, E. J., Reid, J. S., Prins, E. M., Hoffman, J. P., Schmidt, C. C., Miettinen, J. I., and Giglio,
1442 L.: Patterns of fire activity over Indonesia and Malaysia from polar and geostationary satellite
1443 observations, *Atmos. Res.*, 122, 504-519, <https://doi.org/10.1016/j.atmosres.2012.06.011>, 2013.
- 1444 Jamora, J. B., Gudia, S. E. L., Go, A. W., Giduquio, M. B., and Loretero, M. E.: Potential CO2
1445 reduction and cost evaluation in use and transport of coal ash as cement replacement: A case in
1446 the Philippines, *Waste Manage.*, 103, 137-145, <https://doi.org/10.1016/j.wasman.2019.12.026>,
1447 2020.
- 1448 Jose, S., Gharai, B., Niranjana, K., and Rao, P.: Investigation on seasonal variations of aerosol
1449 properties and its influence on radiative effect over an urban location in central India, *Atmos.*
1450 *Environ.*, 133, 41-48, <https://doi.org/10.1016/j.atmosenv.2016.03.029>, 2016.
- 1451 Kaskaoutis, D., Kosmopoulos, P., Kambezidis, H., and Nastos, P.: Aerosol climatology and
1452 discrimination of different types over Athens, Greece, based on MODIS data, *Atmos. Environ.*,
1453 41, 7315-7329, <https://doi.org/10.1016/j.atmosenv.2007.05.017>, 2007.
- 1454 [Kaskaoutis, D., Badarinath, K., Kumar Kharol, S., Rani Sharma, A., and Kambezidis, H.:](#)
1455 [Variations in the aerosol optical properties and types over the tropical urban site of Hyderabad,](#)
1456 [India, *Journal of Geophysical Research: Atmospheres*, 114,](#)
1457 <https://doi.org/10.1029/2009JD012423>, 2009.
- 1458 [Kiely, L., Spracklen, D. V., Wiedinmyer, C., Conibear, L., Reddington, C. L., Archer-Nicholls,](#)
1459 [S., Lowe, D., Arnold, S. R., Knute, C., and Khan, M. F.: New estimate of particulate emissions](#)
1460 [from Indonesian peat fires in 2015, *Atmospheric Chemistry and Physics*, 19, 11105-11121,](#)
1461 <https://doi.org/10.5194/acp-19-11105-2019>, 2019.
- 1462 Kim, J.-S., and Park, K.: Atmospheric aging of Asian dust particles during long range transport,
1463 *Aerosol Sci. Tech.*, 46, 913-924, <https://doi.org/10.1080/02786826.2012.680984>, 2012.

- 1464 Kirchstetter, T. W., Novakov, T., and Hobbs, P. V.: Evidence that the spectral dependence of
1465 light absorption by aerosols is affected by organic carbon, *J. Geophys. Res.- Atmos.*, 109,
1466 <https://doi.org/10.1029/2004JD004999>, 2004.
- 1467 Koven, C. D., and Fung, I.: Inferring dust composition from wavelength-dependent absorption in
1468 Aerosol Robotic Network (AERONET) data, *J. Geophys. Res.- Atmos.*, 111,
1469 <https://doi.org/10.1029/2005JD006678>, 2006.
- 1470 Kudo, R., Nishizawa, T., and Aoyagi, T.: Vertical profiles of aerosol optical properties and the
1471 solar heating rate estimated by combining sky radiometer and lidar measurements, *Atmos. Meas.*
1472 *Tech.*, 9, 3223-3243, <https://doi.org/10.5194/amt-9-3223-2016>, 2016.
- 1473 Kumar, K. R., Sivakumar, V., Reddy, R. R., Gopal, K. R., and Adesina, A. J.: Identification and
1474 classification of different aerosol types over a subtropical rural site in Mpumalanga, South
1475 Africa: seasonal variations as retrieved from the AERONET Sunphotometer, *Aerosol Air Qual.*
1476 *Res.*, 14, 108-123, <https://doi.org/10.4209/aaqr.2013.03.0079>, 2014.
- 1477 Kumar, K. R., Yin, Y., Sivakumar, V., Kang, N., Yu, X., Diao, Y., Adesina, A. J., and Reddy,
1478 R.: Aerosol climatology and discrimination of aerosol types retrieved from MODIS, MISR and
1479 OMI over Durban (29.88 S, 31.02 E), South Africa, *Atmos. Environ.*, 117, 9-18,
1480 <https://doi.org/10.1016/j.atmosenv.2015.06.058>, 2015.
- 1481 Kuttippurath, J., and Raj, S.: Two decades of aerosol observations by AATSR, MISR, MODIS
1482 and MERRA-2 over India and Indian Ocean, *Remote Sens. Environ.*, 257, 112363,
1483 <https://doi.org/10.1016/j.rse.2021.112363>, 2021.
- 1484 Lee, H.-H., Iraqui, O., Gu, Y., Yim, S. H.-L., Chulakadabba, A., Tonks, A. Y.-M., Yang, Z., and
1485 Wang, C.: Impacts of air pollutants from fire and non-fire emissions on the regional air quality in
1486 Southeast Asia, *Atmos. Chem. Phys.*, 18, 6141-6156, <https://doi.org/10.5194/acp-18-6141-2018>,
1487 2018.
- 1488 [Lee, J., Kim, J., Song, C., Kim, S., Chun, Y., Sohn, B., and Holben, B.: Characteristics of aerosol](#)
1489 [types from AERONET sunphotometer measurements, *Atmospheric Environment*, 44, 3110-](#)
1490 [3117, <https://doi.org/10.1016/j.atmosenv.2010.05.035>, 2010.](#)
- 1491 Li, G., Bei, N., Cao, J., Huang, R., Wu, J., Feng, T., Wang, Y., Liu, S., Zhang, Q., and Tie, X.: A
1492 possible pathway for rapid growth of sulfate during haze days in China, *Atmos. Chem. Phys.*, 17,
1493 3301-3316, <https://doi.org/10.5194/acp-17-3301-2017>, 2017.
- 1494 Li, J., Carlson, B. E., and Lacis, A. A.: Application of spectral analysis techniques in the
1495 intercomparison of aerosol data: 1. An EOF approach to analyze the spatial-temporal variability
1496 of aerosol optical depth using multiple remote sensing data sets, *J. Geophys. Res.- Atmos.*, 118,
1497 8640-8648, <https://doi.org/10.1002/jgrd.50686>, 2013.
- 1498 Li, Z., Niu, F., Fan, J., Liu, Y., Rosenfeld, D., and Ding, Y.: Long-term impacts of aerosols on
1499 the vertical development of clouds and precipitation, *Nat. Geosci.*, 4, 888-894,
1500 <https://doi.org/10.1038/ngeo1313>, 2011.

1501 Lin, N.-H., Sayer, A. M., Wang, S.-H., Loftus, A. M., Hsiao, T.-C., Sheu, G.-R., Hsu, N. C.,
1502 Tsay, S.-C., and Chantara, S.: Interactions between biomass-burning aerosols and clouds over
1503 Southeast Asia: Current status, challenges, and perspectives, *Environ. Pollut.*, 195, 292-307,
1504 <https://doi.org/10.1016/j.envpol.2014.06.036>, 2014.

1505 Lloyd, S.: Least squares quantization in PCM, *IEEE T. Inform. Theory*, 28, 129-137,
1506 <https://doi.org/10.1109/TIT.1982.1056489>, 1982.

1507 Lynch, P., Reid, J. S., Westphal, D. L., Zhang, J., Hogan, T. F., Hyer, E. J., Curtis, C. A., Hegg,
1508 D. A., Shi, Y., and Campbell, J. R.: An 11-year global gridded aerosol optical thickness
1509 reanalysis (v1. 0) for atmospheric and climate sciences, *Geosci. Model Dev.*, 9,
1510 <https://doi.org/10.5194/gmd-9-1489-2016>, 2016.

1511 [Markowicz, K., Zawadzka-Manko, O., Lisok, J., Chilinski, M., and Xian, P.: The impact of](https://doi.org/10.1016/j.jaerosci.2020.105627)
1512 [moderately absorbing aerosol on surface sensible, latent, and net radiative fluxes during the](https://doi.org/10.1016/j.jaerosci.2020.105627)
1513 [summer of 2015 in Central Europe, *Journal of Aerosol Science*, 151, 105627,](https://doi.org/10.1016/j.jaerosci.2020.105627)
1514 <https://doi.org/10.1016/j.jaerosci.2020.105627>, 2021.

1515 Matsumoto, J., Olaguera, L. M. P., Nguyen-Le, D., Kubota, H., and Villafuerte, M. Q.:
1516 Climatological seasonal changes of wind and rainfall in the Philippines, *Int. J. Climatol.*, 40,
1517 4843-4857, <https://doi.org/10.1002/joc.6492>, 2020.

1518 [Mims III, F. M.: A 30-Year Climatology \(1990–2020\) of Aerosol Optical Depth and Total](https://doi.org/10.1175/BAMS-D-21-0010.1)
1519 [Column Water Vapor and Ozone over Texas, *Bulletin of the American Meteorological Society*,](https://doi.org/10.1175/BAMS-D-21-0010.1)
1520 [103, E101-E109, https://doi.org/10.1175/BAMS-D-21-0010.1, 2022.](https://doi.org/10.1175/BAMS-D-21-0010.1)

1521 Moosmüller, H., and Sorensen, C.: Small and large particle limits of single scattering albedo for
1522 homogeneous, spherical particles, *J. Quant. Spectrosc. Ra.*, 204, 250-255,
1523 <https://doi.org/10.1016/j.jqsrt.2017.09.029>, 2018.

1524 Mora, M., Braun, R. A., Shingler, T., and Sorooshian, A.: Analysis of remotely sensed and
1525 surface data of aerosols and meteorology for the Mexico Megalopolis Area between 2003 and
1526 2015, *J. Geophys. Res.- Atmos.*, 122, 8705-8723, <https://doi.org/10.1002/2017JD026739>, 2017.

1527 Nakata, M., Mukai, S., and Yasumoto, M.: Seasonal and regional characteristics of aerosol
1528 pollution in east and southeast Asia, *Frontiers in Environmental Science*, 6, 29,
1529 [2018-https://doi.org/10.3389/fenvs.2018.00029](https://doi.org/10.3389/fenvs.2018.00029), 2018.

1530 Fires and Smoke in Borneo: [https://earthobservatory.nasa.gov/images/40182/fires-and-smoke-in-](https://earthobservatory.nasa.gov/images/40182/fires-and-smoke-in-borneo)
1531 [borneo](https://earthobservatory.nasa.gov/images/40182/fires-and-smoke-in-borneo)), 2009.

1532 Nguyen, P., Shearer, E. J., Tran, H., Ombadi, M., Hayatbini, N., Palacios, T., Huynh, P.,
1533 Braithwaite, D., Updegraff, G., and Hsu, K.: The CHRS Data Portal, an easily accessible public
1534 repository for PERSIANN global satellite precipitation data, *Scientific Data*, 6, 1-10,
1535 <https://doi.org/10.1038/sdata.2018.296>, ~~2019~~2019a.

1536 [Nguyen, T. T., Pham, H. V., Lasko, K., Bui, M. T., Laffly, D., Jourdan, A., and Bui, H. Q.:](https://doi.org/10.1016/j.jaerosci.2020.105627)
1537 [Spatiotemporal analysis of ground and satellite-based aerosol for air quality assessment in the](https://doi.org/10.1016/j.jaerosci.2020.105627)

1538 [Southeast Asia region, *Environmental Pollution*, 255, 113106,](#)
1539 <https://doi.org/10.1016/j.envpol.2019.113106>, 2019b.

1540 North, G. R., Bell, T. L., Cahalan, R. F., and Moeng, F. J.: Sampling errors in the estimation of
1541 empirical orthogonal functions, *Mon. Weather Rev.*, 110, 699-706, <https://doi.org/10.1175/1520->
1542 0493(1982)110<0699:SEITEO>2.0.CO;2, 1982.

1543 O'Neill, N., Eck, T., Smirnov, A., Holben, B., and Thulasiraman, S.: Spectral discrimination of
1544 coarse and fine mode optical depth, *J. Geophys. Res.- Atmos.*, 108,
1545 <https://doi.org/10.1029/2002JD002975>, 2003.

1546 Oanh, N. [K., Upadhyay, N., Zhuang, Y.-H., Hao, Z.-P., Murthy, D., Lestari, P., Villarin, J.,](#)
1547 [Chengchua, K., Co, H., and Dung, N.: Particulate air pollution in six Asian cities: Spatial and](#)
1548 [temporal distributions, and associated sources, *Atmospheric environment*, 40, 3367-3380,](#)
1549 <https://doi.org/10.1016/j.atmosenv.2006.01.050>, 2006.

1550 [Oanh, N. T. K., Permadi, D. A., Hopke, P. K., Smith, K. R., Dong, N. P., and Dang, A. N.:](#)
1551 Annual emissions of air toxics emitted from crop residue open burning in Southeast Asia over
1552 the period of 2010–2015, *Atmos. Environ.*, 187, 163-173,
1553 <https://doi.org/10.1016/j.atmosenv.2018.05.061>, 2018.

1554 [Ong, H. J. J., Lagrosas, N., Uy, S. N., Gacal, G. F. B., Dorado, S., Tobias Jr, V., and Holben, B.:](#)
1555 [Determination of Monthly Aerosol Types in Manila Observatory and Notre Dame of Marbel](#)
1556 [University from Aerosol Robotic Network \(AERONET\) measurements, AGU Fall Meeting](#)
1557 [Abstracts, 2016, A54E-03,](#)

1558 Pace, G., Sarra, A. d., Meloni, D., Piacentino, S., and Chamard, P.: Aerosol optical properties at
1559 Lampedusa (Central Mediterranean). 1. Influence of transport and identification of different
1560 aerosol types, *Atmos. Chem. Phys.*, 6, 697-713, <https://doi.org/10.5194/acp-6-697-2006>, 2006.

1561 Pandolfi, M., Alados-Arboledas, L., Alastuey, A., Andrade, M., Angelov, C., Artiñano, B.,
1562 Backman, J., Baltensperger, U., Bonasoni, P., and Bukowiecki, N.: A European aerosol
1563 phenomenology–6: scattering properties of atmospheric aerosol particles from 28 ACTRIS sites,
1564 *Atmos. Chem. Phys.*, 18, 7877-7911, <https://doi.org/10.5194/acp-18-7877-2018>, 2018.

1565 Petters, M. D., Carrico, C. M., Kreidenweis, S. M., Prenni, A. J., DeMott, P. J., Collett Jr, J. L.,
1566 and Moosmüller, H.: Cloud condensation nucleation activity of biomass burning aerosol, *J.*
1567 *Geophys. Res.- Atmos.*, 114, <https://doi.org/10.1029/2009JD012353>, 2009.

1568 Plymale, N. T., Szekely, J. E., and Rubinstein, A. H.: Statistical Cluster Analysis of Global
1569 Aerosol Optical Depth for Simplified Atmospheric Modeling, *J. Appl. Meteorol. Clim.*,
1570 <https://doi.org/10.1175/JAMC-D-21-0150.1>, 2021.

1571 PSA: Highlights of the Philippine population 2015 census of population, Philippine Statistics
1572 Authority, 2016.

- 1573 [Qi, Y., Ge, J., and Huang, J.: Spatial and temporal distribution of MODIS and MISR aerosol](#)
1574 [optical depth over northern China and comparison with AERONET, Chinese science bulletin,](#)
1575 [58, 2497-2506, <https://doi.org/10.1007/s11434-013-5678-5>, 2013.](#)
- 1576 [Ramage, C. S.: Monsoon meteorology, Academic Press, New York, 1971.](#)
- 1577 Randles, C., Da Silva, A., Buchard, V., Colarco, P., Darmenov, A., Govindaraju, R., Smirnov,
1578 A., Holben, B., Ferrare, R., and Hair, J.: The MERRA-2 aerosol reanalysis, 1980 onward. Part I:
1579 System description and data assimilation evaluation, *J. Climate*, 30, 6823-6850,
1580 <https://doi.org/10.1175/JCLI-D-16-0609.1>, 2017.
- 1581 Reid, J., Koppmann, R., Eck, T., and Eleuterio, D.: A review of biomass burning emissions part
1582 II: intensive physical properties of biomass burning particles, *Atmos. Chem. Phys.*, 5, 799-825,
1583 <https://doi.org/10.5194/acp-5-799-2005>, 2005.
- 1584 Reid, J., Xian, P., Hyer, E., Flatau, M., Ramirez, E., Turk, F., Sampson, C., Zhang, C., Fukada,
1585 E., and Maloney, E.: Multi-scale meteorological conceptual analysis of observed active fire
1586 hotspot activity and smoke optical depth in the Maritime Continent, *Atmos. Chem. Phys.*, 12,
1587 2117, <https://doi.org/10.5194/acp-12-2117-2012>, 2012.
- 1588 Reid, J., Maring, H., Narisma, G., van den Heever, S., Di Girolamo, L., Ferrare, R., Holz, R.,
1589 Lawson, P., Mace, G., and Simpas, J.: The coupling between tropical meteorology, aerosol
1590 lifecycle, convection, and radiation, during the Cloud, Aerosol and Monsoon Processes
1591 Philippines Experiment (CAMP 2 Ex), *B. Am. Meteorol. Soc.*, [https://doi.org/10.1175/BAMS-](https://doi.org/10.1175/BAMS-D-21-0285.1)
1592 [D-21-0285.1](https://doi.org/10.1175/BAMS-D-21-0285.1), 2023.
- 1593 Reid, J. S., Hobbs, P. V., Liousse, C., Martins, J. V., Weiss, R. E., and Eck, T. F.: Comparisons
1594 of techniques for measuring shortwave absorption and black carbon content of aerosols from
1595 biomass burning in Brazil, *J. Geophys. Res.- Atmos.*, 103, 32031-32040,
1596 <https://doi.org/10.1029/98JD00773>, 1998.
- 1597 Reid, J. S., Hyer, E. J., Johnson, R. S., Holben, B. N., Yokelson, R. J., Zhang, J., Campbell, J. R.,
1598 Christopher, S. A., Di Girolamo, L., and Giglio, L.: Observing and understanding the Southeast
1599 Asian aerosol system by remote sensing: An initial review and analysis for the Seven Southeast
1600 Asian Studies (7SEAS) program, *Atmos. Res.*, 122, 403-468,
1601 <https://doi.org/10.1016/j.atmosres.2012.06.005>, 2013.
- 1602 Reid, J. S., Lagrosas, N. D., Jonsson, H. H., Reid, E. A., Sessions, W. R., Simpas, J. B., Uy, S.
1603 N., Boyd, T., Atwood, S. A., and Blake, D. R.: Observations of the temporal variability in
1604 aerosol properties and their relationships to meteorology in the summer monsoonal South China
1605 Sea/East Sea: the scale-dependent role of monsoonal flows, the Madden-Julian Oscillation,
1606 tropical cyclones, squall lines and cold pools, *Atmos. Chem. Phys.*, 15, 1745-1768,
1607 <https://doi.org/10.5194/acp-15-1745-2015>, 2015.
- 1608 [Rizza, U., Mancinelli, E., Morichetti, M., Passerini, G., and Virgili, S.: Aerosol optical depth of](#)
1609 [the main aerosol species over Italian cities based on the NASA/MERRA-2 model reanalysis,](#)
1610 [Atmosphere, 10, 709, <https://doi.org/10.3390/atmos10110709>, 2019.](#)

1611 Rolph, G., Stein, A., and Stunder, B.: Real-time environmental applications and display system:
1612 READY, Environ. Modell. Softw., 95, 210-228, <https://doi.org/10.1016/j.envsoft.2017.06.025>,
1613 2017.

1614 [Ross, A. D., Holz, R. E., Quinn, G., Reid, J. S., Xian, P., Turk, F. J., and Posselt, D. J.: Exploring
1615 the first aerosol indirect effect over Southeast Asia using a 10-year collocated MODIS, CALIOP,
1616 and model dataset, Atmospheric Chemistry and Physics, 18, 12747-12764,
1617 <https://doi.org/10.5194/acp-18-12747-2018>, 2018.](#)

1618 Ross, J. L., Hobbs, P. V., and Holben, B.: Radiative characteristics of regional hazes dominated
1619 by smoke from biomass burning in Brazil: Closure tests and direct radiative forcing, J. Geophys.
1620 Res.- Atmos., 103, 31925-31941, <https://doi.org/10.1029/97JD03677>, 1998.

1621 Saleh, R., Hennigan, C., McMeeking, G., Chuang, W., Robinson, E., Coe, H., Donahue, N., and
1622 Robinson, A.: Absorptivity of brown carbon in fresh and photo-chemically aged biomass-
1623 burning emissions, Atmos. Chem. Phys., 13, 7683-7693, [https://doi.org/10.5194/acp-13-7683-
1624 2013](https://doi.org/10.5194/acp-13-7683-2013), 2013.

1625 Schlosser, J. S., Braun, R. A., Bradley, T., Dadashazar, H., MacDonald, A. B., Aldhaif, A. A.,
1626 Aghdam, M. A., Mardi, A. H., Xian, P., and Sorooshian, A.: Analysis of aerosol composition
1627 data for western United States wildfires between 2005 and 2015: Dust emissions, chloride
1628 depletion, and most enhanced aerosol constituents, J. Geophys. Res.- Atmos., 122, 8951-8966,
1629 <https://doi.org/10.1002/2017JD026547>, 2017.

1630 Schuster, G., Dubovik, O., and Arola, A.: Remote sensing of soot carbon—Part 1: Distinguishing
1631 different absorbing aerosol species, Atmos. Chem. Phys., 16, 1565-1585,
1632 <https://doi.org/10.5194/acp-16-1565-2016>, 2016.

1633 Schuster, G. L., Dubovik, O., ~~Holben, B. N., and Clothiaux, E. E.: Inferring black carbon content
1634 and specific absorption from Aerosol Robotic Network (AERONET) aerosol retrievals, J.
1635 Geophys. Res.- Atmos., 110, <https://doi.org/10.1029/2004JD004548>, 2005.~~
1636 ~~Schuster, G. L., Dubovik, O., and Holben, B. N.: Angstrom exponent and bimodal aerosol size
1637 distributions, J. Geophys. Res.- Atmos., 111, <https://doi.org/10.1029/2005JD006328>, 2006.~~

1638 Sharma, M., Kaskaoutis, D. G., Singh, R. P., and Singh, S.: Seasonal variability of atmospheric
1639 aerosol parameters over Greater Noida using ground sunphotometer observations, Aerosol Air
1640 Qual. Res., 14, 608-622, <https://doi.org/10.4209/aaqr.2013.06.0219>, 2014.

1641 Shen, Z., Liu, J., Horowitz, L., Henze, D., Fan, S., Mauzerall, D. L., Lin, J.-T., and Tao, S.:
1642 Analysis of transpacific transport of black carbon during HIPPO-3: implications for black carbon
1643 aging, Atmos. Chem. Phys., 14, 6315-6327, <https://doi.org/10.5194/acp-14-6315-2014>, 2014.

1644 [Sinyuk, A., Holben, B. N., Eck, T. F., Giles, D. M., Slutsker, I., Korkin, S., Schafer, J. S.,
1645 Smirnov, A., Sorokin, M., and Lyapustin, A.: The AERONET Version 3 aerosol retrieval
1646 algorithm, associated uncertainties and comparisons to Version 2, Atmospheric Measurement
1647 Techniques, 13, 3375-3411, <https://doi.org/10.5194/amt-13-3375-2020>, 2020.](#)

- 1648 Smirnov, A., Holben, B. N., Dubovik, O., O'Neill, N. T., Eck, T. F., Westphal, D. L., Goroch, A.
1649 K., Pietras, C., and Slutsker, I.: Atmospheric aerosol optical properties in the Persian Gulf, J.
1650 Atmos. Sci., 59, 620-634, [https://doi.org/10.1175/1520-](https://doi.org/10.1175/1520-0469(2002)059<0620:AAOPIT>2.0.CO;2)
1651 0469(2002)059<0620:AAOPIT>2.0.CO;2, 2002.
- 1652 Smith, S. J., Aardenne, J. v., Klimont, Z., Andres, R. J., Volke, A., and Delgado Arias, S.:
1653 Anthropogenic sulfur dioxide emissions: 1850–2005, Atmos. Chem. Phys., 11, 1101-1116,
1654 <https://doi.org/10.5194/acp-11-1101-2011>, 2011.
- 1655 Sorooshian, A., Wang, Z., Feingold, G., and L'Ecuyer, T. S.: A satellite perspective on cloud
1656 water to rain water conversion rates and relationships with environmental conditions, J.
1657 Geophys. Res.- Atmos., 118, 6643-6650, <https://doi.org/10.1002/jgrd.50523>, 2013.
- 1658 Stahl, C., Cruz, M. T., Bañaga, P. A., Betito, G., Braun, R. A., Aghdam, M. A., Cambaliza, M.
1659 O., Lorenzo, G. R., MacDonald, A. B., and Hilario, M. R. A.: Sources and characteristics of size-
1660 resolved particulate organic acids and methanesulfonate in a coastal megacity: Manila,
1661 Philippines, Atmos. Chem. Phys., 20, 15907-15935, <https://doi.org/10.5194/acp-20-15907-2020>,
1662 2020.
- 1663 Stahl, C., Crosbie, E., Bañaga, P. A., Betito, G., Braun, R. A., Cainglet, Z. M., Cambaliza, M. O.,
1664 Cruz, M. T., Dado, J. M., and Hilario, M. R. A.: Total organic carbon and the contribution from
1665 speciated organics in cloud water: airborne data analysis from the CAMP 2 Ex field campaign,
1666 Atmos. Chem. Phys., 21, 14109-14129, <https://doi.org/10.5194/acp-21-14109-2021>, 2021.
- 1667 Stein, A., Draxler, R. R., Rolph, G. D., Stunder, B. J., Cohen, M., and Ngan, F.: NOAA's
1668 HYSPLIT atmospheric transport and dispersion modeling system, B. Am. Meteorol. Soc., 96,
1669 2059-2077, <https://doi.org/10.1175/BAMS-D-14-00110.1>, 2015.
- 1670 Stevens, B., and Feingold, G.: Untangling aerosol effects on clouds and precipitation in a
1671 buffered system, Nature, 461, 607-613, <https://doi.org/10.1038/nature08281>, 2009.
- 1672 Sullivan, R. C., Levy, R. C., da Silva, A. M., and Pryor, S. C.: Developing and diagnosing
1673 climate change indicators of regional aerosol optical properties, Scientific Reports, 7, 1-13,
1674 <https://doi.org/10.1038/s41598-017-18402-x>, 2017.
- 1675 Tao, W. K., Chen, J. P., Li, Z., Wang, C., and Zhang, C.: Impact of aerosols on convective
1676 clouds and precipitation, Rev. Geophys., 50, <https://doi.org/10.1029/2011RG000369>, 2012.
- 1677 Tsay, S.-C., Hsu, N. C., Lau, W. K.-M., Li, C., Gabriel, P. M., Ji, Q., Holben, B. N., Welton, E.
1678 J., Nguyen, A. X., and Janjai, S.: From BASE-ASIA toward 7-SEAS: A satellite-surface
1679 perspective of boreal spring biomass-burning aerosols and clouds in Southeast Asia,
1680 Atmospheric environment, 78, 20-34, [2013-<https://doi.org/10.1016/j.atmosenv.2012.12.013>,](https://doi.org/10.1016/j.atmosenv.2012.12.013)
1681 [2013](https://doi.org/10.1016/j.atmosenv.2012.12.013).
- 1682 Van Beelen, A., Roelofs, G., Hasekamp, O., Henzing, J., and Röckmann, T.: Estimation of
1683 aerosol water and chemical composition from AERONET Sun-sky radiometer measurements at
1684 Cabauw, the Netherlands, Atmos. Chem. Phys., 14, 5969-5987, [https://doi.org/10.5194/acp-14-](https://doi.org/10.5194/acp-14-5969-2014)
1685 5969-2014, 2014.

1686 [Wall, C. J., Norris, J. R., Possner, A., McCoy, D. T., McCoy, I. L., and Lutsko, N. J.: Assessing](#)
1687 [effective radiative forcing from aerosol–cloud interactions over the global ocean, Proceedings of](#)
1688 [the National Academy of Sciences, 119, e2210481119,](#)
1689 <https://doi.org/10.1073/pnas.2210481119>, 2022.

1690 Wang, L., Lau, K.-H., Fung, C.-H., and Gan, J.-P.: The relative vorticity of ocean surface winds
1691 from the QuikSCAT satellite and its effects on the geneses of tropical cyclones in the South
1692 China Sea, *Tellus A*, 59, 562-569, <https://doi.org/10.1111/j.1600-0870.2007.00249.x>, 2007.

1693 [Wang, S.-H., Welton, E. J., Holben, B. N., Tsay, S.-C., Lin, N.-H., Giles, D., Stewart, S. A.,](#)
1694 [Janjai, S., Nguyen, X. A., and Hsiao, T.-C.: Vertical distribution and columnar optical properties](#)
1695 [of springtime biomass-burning aerosols over Northern Indochina during 2014 7-SEAS](#)
1696 [campaign, Aerosol and Air Quality Research, 15, 2037-2050,](#)
1697 <https://doi.org/10.4209/aaqr.2015.05.0310>, 2015.

1698 Wu, M.-c., and Choy, C.-w.: An Observational Study of the Changes in the Intensity and Motion
1699 of Tropical Cyclones crossing Luzon, *Tropical Cyclone Research and Review*, 4, 95-109,
1700 <https://doi.org/10.6057/2015TCRRh3.01>, 2016.

1701 Xian, P., Reid, J. S., Atwood, S. A., Johnson, R. S., Hyer, E. J., Westphal, D. L., and Sessions,
1702 W.: Smoke aerosol transport patterns over the Maritime Continent, *Atmos. Res.*, 122, 469-485,
1703 <https://doi.org/10.1016/j.atmosres.2012.05.006>, 2013.

1704 [Xiao, N., Shi, T., Calder, C. A., Munroe, D. K., Berrett, C., Wolfenbarger, S., and Li, D.: Spatial](#)
1705 [characteristics of the difference between MISR and MODIS aerosol optical depth retrievals over](#)
1706 [mainland Southeast Asia, Remote Sensing of Environment, 113, 1-9,](#)
1707 <https://doi.org/10.1016/j.rse.2008.07.011>, 2009.

1708 Xie, Y., Li, Z., Zhang, Y., Zhang, Y., Li, D., Li, K., Xu, H., Zhang, Y., Wang, Y., and Chen, X.:
1709 Estimation of atmospheric aerosol composition from ground-based remote sensing
1710 measurements of Sun-sky radiometer, *J. Geophys. Res.- Atmos.*, 122, 498-518,
1711 <https://doi.org/10.1002/2016JD025839>, 2017.

1712 [Yang, S., Lau, W. K., Ji, Z., Dong, W., and Yang, S.: Impacts of radiative effect of pre-monsoon](#)
1713 [biomass burning aerosols on atmospheric circulation and rainfall over Southeast Asia and](#)
1714 [southern China, Climate Dynamics, 59, 417-432, https://doi.org/10.1007/s00382-021-06135-7,](#)
1715 [2022.](#)

1716 [Yumul Jr, G. P., Cruz, N. A., Dimalanta, C. B., Servando, N. T., and Hilario, F. D.: The 2007 dry](#)
1717 [spell in Luzon \(Philippines\): its cause, impact and corresponding response measures, Climatic](#)
1718 [change, 100, 633-644, https://doi.org/10.1007/s10584-009-9677-0](#), 2010.

1719 [Zhao, G., Di Girolamo, L., Dey, S., Jones, A. L., and Bull, M.: Examination of direct cumulus](#)
1720 [contamination on MISR-retrieved aerosol optical depth and angstrom coefficient over ocean,](#)
1721 [Geophysical Research Letters, 36, https://doi.org/10.1029/2009GL038549](#), 2009.

1722 Zhao, G., Zhao, C., Kuang, Y., Bian, Y., Tao, J., Shen, C., and Yu, Y.: Calculating the aerosol
1723 asymmetry factor based on measurements from the humidified nephelometer system, *Atmos.*
1724 *Chem. Phys.*, 18, 9049-9060, <https://doi.org/10.5194/acp-18-9049-2018>, 2018.